Rapid Prototyping of a Programmable Controller for Digital Microfluidic Systems

by

Miguel Angel Murran

B.A.Sc., The University of British Columbia, 2010

A THESIS SUBMITTED IN PARTIAL FULFILLMENT OF
THE REQUIREMENTS FOR THE DEGREE OF

MASTER OF APPLIED SCIENCE

in

The College of Graduate Studies

(Electrical Engineering)

THE UNIVERSITY OF BRITISH COLUMBIA

(Okanagan)

March, 2012

Abstract

Digital microfluidic (DMF) devices can be used to perform complete chemical or biochemical analysis on miniscule droplets; thus they have the potential to replace large and expensive laboratory facilities. Droplets are manipulated on a DMF device by the application of electrical signals to an array of electrodes. Several droplet operations including transport, mixing, and splitting can be performed by the sequential timing of these electrical signals. However, the reliability and successful operation of a DMF device largely depend on improving its controller hardware and fabrication quality. A closed-loop controller uses feedback information to compensate for modeling and run-time uncertainties; thus the controller can improve the accuracy and robustness of droplet operations on a DMF device.

In this thesis, a low cost and fully-customizable closed-loop controller is prototyped for DMF devices. This controller incorporates a calibration-free droplet position sensing technique capable of estimating the position of any type of droplet anywhere on a DMF device. The controller was simulated to evaluate its feasibility of improving the control of a droplet prior to prototyping. Simulation results demonstrate that unprecedented control over droplet position, velocity, and acceleration can be achieved with the proposed controller. In addition, these simulation observations revealed that

pulse train actuation was feasible for controlling the incremental position, velocity, and acceleration of a droplet in a DMF device. Finally, a portable, low-cost closed-loop control system was built using off-the-shelf components. The proposed controller was integrated with a DMF device to experimentally demonstrate its potential of enhancing the control of droplet transport operations by sub-electrode droplet positioning. The prototyped controller can monitor and control the position of a droplet in real-time with an unparalleled degree of accuracy and repeatability. A final contribution was to optimize the fabrication process for a defect-free DMF device using basic microfabrication.

The outcome of this research will allow for complete control over the droplet transport operation. This controller can also be used for more complex droplet operations including mixing and splitting droplets in DMF devices. In addition, the proposed closed-loop controller hardware can serve as a prototype development environment for promoting the commercialization of DMF technology.

Preface

The research conducted in this thesis was performed in the Advanced Control and Intelligent Systems (ACIS) Laboratory at the University of British Columbia under the supervision of Dr. Homayoun Najjaran. Some parts of this thesis have been accepted in peer-reviewed journal articles [1] and others have been published in conference proceedings [2, 3]. My supervisor, Dr. Homayoun Najjaran, was a co-author for all publications.

The capacitance-based droplet position sensing technique in Chapter 2 was accepted for publication in Lab On a Chip [1]. I was responsible for developing the methodology and writing the article.

The optimization of the capacitance-based droplet position sensing technique through DMF parameters introduced in Chapter 2 was published in a conference proceeding [2]. I was responsible for developing the methodology and writing the article. Dr. Abbas S. Milani contributed with the design of experiments for statistical analysis and was responsible for editing the article.

A preliminary investigation into estimating droplet position with capacitance was published in a conference proceeding [3]. H. Martin was responsible for data acquisition and analysis and was the main writing author of the article. I was responsible in developing the methodology for estimating

droplet position from electrode capacitances in a 2X2 array of square electrodes and co-writing the article. R. L'Orsa was responsible for editing the article.

List of Publications

- **M. Murran** and H. Najjaran, *Capacitance-based Droplet Position Estimator for Digital Microfluidic Devices*, Lab On a Chip, 2012. (In press)
- **M. Murran**, A. Milani and H. Najjaran, *Capacitance-based droplet position sensing optimization through digital microfluidic parameters*, ASME 9th International Conference on Nanochannels, Microchannels, and Minichannels (ICNMM), Edmonton, AB, Canada, June 2011.
- H. Martin, **M. Murran** and R. L'Orsa, H. Najjaran, *Experimental technique for sensing droplet position in digital microfluidic systems using capacitance measurement*, ASME International Mechanical Engineering Congress and Exposition, Vancouver, November 2010.

Table of Contents

List of Tables

List of Figures

Acknowledgements

The work presented in this thesis was made possible thanks to the encouragement and support of those with which I have had the pleasure to work, laugh, and play. The following co-workers and friends have contributed to my academic success.

I would like to begin by thanking my supervisor, mentor, and friend; Professor Homayoun Najjaran. I have come a long way since we first discussed the possibilities of graduate studies after one of his lectures on control systems. His support and guidance through the application process helped earn me the Alexander Graham Bell Canada Graduate Scholarship (CGS) award to fund my school and life expenses. The following summer, I was awarded the Michael Smith Foreign Study Supplements (CGS) to fund an international research internship in Kyoto University, Japan. Professor Najjaran not only guided me in my research, but shared with me his life experiences, influencing my own life decisions for the better. His minimal-intervention approach to supervision has motivated me to become more independent and ambitious - for which I will always be grateful. I know now that I made the right decision to join a Master's program under the supervision of Professor Najjaran and look forward to a long professional relationship.

I am honored to have Professors Mina Hoorfar and Jonathan Holzman

as my internal advisory committee members. Mina's enthusiasm and expertise in the field of microfluidics was the motivation necessary to bury myself in technical sources and learn microfluidics from the inside out to avoid perishing under her critique. I really appreciate Professor Holzman's patience and conversations that made this research enjoyable. In addition, I am ever grateful to both professors for sharing laboratory equipment that would have otherwise made my work impossible.

I would like to extend my sincerest appreciations to the members of the Nanometrics Laboratory at Kyoto University, Japan. In particular, I would like to thank my host supervisor and mentor, Professor Hidetoshi Kotera for his hospitality and generosity, making my stay in Japan as comfortable as possible. I am also grateful to Professor Masataka Ohoka who taught me nano-fabrication techniques at Kyoto University. Also, I would like to thank Professor Atsuhito Okonogi for offering invaluable assistance in operating laboratory equipment. Finally, I am thankful towards Nagendra Kumar Kamisetty, Kimiko Terakawa, and Miki Ashida for their friendship during my stay in Kyoto, Japan.

In addition, I would like to thank Professor Kyohei Terao for his guidance in the fabrication and testing of a cell electroporation device. Furthermore, I am grateful to have the companionship of the lab members from Kagawa University during my trip in Takamatsu, Kagawa.

Finally, special thanks to my family for their encouragement and support since the start of my academic career. I want to extend a special thanks to my colleague and friend, Reddiprasad Cheekoori. Finally, I wish to thank all who contributed in the completion of my Master Thesis.

Dedication

This thesis is dedicated to my family and friends for their love and support throughout my academic career.

Chapter 1

Introduction

1.1 Overview

In recent years, there has been an increasing interest in miniaturizing sample volumes for laboratory analyses. The main advantages of volume reduction include smaller reaction time as a result of increased surface to volume ratio, higher sensitivity, as well as reduced reagent consumption and waste production [4]. Traditionally, experimental analyses are executed in specialized laboratory equipment that is operated by highly trained personnel. Such laboratory equipment is typically complex, immense, expensive, and high maintenance. Digital microfluidic (DMF) systems thrive in the field of biotechnology with broad applications in cell analyses [5], protein analyses [6], DNA analyses [7], and drug discovery [8]. The motivation behind building DMF devices is their re-programmability, portability, disposability and low power consumption [9].

A DMF system operates on micro-scale droplets over a planar surface. Complete experimental analyses are carried out in DMF devices through basic droplet operations including droplet dispensing, transport, splitting, mixing and merging [10]. A number of actuation techniques have been proposed including the use of chemical gradients [11], electromechanics [12–14],

magnetic field [15], photoradiation [16], surface acoustic waves [17], and thermal gradients [18].Among all droplet actuation mechanisms, electromechanics is the preferred liquid handling technique due to efficient actuation and simple device fabrication [19].

1.2 Device Configuration

Digital microfluidic devices feature a planar plate technology and may appear in two structural configurations: open and closed structures. In an open configuration (Fig. 1.1a), the droplets are positioned over a single bottom plate that houses an array of electrodes. Early open DMF devices were designed with a catena wire (or ground wire) running above the bottom plate electrodes, however the fabrication complexity in suspending a catena wire over the dielectric surface led to the development surface ground wires on the dielectric surface or even completely eliminating the need for ground wires [4]. A closed configuration (Fig. 1.1b) consists of two parallel plates typically separated by a few tens of microns where droplets are placed and manipulated. The lower plate typically houses an array of electrodes, and the upper plate has a single electrode. In either device configuration, the array of electrodes is insulated by a thin ($\sim 1-10\mu m$) dielectric layer to maximize the electric field intensity necessary for actuation, minimize ohmic heating, and prevent electrolysis effects which can result in electrode degradation [20]. In addition, the exposed dielectric layer surface is often coated with another thin ($\sim 50nm$) hydrophobic layer e.g., TEFLON© which minimizes resistance forces that impede the motion of droplets [21].

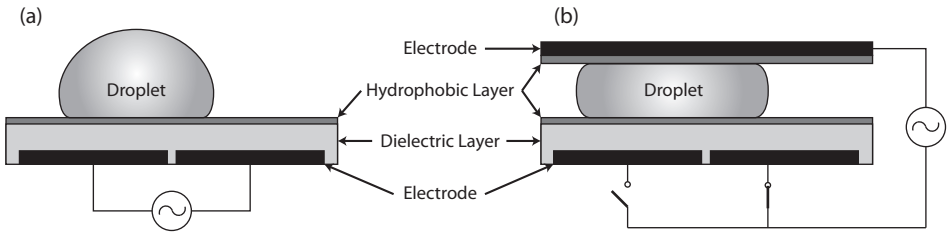

Figure 1.1: Illustration of two device configurations for DMF devices. (a) Open DMF device configuration. (b) Closed DMF device configuration.

Each device configuration has different benefits attributed to the difference in the structure of the device. This research focuses mainly on the closed configuration that suits a wider range of applications because it is capable of performing more droplet operations including dispensing, moving, merging, and splitting. While an open device configuration has difficulties with droplet splitting, it has the ability to displace larger droplet volumes and achieve faster droplet transport speeds because the resistance forces from upper plate are eliminated. Also, an open device configuration has faster droplet mixing and evaporation rates which are both desirable in certain applications including varying the reagent concentration [4, 22]. Finally, an open device configuration enables direct access to samples and reagents on the device surface, therefore facilitating the integration of external sensory instrumentation [23].

1.3 Motivation and Research Purpose

Digital microfluidic devices rely on the ability to manipulate liquid droplet to perform fundamental droplet operations including transporting, splitting,

mixing, and merging of sample and reagent droplets; all essential droplet operations for initiating any chemical reaction. Thus, the findings of this thesis will be applicable to all droplet operations although a large part of the analyses, results, and discussions concentrate on droplet motion as a result of actuation. A unit of droplet displacement (the travel distance between the centers of two adjacent electrodes) requires a single electrical signal with sufficient voltage magnitude and time duration applied to an individual electrode. Larger droplet displacements can be achieved by sequentially energizing consecutive electrodes. The maximum droplet transfer rate, or switching frequency, at which successive electrodes are energized is determined experimentally [20]. In this way, the DMF device features a so called open loop control system that assumes the droplet has completely transferred over an energized electrode within a calibrated actuation time before energizing the next electrode. The open loop control approach relies on pre-calibrated operational conditions due to the lack of feedback information which is necessary to correct for uncertainties projected onto the system operation in the actual working conditions. More precisely, the open loop controller will continue energizing successive electrodes even if the droplet falls behind and fails to interact with the next energized electrode. Although open loop control systems can be implemented easily and at a low cost, the absence of feedback information of this controller cannot compensate for external disturbances that can change the dynamics of the system during the device operation. In addition, in real DMF devices, surface imperfections, e.g., caused by material impurities and foreign particles, impede the motion of a droplet which in certain conditions can completely halt the transport phenomenon. Such

device inherent or externally induced uncertainties significantly compromise the performance and applicability of open loop controllers in DMF devices. On the other hand, a closed loop (feedback) controller uses feedback information to correct for any systematic or random disturbances applied to the system at the cost of an accurate means for measuring the actual output of the system. Specifically in feedback-controlled DMF devices, the controller has a mechanism that senses when a droplet has properly transferred over an energized electrode before proceeding to energize the next electrode.

Shin *et al.* [24] implemented a feedback controller based on visual relay information. The feedback controller locates a droplet over an electrode by detecting a circular object within a designated boundary over an electrode. Once the droplet is detected, an electrical signal is applied to the adjacent electrode to move the droplet further. The process repeats until the droplet reaches a desired location on the DMF device. Visual feedback can be used to detect any type of droplet composition; however, it requires high precision imaging equipment and computational power to analyze images in real time.

Shih *et al.* [25] also used a feedback controller system equipped with an electronic sensor for AC actuation electrical signals. The sensor is a network of passive electrical components in series with the upper ground electrode in a DMF device. The sensor draws power from an AC driving signal to produce a voltage feedback signal whose magnitude increases with the presence of a droplet over the energized electrode. The feedback controller compares the voltage feedback signal against an empirical threshold voltage to determine whether the droplet has successfully transferred over the energized electrode before energizing the next electrode. The threshold voltage

must be calibrated because it depends on the droplet electrical properties and the frequency of the AC driving signal. Thus, this sensing approach has practical use for single-type droplet transport but will be limited for the feedback control systems of DMF devices operating on various samples, e.g., in a throughput experiment, because the sensor impedance must be adjusted and the threshold voltage calibrated for each droplet type separately. Moreover, the applications of a droplet dependent sensing mechanism will be further limited in a lab-on-a-chip (LOC) device housing micro-reactor droplets whose electrical properties change after chemical reactions.

Besides the aforementioned limitations, the existing DMF feedback control systems implement a True/False detection sensing mechanism that reports whether a droplet covers an electrode or not. Despite the simplicity of such detection methods, they require calibration and fail to capture essential droplet dynamic information particularly where the droplets have partial overlap on electrodes. In other words, they can neither position droplets within the interval of two electrodes nor accurately control the velocity and acceleration of droplets. The goal of this thesis is to develop a feedback controller for DMF devices that can operate with any type of droplet composition and can monitor the continuous displacement of a droplet to include the interval between adjacent electrodes. As a result, this research will enable one to not only to control the transport of a droplet but can also be applicable to more complex droplet operations such as splitting in DMF devices with an unprecedented degree of accuracy and repeatability.

1.4 Objectives

The following three objectives led to realizing a fully-customizable controller prototype for DMF devices and ultimately LOC systems:

i) Develop a calibration-free droplet position sensing technique,

ii) Design a closed loop (feedback) controller, and

iii) Build a low-cost, programmable, rapid prototyping platform for the development, testing and tuning of DMF controllers.

1.4.1 Calibration-Free Sensing Technique

Digital microfluidic devices have the ability to accommodate a large variety of chemical species within liquid droplets and can execute a wide range of laboratory analyses on a single device. To benefit from such throughput versatility, the control system requires a droplet sensing technique which can readily operate many types of species simultaneously. The first objective of this thesis is to develop a calibration-free fully electronic and non-intrusive sensing technique for locating the position of any liquid droplet on a DMF device.

1.4.2 Closed Loop Controller

Droplet transport on a DMF device is a key droplet operation for many laboratory analyses, and has been demonstrated in a carefully controlled laboratory environment i.e., tightly regulated actuation voltage, vibration free, constant temperatures, controlled evaporation rates and so forth. However,

any deviation from such controlled conditions can compromise the realization of droplet transport phenomenon or any other droplet operation at large. To alleviate this problem, a closed loop (feedback) controller with position feedback is necessary to provide precise droplet motion by compensating for variations in operating environments. The second objective of this thesis is to analyze, design, and simulate a closed loop controller for DMF devices.

1.4.3 Prototyping Platform

Fabrication and droplet manipulation of DMF devices have so far required very specialized and expensive facilities, which may limit research to only a few well-funded institutions. The motivation for developing a low-cost, fully-customizable controller rapid prototyping platform is twofold: i) to promote DMF research in small-scale institutions, and ii) shorten the period of time for prototyping a laboratory concept into a fully functional commercial product. The third and final objective of this thesis is to build a low-cost programmable rapid prototyping platform for DMF control systems.

1.5 Contributions

To date, much of the research in the field of digital microfluidics has focused on the incorporation of DMF technology into a wide range of chemical and biochemical applications that benefit from micro-scale analysis. Equally important research has concentrated on modeling and understanding the

complex dynamics of droplet actuation. Such droplet system models can predict the performance of DMF devices; a useful tool in the design process of DMF devices. Little research has been done in the field of controlling the non-linear motion of droplet during actuation. Control systems are an important part of complex dynamic systems (or plants) because they continuously monitor the performance of the system to ensure that the transient and steady-state responses are both desirable. In doing so, they constantly calculate the control signals necessary to drive the states of the system (for example position, velocity, acceleration) through an appropriate trajectory that is favorable to the system and also leads to the desired system response. In digital microfluidics, a control system simplifies the process of droplet actuation by converting a simple position command into a series of electrical signals which transports a droplet to the desired position. The work in this thesis focuses on developing a control system for digital microfluidics with strong emphasis on a low-cost and fully customizable platform. The proposed controller platform was built with off-the-shelf components to reduce its cost to a fraction of the cost for systems reported in previous literature. In addition, the controller was designed as module to facilitate the integration of expansion modules e.g. sensors into a single control system to achieve a portable, low power, true Lab-On-a-Chip (LOC) device.

A significant contribution of this thesis was the introduction of a unique, calibration-free droplet position sensing technique. The sensing technique couples a mathematical expression (or estimator) which maps the capacitances of two electrodes covered by a droplet onto the position of the droplet. This sensing technique is non-intrusive and relies on the changes in electrode

capacitance values as a droplet moves across a series of electrodes. The change in capacitance is the direct result of a change in dielectric medium caused by the foreign presence of a droplet between the probed electrodes. The capacitance values of two electrodes are related to a droplet position through a dimensionless ratio of capacitance values. The dimensionless nature of the estimator can be applied to locate the position of any liquid droplet composition. With this sensing technique, the position of droplets can be estimated accurately, even in the interval between adjacent electrodes, a region of interest for precise droplet control. As a result, a feedback sensor employing this technique can report the continuous droplet displacement to a control system. This feedback information is critical to control the intra-electrode position, velocity, and acceleration of droplets in DMF devices.

A second important contribution was the performance optimization of the droplet position sensing technique through DMF physical parameters. A full factorial design was conducted on the droplet position sensing technique to observe the behavior of the position error as a function of the parameters of a DMF device. An empirical model was fitted to the data obtained from the designed simulations and optimized to reduce the position estimate error. Simulation results suggest that the performance of the capacitance based droplet sensing technique studied in this work is dependent on the dielectric thickness, droplet radius, electrode pitch, electrode separation, filler fluid permittivity, and plate gap. Furthermore, iso-performance curves of the performance for this droplet sensing technique were obtained using the empirical model to show the interaction between DMF parameters and aid

in the design of the devices equipped with a this droplet sensing technique.

Another significant contribution has been the development of a technique for estimating the initial value of controller gains by analytical expressions. In this approach, the dynamic system of droplet actuation is modeled after semi-empirical models that are non-linear. Feedback linearization technique is used to linearize the droplet actuation model and apply classical control theory analysis for estimating controller gain values. It is shown that the controller gain values can be estimated from the specification parameters of a 2nd order system including settling time, damping coefficient, and bandwidth. Finally, a position feedback controller model was simulated to analyze its performance in regulating the position, velocity, and acceleration of a droplet in the interval of two adjacent DMF electrodes.

The fourth significant contribution has been the development of a low-cost, fully programmable controller prototyping platform for DMF devices. The prototyping platform was built f off-the-shelf and generic electrical components to reduce cost. The development platform was designed as a modular system to accommodate future add-ins. The development platform consists of a programmable microcontroller and a solid-state switch network that together can execute the most basic droplet operation of droplet transport. More intricate droplet operations such as mixing and splitting droplets are an extension of droplet transport and can easily be programmed into the microcontroller. Two custom-built solid-state switch networks were designed for either DC or AC voltage driving signals of choice. In addition, a position feedback controller is prototyped for DMF devices. The feedback controller utilizes the capacitance-based droplet position sensing previously

presented for locating the position of a droplet. The feedback sensor acts as an external module that interfaces with the microcontroller to relay the position of the droplet.

Another contribution of this thesis was the investigation and full implementation of DC pulse train droplet actuation as an alternative to pure DC and AC actuation signals. The microcontroller can be programmed to actuate a droplet successively across four square electrodes with a train of DC pulses. The pulse duty cycle was varied to observe its effect on the voltage required to complete droplet acutation across four successive electrodes. Strong experimental evidence reveals that higher actuation voltage is required when reducing the duty cycle for successive actuation. On the other hand, smaller actuation voltages are required when increasing the duty cycle. This suggests that droplet inertia assists successive actuation because higher voltages result in the droplet overshoot onto the adjacent electrode; thereby increasing the actuation force due to an increased footprint of the droplet on the next activated electrode. In addition, DC pulse train actuation is a feasible method for incremental droplet displacement and regulating the velocity of droplets by varying the duty cycle of the pulses for a fixed actuation voltage. The benefits of DC pulse train actuation over pure DC actuation include: better control over the displacement of the droplet and reduced droplet footprint deformation.

As a final contribution, optimal fabrication process of DMF devices was achieved without a need for sophisticated facilities and a cleanroom environment. For example, the need for costly deposition of specialized dielectric material such as Parylene C was eliminated through spin coating of a

photoresist layer as an alternative dielectric material while achieving the excellent coating uniformity. This reduces the number of materials needed to fabricate a DMF device, therefore minimizing material costs, simplifying the fabrication process, and reducing device fabrication time significantly.

1.6 Thesis Organization

Chapter 2 introduces the concept of control systems and their application in digital microfluidics. It describes the two types of control systems namely open loop control and closed loop (feedback) control, respectively. Chapter 2 also elaborates the need for position feedback controller in digital microfluidics and describes the presents the proposed calibration-free droplet position sensing technique that is based on multiple electrode capacitance values.

In Chapter 3, a position feedback control system for DMF devices is designed and simulated to control the position, velocity and acceleration of a droplet with DC pulses. The droplet dynamics are modeled after semi-empirical models reported in literature and verified with experimental data. In addition, classical control theory analysis techniques are applied to estimate the controller gain values by analytical expression. Finally, simulation results demonstrate the feasibility of controlling a droplet in the interval of two DMF electrodes with a position feedback controller.

Chapter 4 presents the hardware and software necessary for cost-effective realization of closed loop (feedback) controlled DMF devices with capacitance-based droplet position sensing. The chapter is organized to illustrate a

complete design process from simulation to experimental testing and finally prototyping a portable, low cost, and fully customizable feedback controller. Further, a detailed fabrication recipe is presented to build DMF devices with small feature sizes down to $10\mu m$ without cleanroom facilities. In addition, DC pulse train actuation was investigated as a feasible actuation method for incremental droplet actuation or controlling the droplet transport speed at a fixed actuation voltage by varying the pulse duty cycle.

Finally, the most significant conclusions of this research and future directions are summarized in Chapter 5.

Chapter 2

DMF Control Systems

2.1 Overview

A control system manipulates the input to a system to achieve a desired output. Fig. 2.1 depicts the concept of a typically control system where the input signal is defined as the desired output of the system. A control system is a collection of subsystems that transform an input signal into an appropriate driving signal to control the transient and steady-state responses of a dynamic system (i.e., plant or process). The purpose of any control system is to improve system stability, realize a desirable transient response, and minimize steady-state error [26].

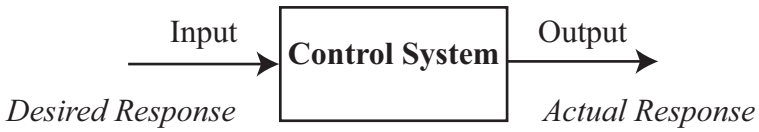

Figure 2.1: Diagram of a universal control system.

Digital microfluidic devices hinge on the ability to manipulate droplets in a specified pattern for performing repetitive and sometimes tedious laboratory protocols involved, for example, in high throughput screening processes. The performance of the DMF devices, similar to any other systems,

can be compromised by both inherent system deficiencies (e.g., design-stage errors, material impurities, or fabrication errors), and runtime or external disturbances (e.g., noise corruption, time-variant system properties, particle adsorption, droplet evaporation, foreign particle contamination, or device failure). A control system is designed to reduce the impact of such undesired factors and minimize the discrepancy between the desired and actual output system response. For the purpose of droplet transport that is the main focus of this research, another benefit of the inclusion of control system in the DMF device is that the control system can remarkably increase the precision of droplet positioning, and hence the control system can regulate the position, velocity, and acceleration for high precision application like micro-conveyors [27].

From the end users' viewpoint, the manipulation of droplets can be substantially facilitated using a control system that can replace a sequential combination of electrical signals into a simple command such as "Move Left" or "Split." As a result, a complete laboratory process can be readily programmed by an untrained user using a handful of high-level commands while the complicated nonlinear droplet motion control schemes - an essential step towards fully automated DMF systems - have been preprogrammed on the device hardware.

The control system can be either open loop that relies on a model of the microfluidic system to predict the output, or closed loop (feedback) which employs a sensing mechanism to measure the actual output of the system, compare it against the desired output response, and generate a corrective control signal. Typically, closed loop control is more robust than

open loop control at the cost of an additional sensing system. However, open loop control can still be useful for simple and repetitive procedures. The following sections describe each control system configuration and its pertinent application in DMF devices.

2.2 Open Loop Control of DMF Systems

Open loop control systems consist of a chain of subsystems and processes with no feedback loops. Fig. 2.2 depicts the functional block diagram of an open loop control system where the input signal propagates down the chain of subsystems. As the input signal transverses through the subsystems, it may be corrupted by noise from external disturbances which significantly affect the performance of the system. As a result, the input signal or desired output may not match the actual output response. For proper system operation, the disturbances must be accounted in the input signal. Tuning the input signal can mitigate the disturbances and is achieved through calibration under control conditions. However, any change to the original conditions significantly affects the performance and output of system.

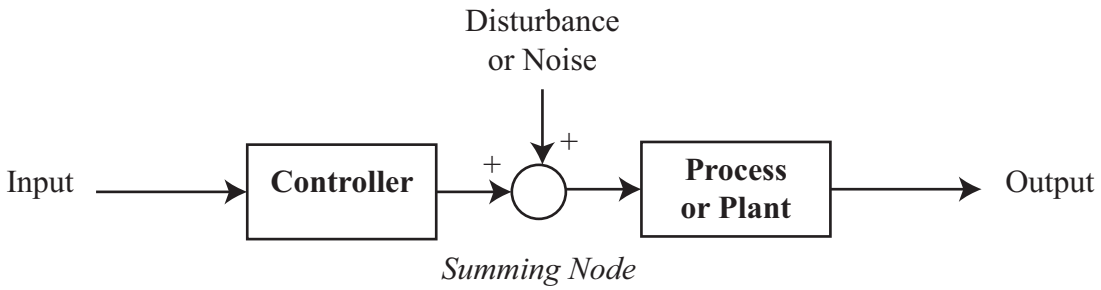

Figure 2.2: Functional block diagram of open loop control systems.

In the case of digital microfluidics, the process subsystem describes the hydrodynamics of a droplet as a function of the electromechanical force. The input to the process subsystem is the electromechanical force whose direction and magnitude depends on the voltage applied to an electrode in the vicinity of the droplet. The output of the process subsystem is the resulting droplet position as a result of the actuation force.

Open loop control systems have been implemented in digital microfluidics to perform a series of droplet operations. Fair *et al.* [20] demonstrated continuous droplet transport across a linear array of electrodes. Fig. 2.3 illustrates the technique to achieve continuous droplet transport on a DMF device. A single DC pulse is applied to an electrode until the droplet completely moves over the energized electrode before sending a pulse to the next electrode. The duration of the pulse is the time required for a droplet to completely move to the adjacent electrode for a given voltage magnitude. The switching frequency is the rate at which successive electrodes are energized and is inversely proportional to the width of the pulse. Clearly, the higher the switching frequency the faster the rate of droplet transfer. It is noted that higher voltage magnitudes yield higher switching frequencies because the electromechanical force is greater.

In addition, different droplet compositions have different switching frequencies [28]. As noted earlier, open loop control systems work well when the operating conditions are fixed. However, an issue arises when multiple droplets with different liquid composition are present in a single DMF device as each droplet has a unique switching frequency found only through calibration. The issue is compounded when two types of droplets merge and

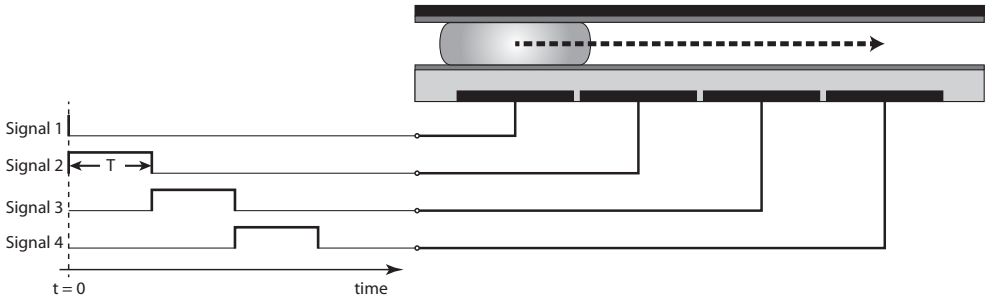

Figure 2.3: Single DC pulse continuous droplet actuation for DMF devices.

their contents are mixed, or react and create another new composition with yet a different switching frequency.

Besides the liquid droplet composition issue, DMF devices are usually filled with a filler liquid medium to reduce the threshold voltage and facilitate transport [20]. The filler liquid surrounding the sample droplets has an effect on the switching frequency that is a function of resistive forces. Specifically, oil filled mediums have lower switching frequency than air filled mediums [20].

Another common problem of DMF devices are surface imperfections due to the presence of foreign particles on the surface. Such superficial contamination can pin the droplet, impede the motion of the droplet, and ultimately halt the transport of droplet to the adjacent electrode. This considerably affects the performance of the open loop controller because the electrical signals will continue to energize the next electrodes one at a time whereas the droplet does not follow the energized electrode.

An open loop control system must track each type of droplet to apply the minimal actuation time necessary for continuous droplet actuation, as

prolonged DC actuation time may result in undesirable side effects including electrochemical reactions, electrolysis, joule heating, and dielectric degradation. On the other hand, shorter DC actuation times may fail to completely displace the droplets across the electrodes continuously. As a result, the applicability of open loop control systems in practical DMF devices is debatable. A better approach to cope with different switching frequencies is to apply the necessary actuation time by monitoring the displacement of a droplet to adjacent electrodes. Although generic open loop control systems are readily integrated, cost effective and available off-the-shelf, their inability to compensate for disturbances has limited their use in DMF devices. Closed loop (feedback) control systems are more complex than open loop control systems mainly because of the sensing mechanism that is specific to the application in hand, but they are capable of correcting the disturbances elaborated above.

2.3 Closed Loop (Feedback) Control of DMF Systems

In closed loop (or feedback) control systems, the output of the system is looped back to the input. Fig. 2.4 illustrates a negative feedback control system where the system output is compared to the input to generate an error signal for the controller. In this way, the negative feedback improves the system stability by automatically correcting for external disturbances. In other words, a feedback control system minimizes the difference between the desired system response and the actual system response. This difference

is essentially an error signal that the controller attempts to bring and maintain near zero. Feedback control systems are self-correcting systems which makes them insensitive to disturbances. However, generally close-loop control systems are more complex than open loop control systems because of the additional feedback sensor that is responsible for looping back the system output. The feedback sensor could be any type of signal that provides valuable information that assists the controller in matching the system output with the desired output (i.e., typically the input of a feedback control system). The performance of any closed loop control system is ultimately limited by the availability and quality of the information in the feedback signal. In other words, a feedback control system can compensate for any disturbances in the system, but it cannot account for the uncertainties associated with the information in the feedback signal. High accuracy and reliable information in the feedback signal will improve the controller performance in achieving a desirable system output.

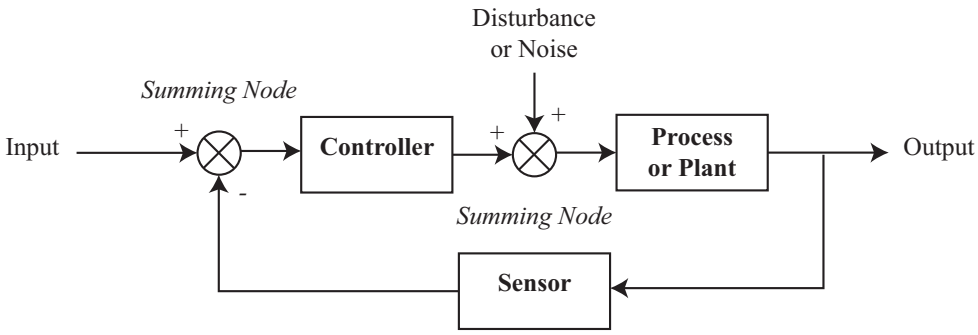

Figure 2.4: Functional block diagram of closed loop control systems.

The success of DMF devices hinges on the ability to execute complete droplet transport considered as the most basic droplet operation. As previ-

ously described, the droplet transport operation requires a single electrical signal applied to an electrode in the vicinity of a droplet. For continuous droplet actuation, sequential electrodes are energized while allowing enough time for the droplet to completely transfer over an electrode before energizing the next electrode. The time for complete droplet transfer over an electrode varies between different droplet compositions and is severely affected by any imperfections on the surface of the DMF device. To compensate for all these disturbances which have a considerable effect on the droplet transfer time, the feedback control system must sense the droplet position.

Shih *et al.* [25] implemented a feedback control system for unit droplet displacement with AC driving voltage. The feedback sensor consists of passive electrical components including capacitors and resistors connected in series with the top ground electrode of the DMF device shown in Fig. 2.5. The sensor draws power from the AC driving signal to produce a voltage signal that is used as a feedback signal. To avoid disrupting the actuation force, the sensor impedance must be tuned such that the majority of the voltage drop from the driving signal occurs across the dielectric layer when a droplet fully overlaps the driving electrode. This sensor tuning is required for each device and for droplets with different electrical properties as the droplet is part of the sensing mechanism. The feedback signal, V_{feed}, is sensitive to changes in frequency and magnitude of the driving signal, electrode size, dielectric thickness, and droplet electrical properties.

Fig. 2.6 illustrates the flowchart of the feedback control system operation. The control system applies voltage to an electrode adjacent to a droplet and at the same time measures the feedback voltage. The controller

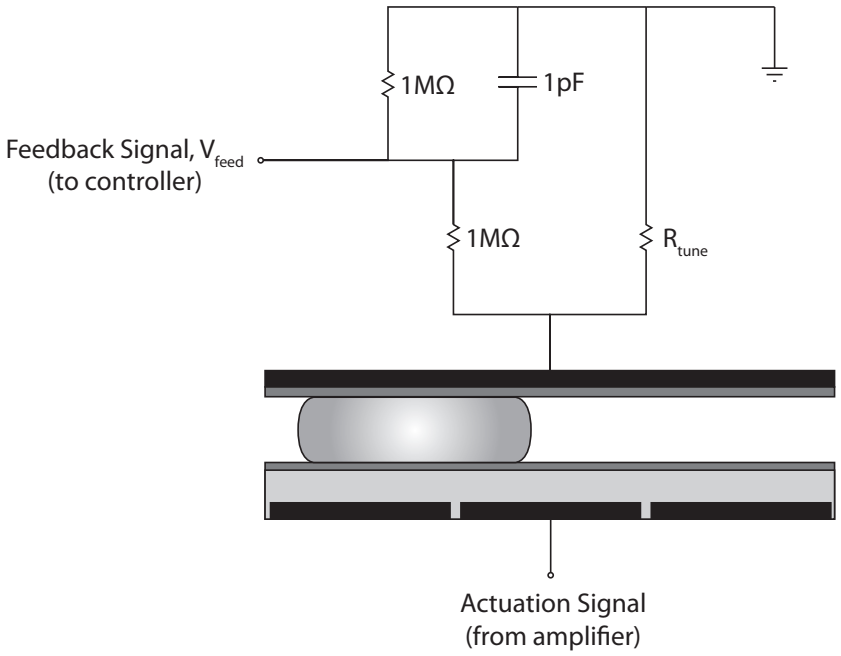

Figure 2.5: Feedback sensor integration proposed by Shih *et al.* [25].

compares the feedback voltage, V_{feed}, with a calibrated threshold voltage, $V_{Threshold}$, to determine whether the droplet transport operation is completed. The threshold voltage is calibrated to equal the feedback voltage when a droplet is completely centered over an electrode. Voltage is applied to an electrode as long as the feedback voltage is less than the calibrated threshold voltage. Once the feedback voltage is equal to or greater than the calibration voltage, a voltage is applied to the next electrode and the process continuous.

This feedback control system is practical, but it has some limitations. First, the feedback controller can only actuate one droplet at a time because driving multiple droplets at once would confuse the control system since the

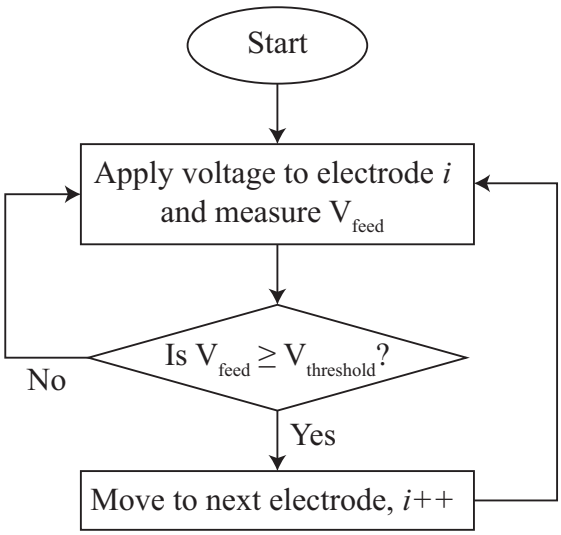

Figure 2.6: Feedback control system finite state machine (FSM).

sensor is attached in series with the driving signal. In addition, driving multiple electrodes will reduce the dielectric impedance, thus reducing the voltage drop across the dielectric layer and affecting the feedback voltage magnitude. Second, the threshold voltage for each electrode is sensitive to variations in electrode sizes and dielectric thickness introduced during the microfabrication process. Finally, the droplet sensing approach is binary, as it is based on a threshold condition over discrete electrodes. Thus, droplets can only be centered over the electrodes with this approach whereas in certain droplet operations such as splitting and mixing in-between electrode positioning is important as well.

Shin *et al.* [24] proposed a visual feedback control system for controlling the position of droplets on a DMF device. The control system follows a three stage process toward controlling the motion of droplets: (1) image acquisition, (2) droplet detection, and (3) actuation. During image acquisition, top

view images of the DMF device are captured with a microscope camera and relayed to a processing unit. During droplet detection, image analysis algorithms such as circular edge detection are used to detect the droplet within a circular area over an electrode. In the last stage, the processing unit applies voltage to the appropriate electrode to actuate the droplet in the desired direction. This process repeats until the droplet reaches its final destination. Unlike the previously described feedback control system, this control system can be applied to any type of liquid droplet as the droplet control operation depends on detecting a circular object from a digital image. However, this approach requires high precision image acquisition instruments with enough resolution to discern a circular object on a DMF device. Another complication is the lighting condition which must be calibrated to optimize the visibility of the meniscus in clear liquid droplets. Furthermore, special materials are needed to fabricate a conductive transparent upper plate (e.g., Indium Tin Oxide (ITO) coated glass) in the DMF device to allow light to pass through the upper plate for clear image of the droplet. The circular edge detection algorithm requires calibration through experimental trials to optimize the detection of droplets within circular areas or boundaries over each electrode in a DMF device. This calibration is essential to reduce false triggering of adjacent electrodes. Furthermore, droplet pinning effects can distort the shape of the droplet to deviate from a circular outline and can confuse the circular edge detection algorithm. Visual feedback control systems require high computational power to analyze real-time images. The high demand for computational power necessary for image analysis limits the speed of visual feedback control systems. Finally, like the previously

described feedback control system, droplets can only be sensed within the vicinity of an electrode. This method is suitable for discrete droplet displacement between electrodes and would not be able to position droplets anywhere within two electrodes.

A droplet sensing mechanism capable of locating droplets in between two electrodes is important in DMF devices, as the position, velocity, and acceleration of droplets can be controlled to enhance the droplet controllability without the need for more and finer electrodes that can further complicate the DMF fabrication process. The following section describes other sensing techniques available in literature with application in feedback controlled DMF devices, and presents the proposed calibration-free continuous droplet sensing technique and optimization.

2.4 Position Feedback

Digital microfluidic devices can contain a large grid array of electrodes to manipulate droplets. To manipulate a droplet in this array of electrodes, one needs to know the position of the droplet. Position feedback is therefore necessary and sufficient to determine which DMF electrode to energize. Apart from visual and voltage droplet sensing techniques described before, other techniques involve evanescent wave, conductance sampling, and capacitance have been proposed in literature.

Valentino *et al.* [29] embedded a waveguide on the dielectric layer for droplet detection. The waveguide is positioned orthogonal to the direction of droplet motion. When a droplet crosses over the waveguide, the presence

of the droplet over the waveguide introduces variations in the refractive index along the direction of the waveguide that cause reflection losses. As a result, a photo-receiver senses a lower light intensity when a droplet crosses over the waveguide. This sensing technique gives localized droplet detection with limited applicability in large scale DMF devices. In addition, waveguide structures, light sources, and photo-receivers must be integrated for every localized droplet sensing area.

Nichols *et al.* [30] described a droplet position sensing algorithm based on conductance sampling. In their approach, every electrode is probed to measure the conductance between the upper and bottom electrodes to form a spatial distribution of conductance measurements. The spatial distribution of conductance measurements is similar to a topographical map with peaks and plateaus. The peaks are high conductance measurements which are caused by the presence of a conductive droplet between the upper and lower electrodes whereas the plateau indicates that no droplet is present under the assumption that the filler medium between the top and bottom electrodes elsewhere is nonconductive. A limitation of this approach is that it requires high electrode density to accurately determine the position or size of a droplet. This is not practical in typical DMF device where the goal is to minimize the droplet volume such that its footprint is roughly equal to the size of a single electrode. Furthermore, conductance sampling is intrusive and hence is not feasible for EWOD devices where direct current has undesirable effects including electrolysis and joule heating.

Chen *et al.* [31] developed a coplanar capacitance sensor that can detect the position of droplets. In this approach, the bottom plate electrodes serve

two purposes: (1) droplet sensing and (2) actuation. A droplet is sensed by detecting a difference in capacitance between two adjacent electrodes on the bottom plate because capacitance is sensitive to the medium between the probed electrodes. The rough droplet position estimate can be deduced from this approach as it requires high electrode density for accurate measurement. As mentioned earlier, increasing the electrode density far smaller than the size of a droplet introduces addressability complications and impacts the efficient use of electrodes. Furthermore, coplanar capacitance sensor relies on fringe capacitance to detect the presence of a droplet. The effect of fringe capacitance quickly diminishes further away from the electrodes. Thus, the dielectric layer thickness must be constraint to be able to detect a droplet over the dielectric layer.

So far, these three droplet sensing techniques implement a binary detection sensor with two output states (On or Off) to infer whether a droplet is present over an electrode or not. An "On" state indicates a droplet is present between spatial probes and is triggered when the probe measurement value is higher than a threshold value. The "Off" state indicates that no droplet is present between the probes and has a probe measurement value less than a threshold condition. In order to pinpoint the location of the droplet, the electrode size must be divided into many small electrodes such that the boundaries of a droplet can be detected to make a relatively accurate estimate about the center position of the droplet. Among the many droplet sensing techniques, capacitance measurement is closest to ideal since it is low power, non-intrusive, portable and has a short response time.

2.4.1 Capacitance-Based Droplet Position Sensing

Capacitance is a measure of electrical charge stored in a capacitor. A capacitor consists of two conducting bodies separated by an insulating medium. When a potential (or voltage) difference is applied between the conducting bodies, electrical charges of equal and opposite magnitude accumulate on the surface of the conducting bodies. These free charges create an electrical field between the positively charged conductor and negatively charged conductor. The energy stored in a capacitor is in the form of the electric field between the conductor bodies. Capacitance is defined as the ratio of electrical charge to potential difference as

$$C = \frac{Q}{V}, \tag{2.1}$$

where C is the capacitance in Farads, Q is the electrical charge in Coulombs, and V is the potential difference between the conductors in volts. The capacitance value only depends on the capacitor geometry and the permittivity of the insulating medium. Capacitance has a wide range of applications in sensing where changes in capacitance are translated to changes in a parameter of interest. For example, capacitance has been used in DMF devices to monitor chemical reactions and identify fluid composition. [32, 33] However in this thesis, capacitance is used to locate the position of any droplet in DMF devices.

A goal of this thesis is to develop a droplet position sensor that requires no calibration and can be used to continuously track the displacement of droplet even in the interval of two adjacent electrodes. The proposed sens-

ing technique uses capacitance of multiple electrodes, an inherent electrical property of EWOD DMF devices, to determine the position of any droplet composition in the interval of two electrodes. As mentioned earlier, capacitance is an electrical property that is sensitive to the presence of a droplet. The estimator uses a dimensionless ratio of electrode capacitances to approximate the droplet position in the interval of two electrodes. The following section derives the formulation of the proposed calibration-free droplet position estimator. The sensor performance is evaluated in 2D and then 3D analytical and numerical simulations of a DMF device. Finally, simulation observations are verified through experimental measurements.

Theoretical Modeling

Fig. 2.7 shows the equivalent electrical circuit of a single control electrode in a DMF system with a generic liquid presented to describe our proposed sensing mechanism. [34–37]

The electrical circuit consists of two parallel circuit networks corresponding to the liquid and ambient region far from the fluid layer interface. The dielectric and hydrophobic layers are modeled as capacitors [34–37]. The ambient medium or filler liquid, such as air, has no free charges and thus is modeled by a capacitor. The model is generalized to include a liquid droplet with an arbitrary conductivity. Hence, the electrical model for the liquid droplet is a parallel capacitor and resistor circuit.

The meniscus at the liquid-liquid or liquid-vapor interface slightly distorts the electrical field between the electrodes. However, its effect is negligible for typical DMF systems where the control electrode width to plate

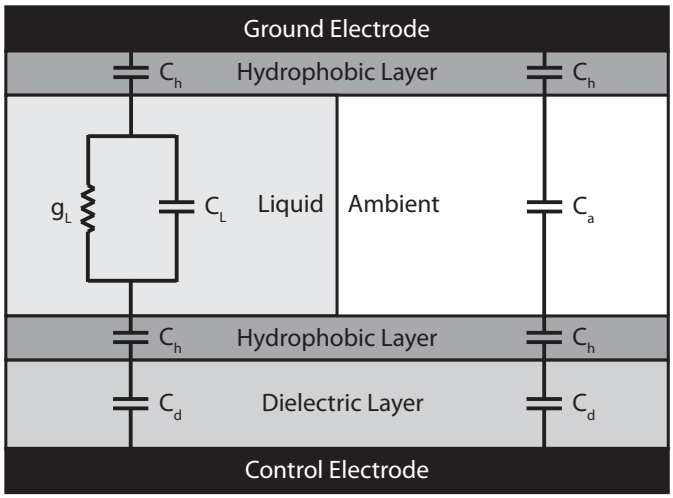

Figure 2.7: Electrical circuit model for a DMF device with a generic liquid and a non-conductive ambient fluid.

gap ratio is large [35–37].

The electrical reactance of a single control electrode is purely capacitive with a capacitance given as

$$C_{eq} = aA + (b - a)A_L, \tag{2.2}$$

where a is a small constant whose magnitude is inversely proportional to the plate gap because the ambient capacitance is the smallest series capacitance, b is a large constant that is inversely proportional to the dielectric layer thickness because the dielectric capacitance is the second smallest series capacitance since (i.e., the liquid droplet is slightly conductive), A is the area of a square electrode, and A_L is the liquid footprint area over the square electrode.

In DMF systems, droplets are translated in a linear direction towards

the adjacent electrode. Consequently, the control electrode capacitance is a function of droplet position because the droplet footprint area directly depends on the droplet position. As a result, the center of the footprint area of a droplet and hence its position can be estimated from the capacitance values of two adjacent electrodes.

Fig. 2.8 illustrates a droplet with a fixed volume partially overlapping two adjacent control electrodes in a DMF system. A droplet with a circular footprint with a radius of r is centered at a distance of x_0 from the center of electrode 1. Electrodes 1 and 2 are squares with a width of L, and a separation gap of L_e.

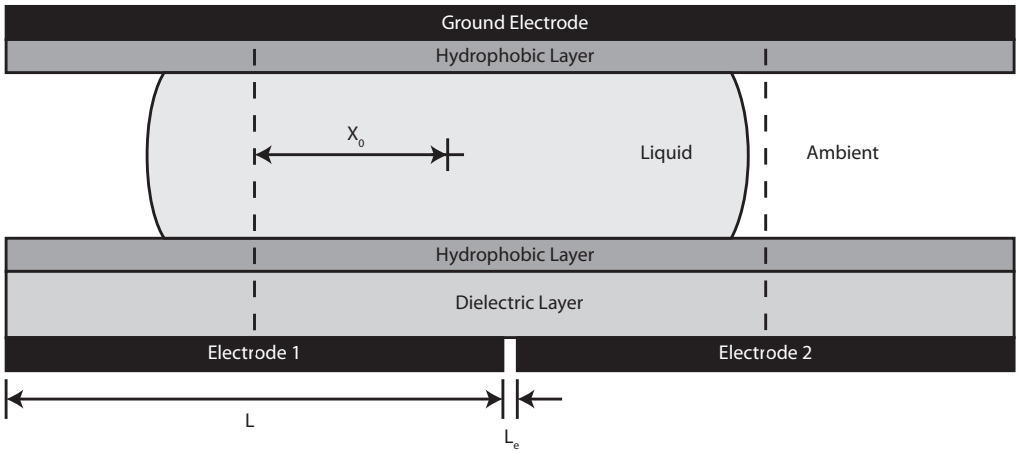

Figure 2.8: Meridian plane of a liquid droplet positioned between two bottom plate electrodes of a DMF device.

At the meridian plane of the droplet, the capacitance per unit length of electrode 1 is given as

$$C_1 = aL + (b - a)\left(r + \frac{L}{2} - x_0\right). \tag{2.3}$$

Similarly, the capacitance of electrode 2 is given as

$$C_2 = aL + (b-a)\left(r - \left(\frac{L}{2} + L_e\right) + x_0\right). \tag{2.4}$$

Normalizing the capacitance of electrode 2 yields a dimensionless ratio that is a function of droplet center position as

$$\frac{C_2}{C_1 + C_2} = \frac{aL + (b-a)\left(r - \left(\frac{L}{2} + L_e\right) + x_0\right)}{2aL + (b-a)(2r - L_e)}. \tag{2.5}$$

Coefficient b is much larger than coefficient a because the dielectric thickness is much smaller than the plate gap. Therefore,

$$\frac{C_2}{C_1 + C_2} \cong \frac{r - \left(\frac{L}{2} + L_e\right) + x_0}{2r - L_e}. \tag{2.6}$$

Typically in order to successfully actuate a droplet in a DMF device, the droplet footprint area must be slightly larger than a single electrode to overlap the adjacent activated electrode. [13, 20] On the other hand, a droplet cannot be much larger than an electrode since there will be a risk of unwanted droplet splitting instead of transportation. Thus, $r \cong \frac{L}{2} + L_e$ is a valid assumption so that Eq. 2.6 can be further simplified as

$$x_0 \cong \frac{C_2}{C_1 + C_2}(L + L_e). \tag{2.7}$$

As a result, the droplet position estimator is independent of the liquid droplet composition because the droplet position is calculated based on a dimensionless ratio of control electrode capacitances. Hence, this proposed approach significantly facilitates the operation of feedback control DMF de-

vices in the experiments with multiple liquid samples whereas the previous approaches reported in the literature require calibrating the device for each liquid sample used [24, 25].

Experimental Setup

A DMF device was fabricated to verify the theoretical observations. The device consists of two overlapping plates separated by a spacer of $0.5mm$. On the bottom plate, a liner array of 2 mm square electrodes was etched onto a $50nm$ copper layer over a glass substrate. A thin PDMS layer of $5.9\mu m$ thickness was spin coated over the square electrode followed by a Teflon AF1600 layer of $60nm$. The upper plate is an ITO microscope slide coated with $60nm$ Teflon AF1600.

Fig. 2.9 shows the schematic of the experimental setup in this research. It consists of a computer, capacitance meter, switch box, DMF device, and microscope camera.

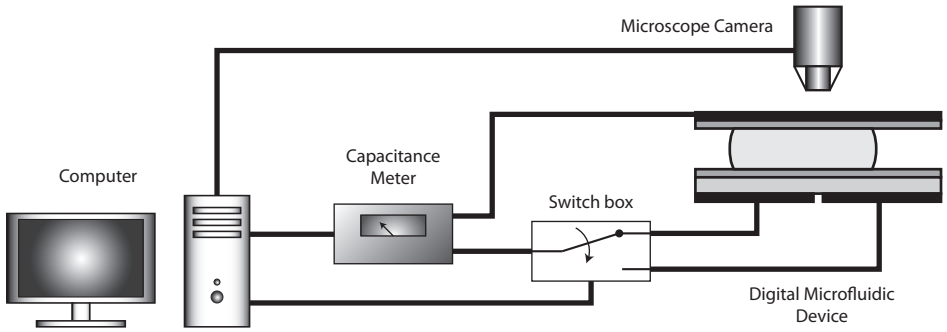

Figure 2.9: Experimental setup schematic for measuring electrode capacitance and droplet position.

In the experimental setup, a National Instrument PXI system equipped

with a digital multimeter (PXI-4072) with a resolution of $0.05pF$ was used for capacitance measurements. The switch box is a de-multiplexer with one input and two outputs that is controlled by the computer. Each output from the switch box is connected to each bottom electrode. The top view images are acquired through the microscope camera positioned directly above the device. The microscope is equipped with a $1.4MPixels$ camera for a position resolution of $7.3\mu m$. The microscope scale was calibrated with a slide micrometer.

The experimental process involves droplet generation, droplet deposition, capacitance measurements, and image acquisition. A Gilson micropipette was used to deposit $2.6\mu L$ of De-Ionized (DI) water droplets with a maximum error of $\pm 1\%$ of volume. A droplet was randomly positioned on the bottom plate electrodes and then caped with the upper plate. The random repetitions will prevent biased error in the measurements. Multiple independent capacitance samples were recorded and at the same time top-view images of the droplet were captured for a few seconds. The actual position of the droplet can be measured by counting the pixels from the image acquired from the microscope (Fig. 2.10).

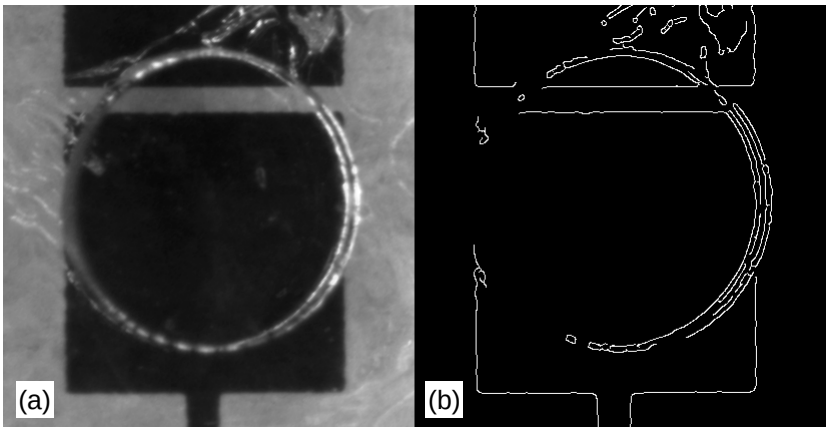

Figure 2.10: Top-view image of DMF device. (a) Original grayscale image. (b) Canny edge detection post-image processing.

Simulation Results

The capacitance-based position estimator performance is evaluated with 2D and 3D analytical and numerical simulations of a DMF device. The analytical simulation solved using MATLAB® produces a closed form mathematical function relating electrode capacitances and droplet position under the assumption that the fringing capacitances are negligible. On the other hand, the numerical simulation performed in COMSOL® solves electrostatic equations in a finite element analysis to provide a more realistic estimate of the actual capacitance by taking the fringing electric fields into account. Therefore, it is expected that the capacitances obtained from numerical simulation are higher than those computed analytically because of the additional fringe capacitance.

In the 2D analysis, a single slice of a droplet is considered to gain a better

insight into the relations between electrode capacitances and droplet position and anticipate sources of errors present in a full 3D analysis. In the 2D analysis, the droplet is modeled with a circular footprint. This assumption is valid when the droplet is stationary as it assumes a symmetrical structure to balance cohesion forces. Top-view images revealed negligible droplet deformation from pinning effects. Furthermore, at slow droplet transport speeds the droplet footprint is fairly circular and does not suffer significant footprint elongation [20]. In later Chapters of this thesis, it is discussed that DC pulse train actuation reduces droplet elongation during transport as the droplet is allowed to resume a structure in equilibrium after the actuation force momentarily disappears. In short, the assumption of a circular droplet profile is typically valid and commonly accepted in the literature. A droplet is positioned in between the centers of two adjacent control electrodes. For each droplet position, the capacitance of each electrode is computed and used to estimate the droplet position with Eq. 2.7. The estimation error is defined as the difference between the estimated position and actual position normalized by the separation distance between the centers of two electrodes $(L + L_e)$.

Simulation parameters were matched to experimental measurements from the fabricated DMF device and are summarized in Table 2.1.

Fig. 2.11 shows a plot of the electrode capacitances at the meridian plane as a function of droplet position. As the droplet travels away from electrode 1 (left electrode), the capacitance of electrode 1 decreases while the capacitance of electrode 2 increases. The flat region on the graph between point (a) and (b) is the result of a larger droplet footprint than the size of

Table 2.1: DMF device parameters.

Parameter	Value
Ambient fluid permittivity, ϵ_a (Air)	1.0
Control electrode pitch, L	$2.0mm$
Control electrode spacing, L_e	$0.2mm$
Dielectric layer permittivity, ϵ_d (PDMS)	2.65
Dielectric layer thickness, t_d	$5.9\mu m$
Droplet resistivity, ρ_L (DI water)	$18M\Omega m$
Droplet permittivity at 20 °C, ϵ_L (DI water)	80.2
Droplet radius, r	$1.05\frac{L}{2} + L_e$
Plate gap, D	$0.5mm$

the electrodes. At point (c), the capacitances of both adjacent electrodes equalize. It is noted that the numerical capacitances are slightly larger than the analytical capacitances due to a minute additional fringe capacitance.

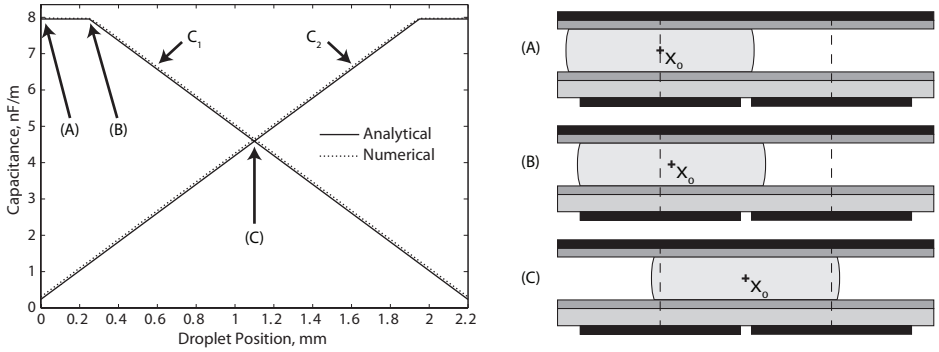

Figure 2.11: Analysis of electrode capacitance at the meridian plane for various droplet positions between the two bottom plate electrodes.

Fig. 2.12 plots the normalized error for multiple droplet positions. The maximum estimate error is less than 4% of the maximum intra electrode

droplet displacement. Three types of error affect the position estimator performance. The initial error manifests itself as a position bias and is present when a droplet centered over an electrode partially overlaps the adjacent electrode. The transition error appears as a curved region in the normalized error plot. From point A to B, the capacitance of electrode 1 remains unchanged while the capacitance of electrode 2 increases. The unbalanced rate of change of electrode capacitance results in a non-linear response of the estimator expressed in Eq. 2.7 leading to the transition error. Finally, a small error is caused by the simplification made from Eq. 2.5 to Eq.2.6.

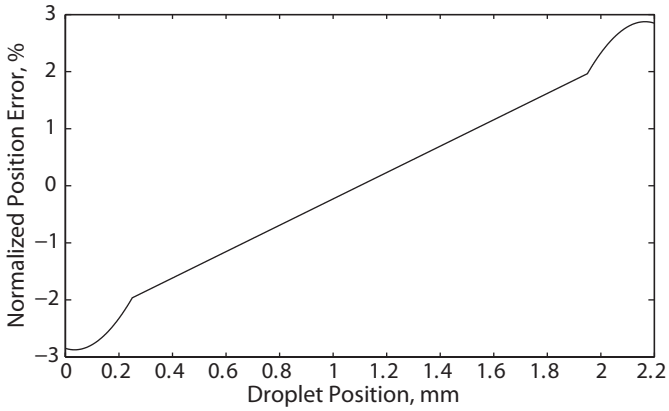

Figure 2.12: Normalized error of the droplet position estimate for various droplet positions between two bottom plate electrodes in a 2D DMF device.

The electrode capacitances for the 3D DMF simulation are plotted in Fig. 2.13. As expected, the capacitance of electrode 1 decreases as the droplet moves towards the adjacent electrode. The electrode capacitance curves have non-linear and linear regions. The non-linear region is caused by the leading and trailing droplet edges as they cross over the boundary of

a square electrode. The linear region occurs when the leading and tailing droplet edges are enclosed within the boundaries of the square electrodes. In both 2D and 3D analyses, analytical and numerical electrode capacitance waveforms have a similar profile; however, numerical capacitance waveforms are slightly higher due the additional fringe capacitance between the droplet vertical boundaries and the electrodes, as it was mentioned earlier.

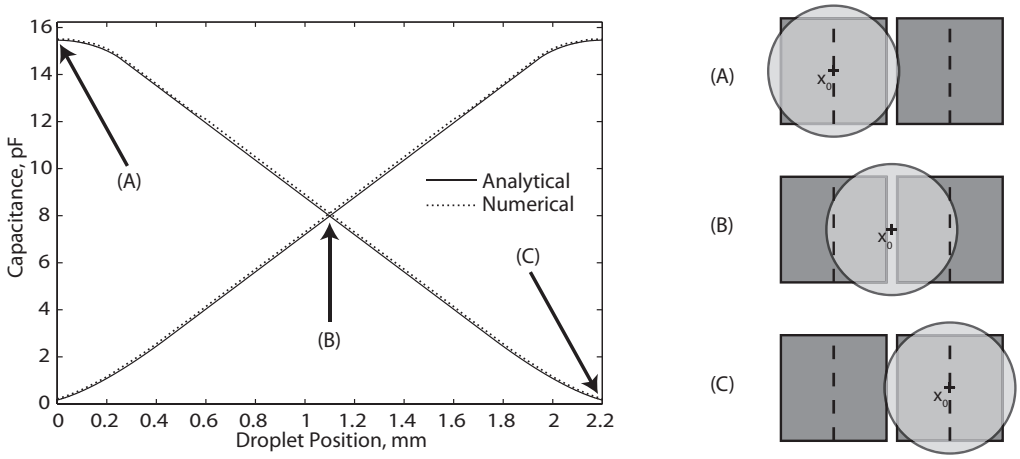

Figure 2.13: 3D analysis of electrode capacitance for various droplet positions between two bottom plate electrodes.

Fig. 2.14 plots the normalized error from the 3D simulations. The normalized error curve resembles a sinusoidal plot. The maximum error is less than 3% of the distance between adjacent bottom plate electrodes and occurs when the droplet is nearly centered over an electrode. As it was discussed earlier, the position estimator is susceptible to three error types; initial, transition, and simplification errors. Numerical error results have a higher initial error and lower transitional error when compared to the analytical error values. The higher initial error in the numerical results is attributed

to the additional fringe capacitance between the droplet vertical boundaries and the adjacent electrode. Although the analytical and numerical waveforms have similar sinusoidal profile, the discrepancies observed in numerical waveform are caused by fringe capacitance.

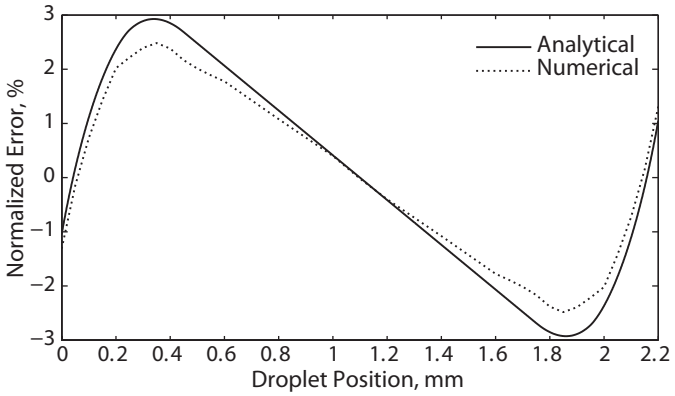

Figure 2.14: Normalized error of the droplet position estimate for various droplet positions between two bottom plate electrodes in a 3D DMF device.

Experimental Results

Fig. 2.15 plots the visual (actual) and capacitive droplet position estimate (estimate) using the line of unity. The visual droplet position was measured from the top-view images taken by the microscope camera. An estimate of the droplet position was computed by Eq. 2.7. Ideally, position estimates should lie along the unity line. More precisely, the proposed position estimator underestimates the displacement in the first half and overestimates the displacement in the second half of the travel distance. However, the estimates are accurate in the start, middle, and end points which are most likely the points of interest for feedback control of droplet operations.

Another important point is that the induced bias errors will in practice help the controller since the underestimated displacement in the first half will let the controller to generate a greater control input and further accelerate the droplet in the first half (i.e., reduce the rise time). In contrast, the overestimated displacement will limit the control input and decrease the overshoot in the second half. The estimation error is once again attributed to the three types of mentioned before. Experimental and simulation results have similar s-curve profiles.

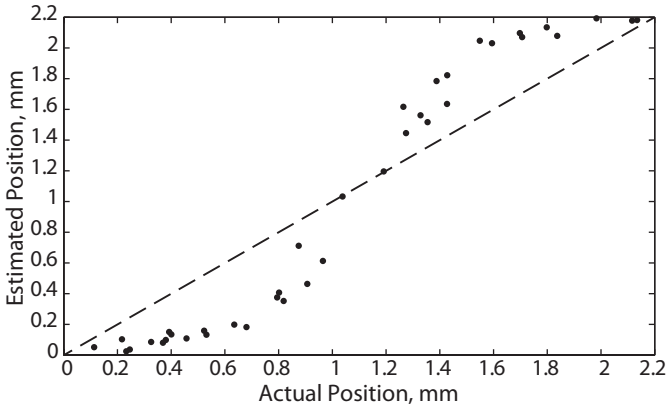

Figure 2.15: Visual and capacitive droplet position plot from experimental measurements.

Fig. 2.16 plots the normalized error of experimental measurements for random droplet positions. The normalized error plot resembles a sinusoidal plot consistent with simulation results presented earlier. The maximum position estimate error is less than 25% of the distance between the adjacent electrodes. It is noted that the error is significantly less in the two extremes and midpoint where accurate estimates are more critical for feedback.

In these experiments, significant efforts were put to minimize the elon-

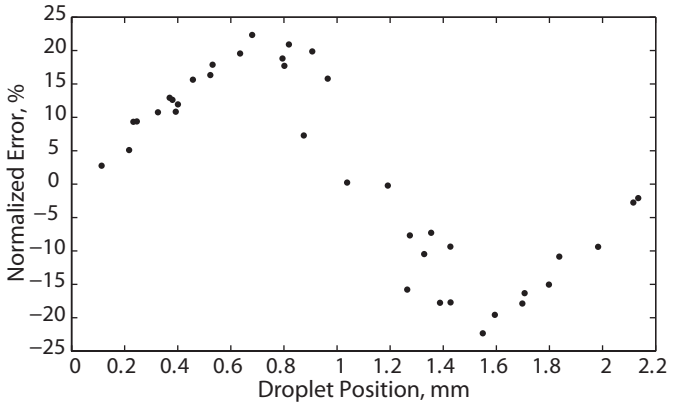

Figure 2.16: Normalized error plot from experimental measurements of DMF device.

gation of droplets. Capacitance measurement was taken under static equilibrium when the droplet assumes a symmetrical structure with a circular footprint. Top view images of the droplet during the experiments reveals negligible droplet pinning effects even after an incremental actuation. The discrepancies between the model and experimental results are explained by variations in droplet diameter. A parameter sensitivity analysis of the model shows that the diameter of the droplet footprint has a significant effect on the magnitude and shape of the error curve. A decrease in the droplet radius decreases the initial error while increasing the transient error. As it was explained earlier, the initial error is a bias due to the overlap on the adjacent electrode when a droplet is centered over an electrode. The magnitude of the bias error decreases when the droplet diameter is smaller than the pitch of an electrode - the sum of electrode width and inter-electrode gap ($L + L_e$). The transient error arises as the leading and tailing droplet edges cross over the square electrode footprint. When the droplet moves away from the center of

an electrode, the overlapped area between the droplet and electrode varies non-linearly. Therefore, smaller droplet diameter increases the magnitude of the transient error producing an s-shape profile. Simulation results with smaller a droplet diameter support this observation. A closer look at top view images of the droplet shows that the outermost droplet diameter was used for simulation results; however, the inner droplet diameter (or circular footprint diameter) is 20% smaller than the outer radius due to the plate gap separation. Reviewing simulation results with a droplet circular footprint to match the inner droplet diameter from the experimental setup yields more convincing results which are in strong agreement with the experimental data. However, this source of error can be mitigated by constraining the droplet volume that its footprint slightly overlaps adjacent electrodes when centered over an electrode, or by reducing the plate gap size in which case the droplet inner and outermost radii are the same. This constraint is necessary in practical DMF devices to facilitate continuous droplet actuation. Another significant source of error is the effect of droplet misalignment where the droplet is situated off-center from the meridian plane. In this case, the transition error increases because the curve length of the leading and tailing droplet edges increases; hence, increasing the position range over which the overlapped area between the droplet and electrode varies nonlinearly. In practice, the actuation forces naturally center the droplet on the meridian plane thereby minimizing this source of error. Finally, instrumental errors arising from the droplet dispenser and capacitance meter, though small, have some effect on the outcome of this droplet position estimator.

Summary

The position of any type of droplet can be estimated in a DMF system with a certain degree of uncertainty. The droplet position estimator can monitor the continuous displacement of any type of droplet in the interval between two electrodes. The proposed droplet sensing technique incorporates an estimator that approximates the position of a droplet anywhere in between electrodes independent of droplet composition. The fact that this sensing technique performs independent from the electrical properties of the droplet means that sensor implementation requires no calibration i.e., a desirable advantage over previous sensing techniques in particular when dealing with a diverse collection of droplet compositions in a single DMF device. Although, this analysis considered a linear droplet position sensing, this approach can be expanded onto a two dimensional grid of x-y electrodes by treating a group of two adjacent electrodes in either x or y directions.

Another distinguishing advantage of this approach is that the sensor captures the continuous displacement of the droplet; valuable information for any feedback controller to correct disturbances in droplet position, velocity and acceleration in the domain of intra electrodes. This sensing approach has the potential to increase the droplet positioning resolution in applications including micro-conveyors whose position resolution and repeatability is limited by the size of the electrodes.

The nature of a DMF system produces a sinusoidal position bias in the state estimator that induces an error in position measurements. However, this sinusoidal bias in the position estimator can benefit the control system

to reduce rise time and overshoot.

2.4.2 Optimization of Capacitance-Based Droplet Position Sensing

It the previous section, it was found that the performance of the calibration-free droplet position sensor is sensitive to changes in the parameters of a DMF device. It is of interest to study the sensitivity of the position estimate accuracy on the structural and material parameters of a DMF device including dielectric permittivity, dielectric thickness, droplet radius, electrode pitch, electrode separation, filler fluid permittivity, and plate gap. A numerical model was constructed to evaluate the performance of the capacitance based droplet sensor. A full factorial sensitivity analysis was designed to evaluate the changes in the sensor performance from simulations. Finally, an empirical model was developed to fit to the simulation results, and the performance of the capacitance droplet sensor was optimized. In addition, performance curves were generated from the empirical model to facilitate the design and fabrication of similar DMF devices.

Methodology

The lower plate of the proposed DMF model (Fig. 2.17) consists of two adjacent control electrodes, electrode 1 and electrode 2, respectively. A thin dielectric layer insulates each of the control electrodes. The upper plate for the DMF model is a continuous electrode. The droplet was modeled with a circular footprint as discussed in the previous section.

The droplet is centered over electrode 1 and incrementally displaced

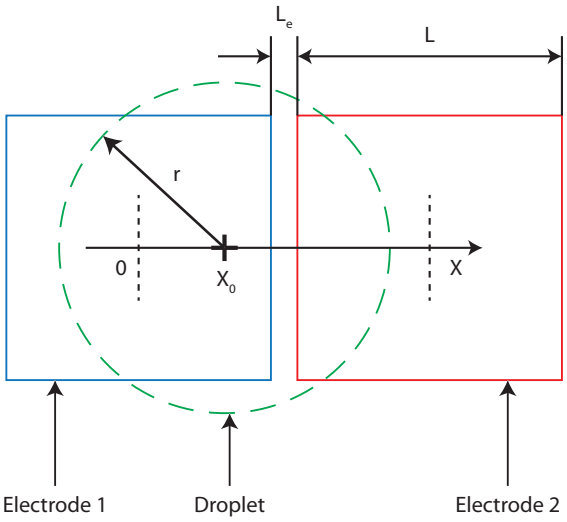

Figure 2.17: Top-view of a reagent droplet over two adjacent control electrodes of the lower plate.

towards the center of electrode 2. The capacitances of electrode 1 and 2 are recorded as droplet is displaced. The position of the droplet is estimated in the same manner described by Eq. 2.7.

The error in the droplet position estimate is observed over the droplet displacement. The estimate error is composed of two errors: an initial error and transient error. The initial error occurs when a droplet is centered over an electrode. The small droplet overlap on the adjacent electrode due to the circular droplet footprint increases the capacitance of the adjacent electrode which offsets the estimate. On the other hand, the transient error occurs when the leading and tailing droplet edges cross the boundaries of the electrodes. The nonlinear increase or decrease of electrode capacitance caused by the curvature of the droplet affects the position estimate and hence the performance of the droplet position sensor. The magnitudes of

the initial and transient errors are dependent on the material and structural parameters of the DMF model.

A two-level full factorial design was used to observe the changes in the droplet sensor performance to varying parameters of the DMF device. The parameters of interest include dielectric permittivity, dielectric thickness, droplet radius, electrode pitch, electrode separation, filler fluid permittivity, and plate gap. The response variable is the maximum error between the simulated and estimated droplet positions. In a two-level factorial design, each parameter has a lower and upper value. The levels of each parameter were taken from earlier publications [2, 20, 22, 23, 31] and summarized in Table 2.2.

Table 2.2: Typical parameter levels of DMF devices.

Parameter	Low level	High level
Dielectric layer permittivity, ϵ_1	2.65 (PDMS)	3.15 (ParyleneC)
Filler fluid permittivity, ϵ_2	1.0 (Air)	2.8 (Silicone Oil)
Dielectric layer thickness, d_1	$1\mu m$	$20\mu m$
Plate gap, d_2	$100\mu m$	$500\mu m$
Electrode pitch, L	$1.0mm$	$2.5mm$
Electrode separation, L_e	$50\mu m$	$200\mu m$
Droplet radius, r	$r_{low} = 1.05\frac{L}{2} + L_e$	$r_{high} = \frac{\sqrt{2}L}{2}$

For each simulation of a treatment combination, the maximum position error was recorded. Dominant factors are identified in a normal probability plot of factor effects [32]. In such plots, non-dominant factors are distributed on a straight line with a nearly zero mean and a negligible variance. In

contrast, dominant factors would deviate from the straight line and have non-zero mean. Fig. 2.18 illustrates dominant and non-dominant factors in a normal plot.

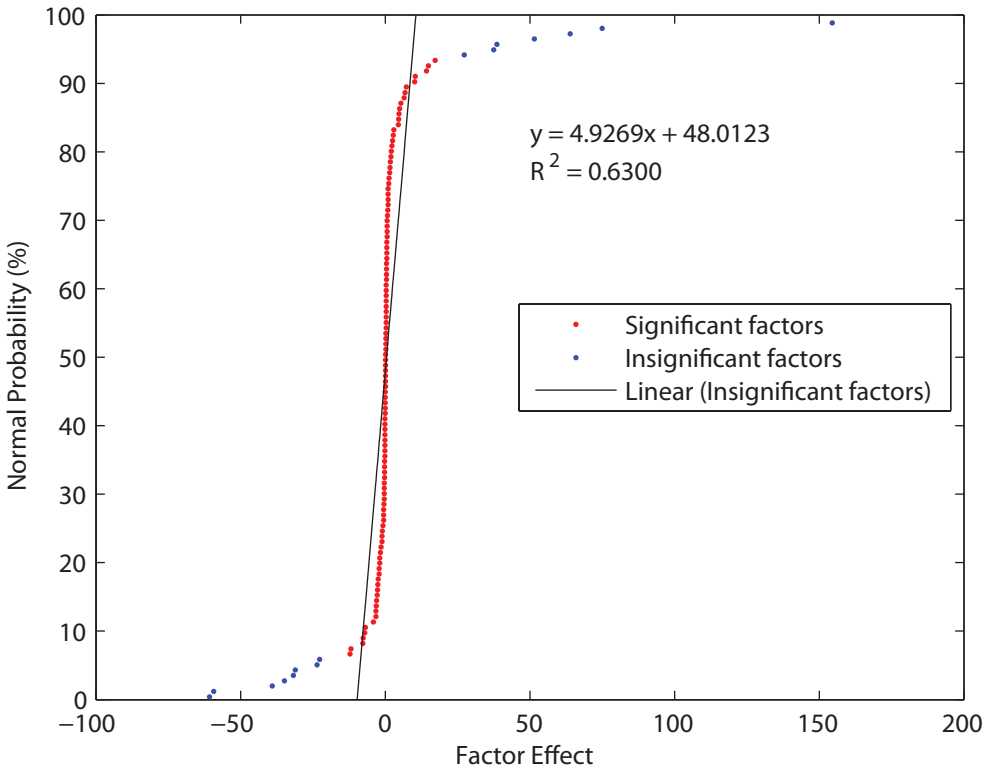

Figure 2.18: Normal plot of factor effects.

An alternative method for screening dominant factors is through the comparison of factor percent contributions [32]. Percent contribution of dominant factors is higher when compared to those of non-dominant factors. A factor was considered dominant if its percent contribution or effect meets or exceeds 1% or 20, respectively. The percent contribution and effect of

dominant factors are summarized in Table 2.3.

Table 2.3: Percent contribution and effect of dominant factors.

Factor	Percent contribution	Effect
L	43.59	154.52
r	10.27	75.00
d_1	7.45	63.87
$d_1 * d_2$	6.76	-60.86
d_2	6.42	-59.32
$L * r$	4.85	51.52
L_e	2.79	-39.06
$\epsilon_2 * d_1$	2.72	38.56
ϵ_2	2.57	37.48
$L_e * r$	2.23	-34.94
$\epsilon_2 * d_1 * d_2$	1.85	-31.81
$\epsilon_2 * d_2$	1.77	-31.11
$d_1 * L$	1.37	27.35
$d_2 * L$	1.01	-23.57
$d_1 * d_2 * L$	0.94	-22.70

After identifying dominant factors, an empirical model was fitted to the simulation data. A linear regression of dominant factors was used to model the response as a function of main and interaction effects of the dominant

factors. The general regression model is described as

$$\begin{aligned} e_{max} = \alpha_1\epsilon_2 + \alpha_2 d_1 + \alpha_2 d_2 + \alpha_4 L + \alpha_5 L_e + \\ \alpha_6 r + \alpha_7\epsilon_2 d_1 + \alpha_8\epsilon_2 d_2 + \alpha_9 d_1 d_2 + \\ \alpha_{10} d_1 L + \alpha_{11} d_2 L + \alpha_{12} L r + \alpha_{13} L_e + \\ \alpha_{14}\epsilon_2 d_1 d_2 + \alpha_{15} d_1 d_2 L + \alpha_{16}, \end{aligned} \tag{2.8}$$

where e_{max} is the maximum estimate error and α_1 - α_{16} are model coefficients of dominant factors.

The values of the model coefficients, α_1 - α_{16}, are summarized in Table 2.4. The empirical model fits the simulation data with an adjusted R^2 value of 96.12%.

Simulation and empirical model responses of various factor combinations are plotted in Fig. 2.19. The empirical model reasonably follows the simulation results.

Table 2.4: Empirical model coefficients.

Model coefficients	Fitting values
α_1	18.7
α_2	31.9
α_3	-29.7
α_4	77.3
α_5	-19.5
α_6	37.5
α_7	19.3
α_8	-15.6
α_9	-30.4
α_{10}	13.7
α_{11}	-11.8
α_{12}	25.8
α_{13}	-17.5
α_{14}	-15.9
α_{15}	-11.4
α_{16}	154.5

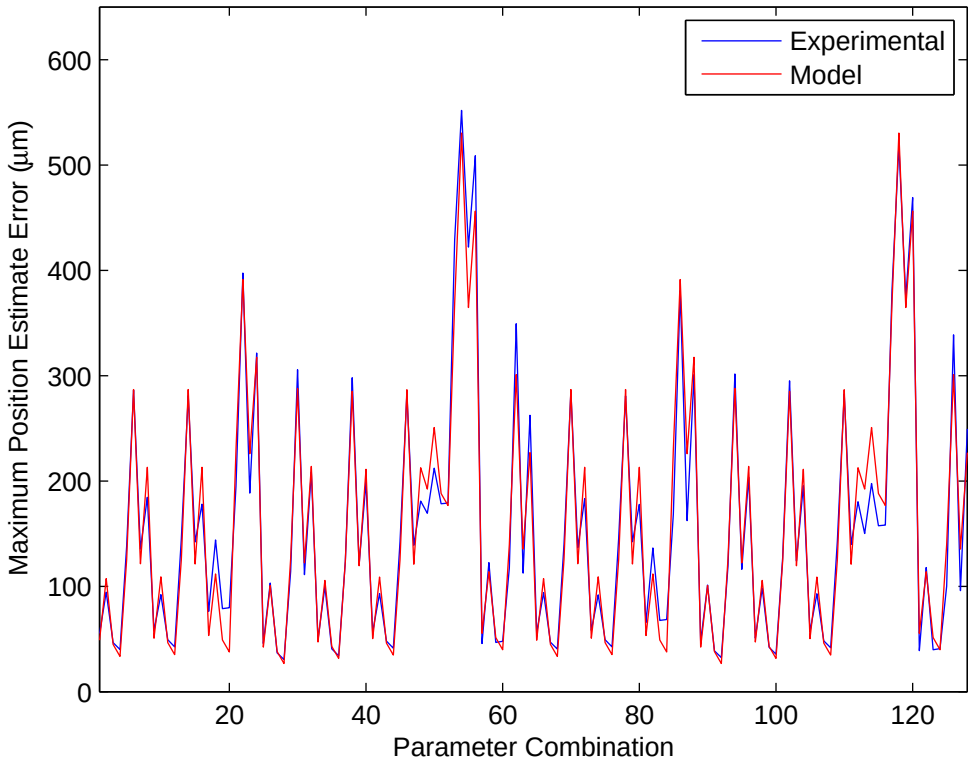

Figure 2.19: Experimental and empirical model response for full factorial combinations.

Results and Discussions

The performance of the capacitance-based droplet sensor depends on certain parameters of a DMF device. Studying simulation results show that the dielectric thickness, droplet radius, electrode pitch, electrode separation, filler fluid permittivity, and plate gap have the greatest effect on the droplet position estimate error. Optimizing the empirical model over the input variables range revealed that there is a point for which the maximum estimate error is minimized down to $27\mu m$. The parameter values that yield this point of minimal estimate error are summarized in Table 2.5.

Table 2.5: Optimal parameter levels of the DMF device.

Parameter	Optimal value
ϵ_2	1.0 (Air)
d_1	$20\mu m$
d_2	$500\mu m$
L	$1.0mm$
L_e	$200\mu m$
r	$r_{high} = \frac{\sqrt{2}L}{2}$

The optimal point of the empirical model is consistent with our initial intuition to minimize the initial and transient errors in the droplet position estimate. The initial error in the position estimate is due to the small droplet overlap on the adjacent electrode when the droplet is centered over an electrode. The initial error is decreased by decreasing the change in the electrode capacitance between no droplet overlap and full droplet overlap. This is achieved by increasing the dielectric thickness. The transient error

is caused by the nonlinear change in electrode capacitance that is the result of the droplet edge curvature crossing the electrode boundaries. This effect is mitigated by increasing the droplet radius while decreasing the electrode pitch because the curvature of the droplet crossing electrode boundaries decreases. As a result, the nonlinear change in electrode capacitance is reduced.

Finally, isoperformance curves are indispensable for exploring different design and fabrication options of a DMF device. An isoperformance curve reveals parameter combinations that can yield a constant output response. The output response of interest was taken to be the maximum position estimate error from a capacitance based droplet sensor for DMF devices. Using the proposed empirical model at the optimal point, isoperformance curves for filler fluid permittivity, electrode separation, dielectric thickness, plate gap and droplet radius are plotted with respect to electrode pitch in Fig. 2.20-2.24, respectively. Each plot contains three contours corresponding to a maximum droplet position estimate error of $50\mu m$, $100\mu m$, and $200\mu m$.

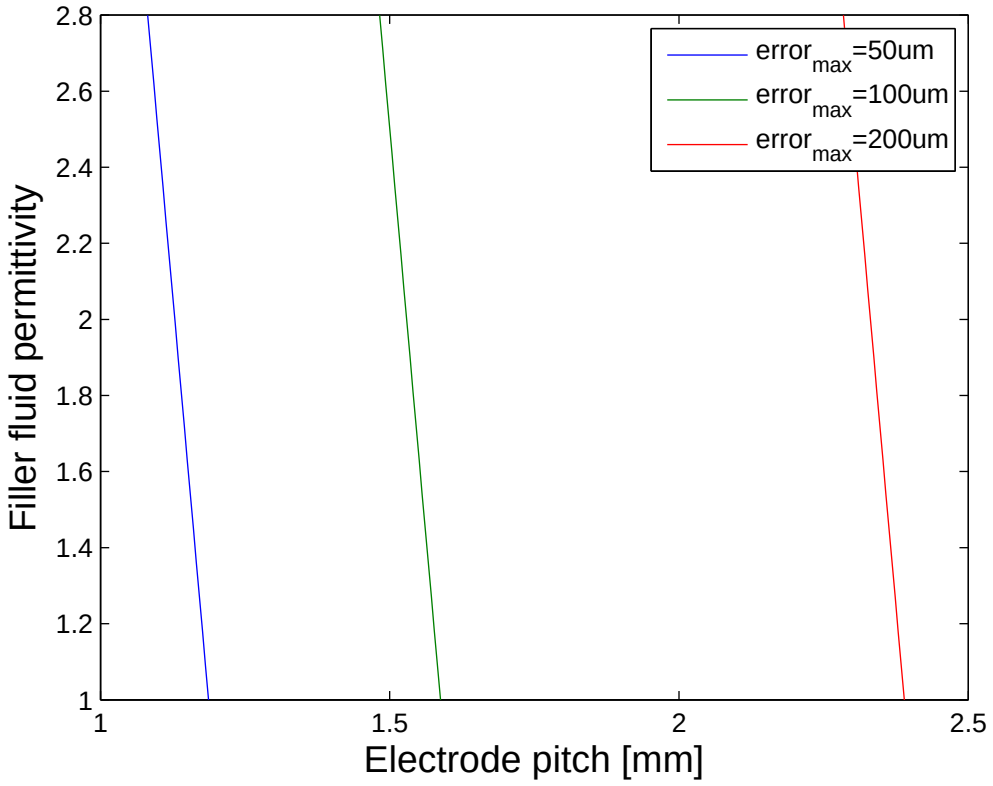

Figure 2.20: Isoperformance curves for filler fluid permittivity and electrode pitch.

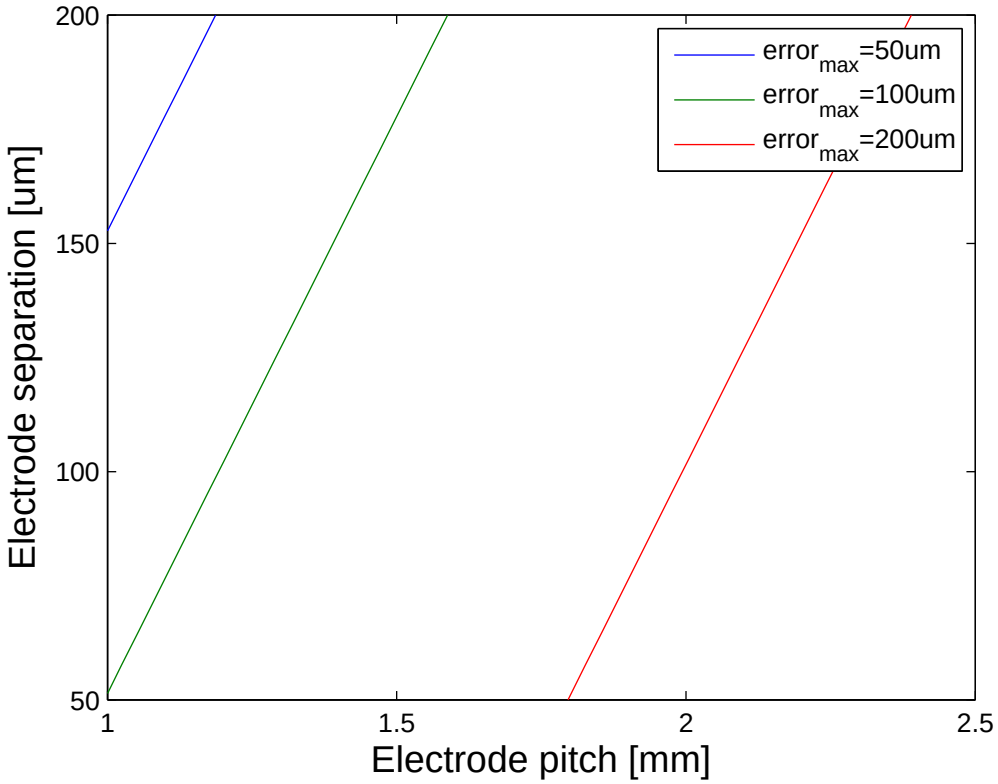

Figure 2.21: Isoperformance curves for electrode separation and electrode pitch.

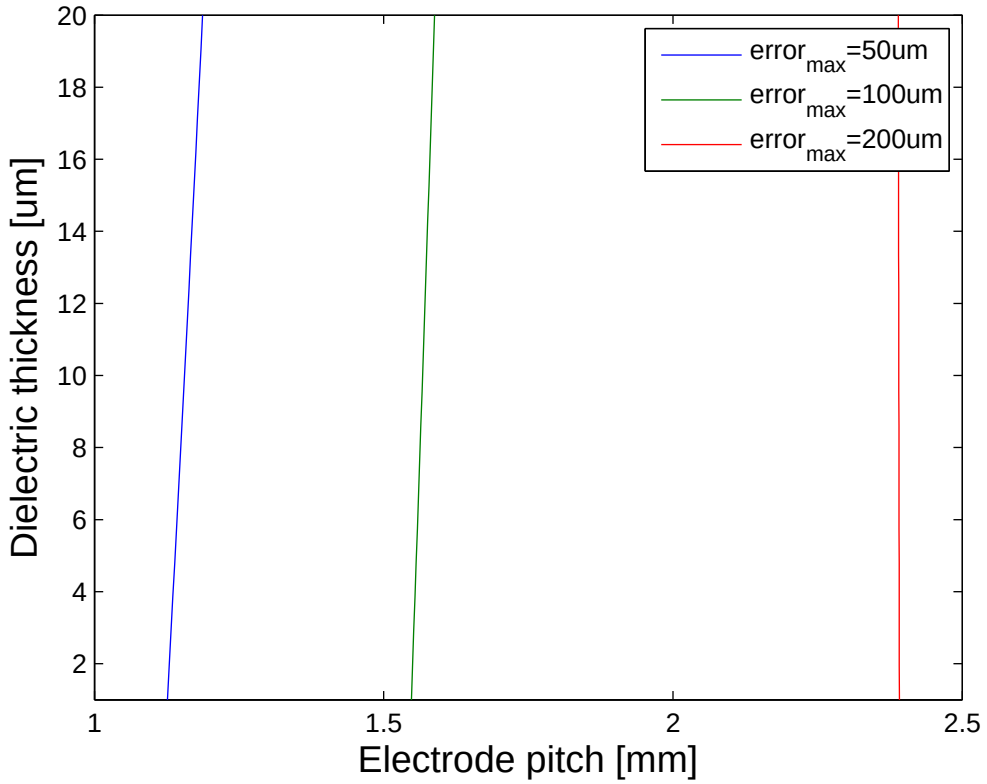

Figure 2.22: Isoperformance curves for dielectric thickness and electrode pitch.

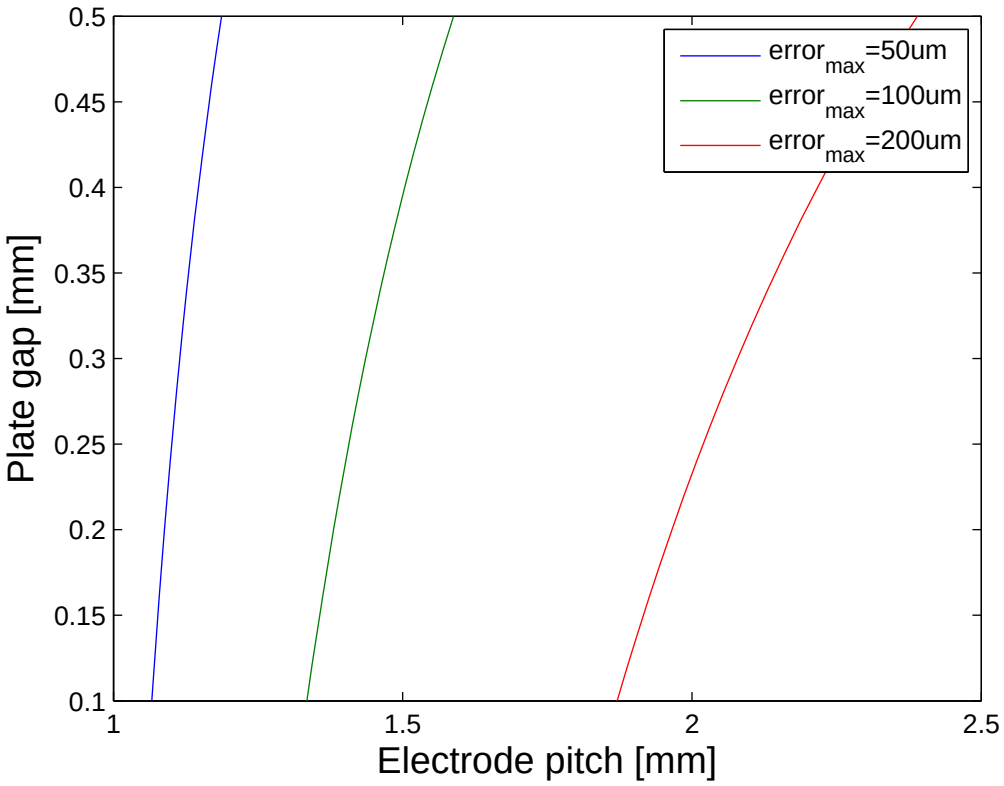

Figure 2.23: Isoperformance curves for plate gap and electrode pitch.

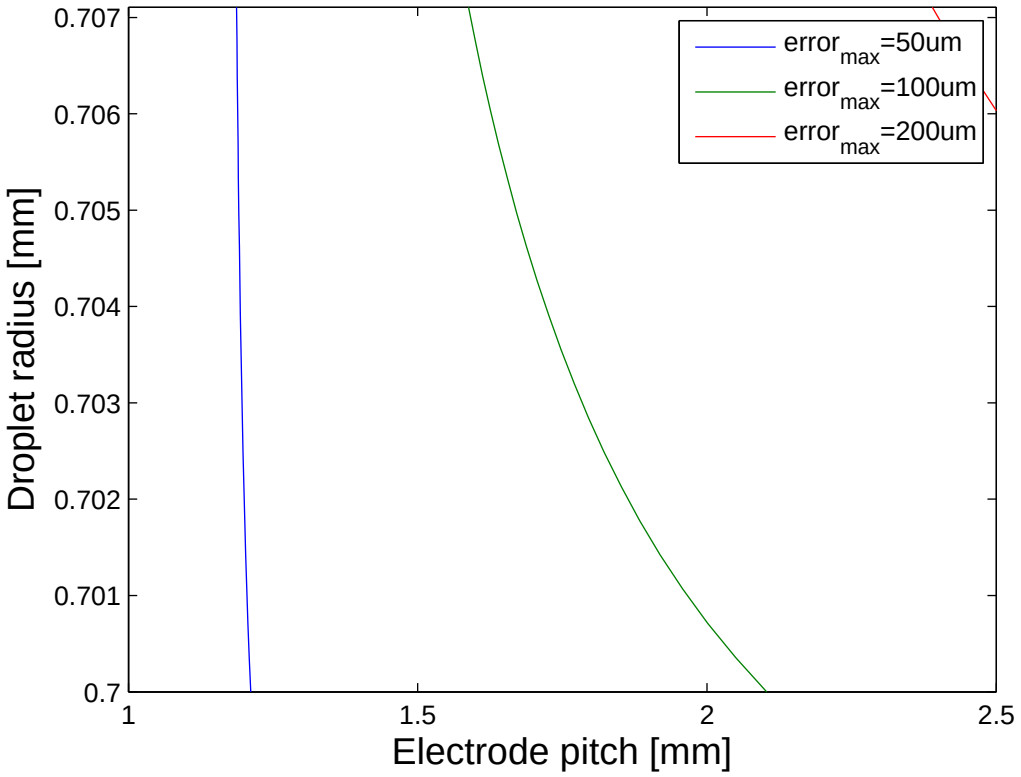

Figure 2.24: Isoperformance curves for droplet radius and electrode pitch.

Summary

The performance of droplet position sensor for a DMF device was optimized by minimizing the position estimate error. The response of the droplet sensor was simulated for various combinations of material and structural parameters in a DMF device. An empirical model was fitted to the system response obtained from simulations. Optimization of the sensor performance was achieved by optimizing the empirical model. It was found that the performance of the sensor under study is influenced most by electrode pitch followed by droplet radius, dielectric thickness, plate gap, electrode separation, and filler fluid permittivity. It is interesting to note that the optimal sensor performance is not limited to particular combination of DMF parameters. Isoperformance curves for the sensor performance show the interactions between paired DMF parameters such that the maximum position estimate error remains constant. The isoperformance curves also show that the filler fluid permittivity and dielectric thickness have less effect on the sensor performance than the others and are independent of the electrode pitch. In contrast, the effect of electrode separation, droplet radius, and plate gap varies as a function of electrode pitch.

Minimizing the error of droplet position sensors can significantly improve the performance of a closed loop droplet controller that is considered to be an essential component for fully automated DMF platforms.

Chapter 3

Analysis and Design of a DMF Feedback Controller

3.1 Overview

Control systems have improved the accuracy and robustness of droplet actuation in DMF devices. However, previous control systems have not demonstrated the ability to control droplets in the interval of two DMF electrodes and hence manipulating a desired response necessary for certain droplet operations such as droplet transport, splitting, merging and mixing. The location between two adjacent DMF electrodes is not a naturally stable position for a droplet to stop because in between electrodes there is no equilibrium point where the net actuation forces from an activated electrode is naturally minimized. To achieve intra-electrode droplet positioning, a control system needs a droplet position feedback signal to decide which leading or tailing electrode to energize to generate a state of equilibrium in between two electrodes. In this section, a position feedback control system is designed and simulated to demonstrate the feasibility of controlling the position, velocity, and acceleration of a droplet in DMF devices prior to

prototyping.

A control system is a collection of subsystems some of which are simple amplifiers (or gains) whose purpose is to amplify the magnitude or change the form of an input signal which has a direct effect on the output response of the system. Such gains must be strategically chosen to achieve the desired system output response. In general, low gains result in a stable but slow system response where the output value takes a long period of time to reach the steady-state (desired) value. Increasing the gain values speed up the system response, however, there is a threshold gain value known as the critical value beyond which the system response begins to oscillate and eventually the system becomes unstable. The controller gains can be estimated using classical control theory analysis, but first the system must be described by a transfer function that is a linear time-invariant mathematical expression relating the input and output of a system.

Estimating the controller grains nearest to the desired critical value can be a challenge for intricate systems including DMF systems. The dynamic behavior of droplet actuation stems from the complex interactions of electrostatic and hydrodynamic effects. Numerical models [38] coupled electrostatic and hydrodynamic interactions to compute the driving and opposing forces for droplets in motion. However, numerical models are computationally exhaustive because they solve electro-hydrodynamics governing equations in time and space domains. Furthermore, classical control theory analysis is required to estimate the controller gains cannot be applied to numerical models as its output is in the form of a dataset with no explicit mathematical expression describing the dynamic system behavior that relates to

the output to the input over time. Although a regression model can be fitted and verified experimentally to the numerical input and output data to apply the classical control theory analysis to numerical models, the lack of information about a general form of the model (the order of the transfer function, zeros, and poles) can lead to counter intuitive results.

Semi-empirical droplet dynamic models exist in which electrostatic and hydrodynamic phenomena are treated separately [39]. Semi-empirical models describe the dynamics of droplet motion with mathematical expressions which can be reduced to a transfer function for the classical control theory analysis. Unlike numerical models, the application of semi-empirical models is restricted to certain system conditions.

In the following sections, a position feedback controller for DMF devices is designed and simulated. In addition, a technique to analytical estimate the controller gains is presented. The electromechanical driving force is modeled based on the conservation of energy [34, 37, 39, 40]. Feedback linearization was used to linearize the nonlinear relationship between the driving force and the applied voltage. Threshold and saturation conditions were accounted by using intermediate actuation voltages. The performance of two position feedback control systems namely proportional (P-action) controller and proportional-derivative (PD-action) controller were designed and compared. The performance of both controllers was evaluated by simulating the position, velocity, and acceleration control of a droplet in a DMF device. Simulation results demonstrate the possibility of controlling the position of a droplet in the interval of two adjacent DMF electrodes using feedback control. Also, the model is used to demonstrate the use of pulse

width modulated actuation signal that is the subject of further discussion in Chapter 4.

3.2 System Modeling

The motion of a droplet in a DMF device can be modeled by balancing all driving and opposing forces acting on the liquid droplet [39]. The governing equation for describing the dynamic motion of a droplet can be described as [39, 41]

$$m\frac{dv}{dt} = F_{drive} - F_{wall} - F_{filler} - F_{tpcl}, \tag{3.1}$$

where m is the mass of the droplet, v is the velocity of the droplet, F_{drive} is the electromechanical force generated by the application of voltage to a DMF electrode beneath the droplet, F_{wall} is the net shear force experienced at the liquid-solid interface on the upper and lower DMF plates, F_{filler} is the drag force acting on the droplet as it transverses through the surrounding fluid, F_{tpcl} is the three-phase contact line force proposed by Ren *et al.* [41] to account for energy losses due to the absorption and desorption of fluid particles around the three-phase contact line [42].

The DMF device was modeled in the similar manner previously described in Chapter 2 where the droplet meniscus was found negligible as its effect on the electric field distribution is minimal particularly in DMF devices in which the ratio of electrode width to plate gap is large [35–37]. In addition, the droplet footprint was assumed to have a circular profile that is a valid assumption under the static equilibrium where cohesion forces are balanced

throughout the droplet. This assumption may also be valid at slow droplet transport speeds as the droplet footprint is fairly circular and does not suffer significant footprint elongation [20]. In Chapter 4 of this thesis, it is discussed that DC pulse train actuation reduces droplet elongation during transport as the droplet is allowed to resume a circular profile inscribed in equilibrium after the actuation force momentarily disappears.

The electromechanical force was estimated based on the conservation of energy [34, 37, 39, 40]. The magnitude of the electromechanical force is estimated as [43]

$$F_{drive} = \frac{dU}{dx} = \frac{d}{dx}\frac{CV^2}{2} = \frac{\epsilon_{rd}\epsilon_{rh}}{t_h\epsilon_{rd} + t_d\epsilon_{rh}}\frac{V^2}{2}\frac{dA}{dx}, \tag{3.2}$$

where U is the energy confined in the system, C is the capacitance between the droplet and energized electrode, V is voltage applied to the energized DMF electrode, ϵ_{rd} and ϵ_{rh} are the dielectric and hydrophobic layer permittivity, t_h and t_d are the dielectric and hydrophobic layer thicknesses, A is the overlapping area between the droplet and the energized electrode.

It is clear that the magnitude of the electromechanical force is a function of DMF device parameters, applied voltage, as well as the droplet position due the last derivative term of $\frac{dA}{dx}$. Fig. 3.1 plots the change of droplet area dA as a droplet is transitioned from the center of one electrode to the second adjacent electrode. The rate of the of wetted area varies as a nonlinear function since the curved droplet leading and trailing edges cross the linear boundaries of the square DMF electrodes. As a result, the electromechanical force model is a nonlinear function of droplet position

which must be linearized to allow one to use the classical control theory analysis to estimate controller gains.

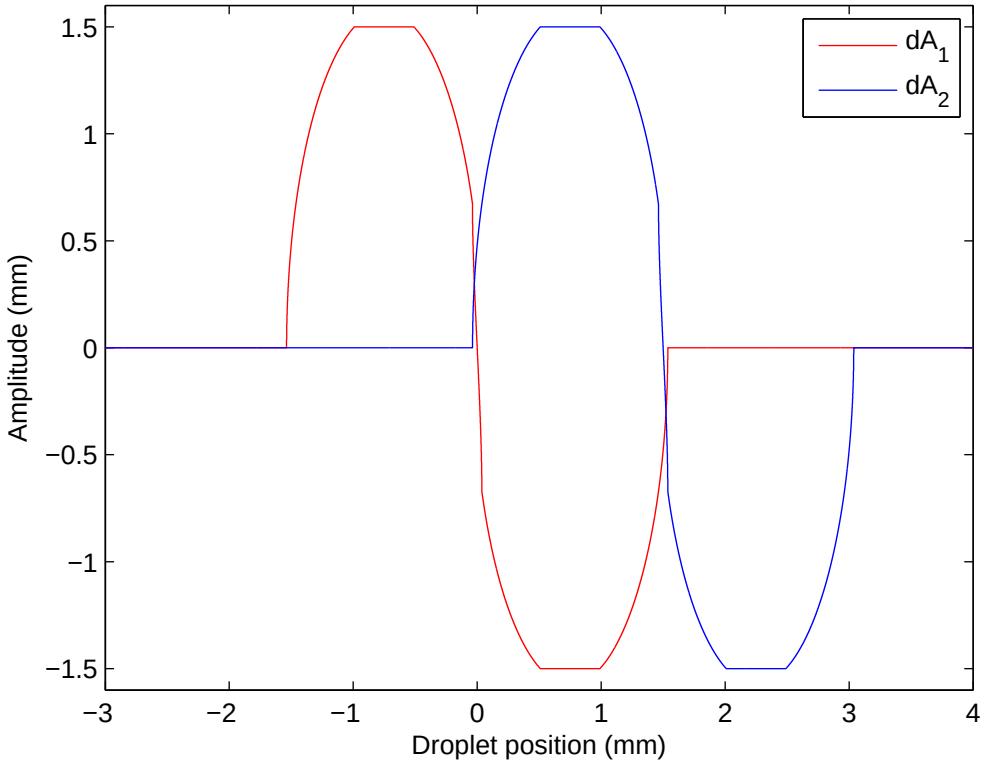

Figure 3.1: Rate of change of droplet/electrode overlapping area for two adjacent DMF electrodes as the droplet transitions from the center of an electrode to the next electrode. The DMF electrodes were square shape with a width of 1.5mm. The radius of the droplet footprint was 0.787mm.

In real DMF devices, two threshold conditions exist which have an effect on droplet motion. At the low end of driving voltages, hysteresis and droplet pinning effects prevent the motion of droplet until the actuation voltage surpasses a threshold [20]. At high driving voltages, the intensity of

electric fields at the three-phase contact line causes nonlinear interactions which reduce the effectiveness of the actuation force [44]. Although these threshold conditions are not directly accounted for by this electromechanical force model, in this study the operating actuation voltage magnitude is fixed fix to intermediate voltages far from either threshold voltage level through Pulse Width Modulation (PWM). By setting the actuation voltage to a level between the low- and high- voltage threshold conditions, an incremental step displacement of the droplet can be achieved with a single DC voltage pulse applied to an adjacent electrode. In Chapter 4, experimental results demonstrate that droplets can be displaced with DC voltage pulses. Furthermore, the magnitude of the step displacement can be controlled by varying the DC voltage pulse width.

The wall force is estimated from a one-dimensional model which assumes a parabolic velocity profile and no-slip conditions at the liquid-solid interfaces. Ahmadi *et al.* [45] demonstrated limitations of one-dimensional model as they overestimate the magnitude of the shear stress at higher droplet transport speeds (or higher Reynolds numbers).However, at low droplet transport speeds which is the case in this study, one-dimensional model have simple computation and yield an acceptable approximation comparable to more complex two-dimensional models because the wall force is not the dominant opposing force [45]. The net wall force exerted on the droplet from the upper and lower plates is estimated as [39]

$$F_{wall} = (\frac{6\mu_d v}{h})(2\pi r^2), \tag{3.3}$$

where μ_d is the viscosity of the droplet, v is the droplet average velocity, h is plate gap between upper and bottom plates of a DMF device, r is the radius of the droplet footprint.

The filler force is the drag force on the droplet as it moves through a viscous ambient fluid. Often in DMF devices, silicon oil is used as the ambient fluid to minimize evaporation rates of droplets and opposing forces at the cost of higher drag force which become more dominant only in extremely high velocities which hardly the case in DMF systems. Bahadur and Garimella [39] estimate the filler force as the drag force on cylindrical rigid body in a cross flow as

$$F_{filler} = \frac{1}{2} C_D \rho_f v^2 (2rh), \tag{3.4}$$

where C_D is the drag coefficient which is approximated by $\frac{24}{Re}$ [43] under low Reynolds numbers typically less than 10, and ρ_f is the filler fluid density. The Reynold number for a DMF droplet is $Re = \frac{\rho_d v L}{\mu_d}$, where ρ_d is the droplet fluid density and L is the DMF electrode width.

The triple point contact line force arises from the energy dissipation due to liquid particles adhering and detaching at the three-phase contact line. Ren *et al.* [41] estimate the energy loss from molecular interactions as an opposing force that is proportional to the droplet velocity as

$$F_{tpcl} = \zeta v (4\pi r), \tag{3.5}$$

where ζ is the contact line friction coefficient.

3.3 Theoretical Controller Gain Estimation

To estimate the controller gains, the droplet dynamic system must be reduced to a set of linear time-invariant (LTI) equations for classical control theory analysis. Fig. 3.2 illustrated the desired reduced block diagram for the feedback control system where subsystems are represented by a transfer function. With this block diagram, one can reduce the system into a single block to analyze the response of the closed loop system and estimate the controller gains.

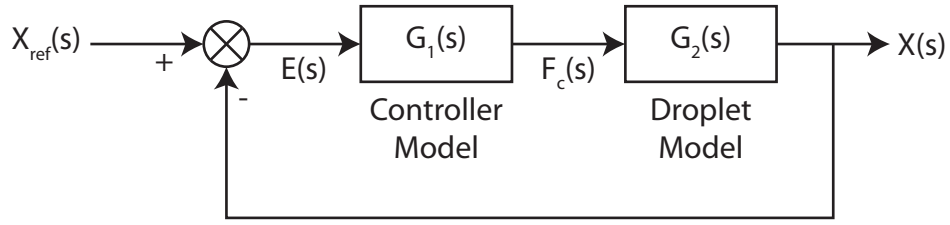

Figure 3.2: Desired block diagram representation for estimating controller grains.

Fig 3.3 illustrates the block diagram for the droplet model which includes blocks describing the droplet inertia, driving force, and all opposing forces (F_{wall}, F_{filler}, and F_{tpcl}). The coefficient a_1 in the electromechanical force model which substitutes for $a_1 = \frac{1}{2}\frac{\epsilon_{rd}\epsilon_{rh}}{t_h\epsilon_{rd}+t_d\epsilon_{rh}}$. The block diagram is a graphical representation of the governing equation of droplet motion. With the exception of the nonlinear electromechanical force model, all blocks can be reduced into a single block.

Fig. 3.4 illustrates an equivalent block diagram representation where the droplet momentum and opposing forces have been combined into a single block. The droplet dynamic motion is described by a single second order

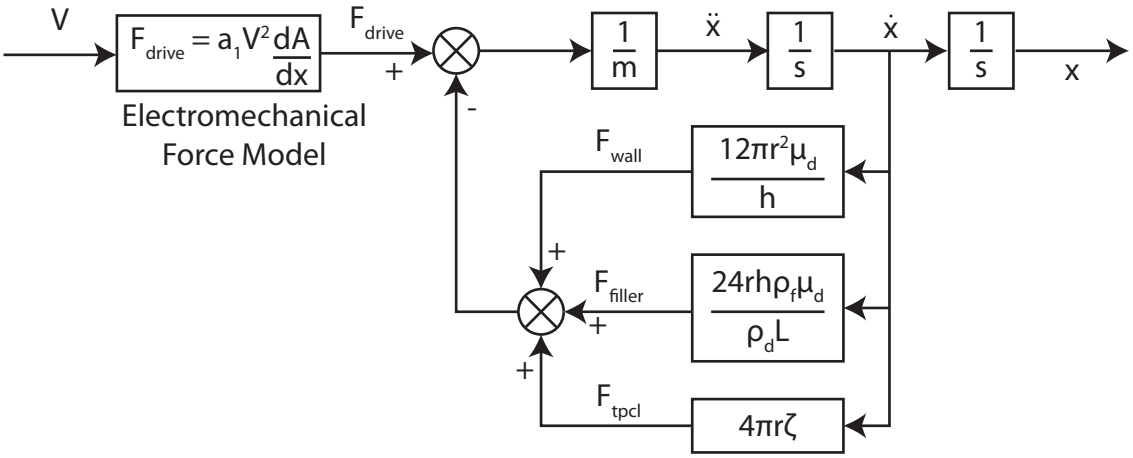

Figure 3.3: Block diagram representation of the droplet dynamic system.

system equivalent to a mass and damper system. The magnitude of the damper c is equal to the sum of all opposing forces as

$$c = \frac{12\pi r^2 \mu_d}{h} + \frac{24rh\rho_f \mu_d}{\rho_d L} + 4\pi r\zeta. \tag{3.6}$$

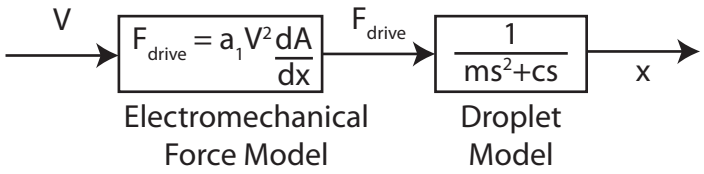

Figure 3.4: Equivalent block diagram representation of the droplet dynamic system.

The electromechanical model cannot be combined with the droplet model because the driving force is proportional to the voltage square a nonlinear transformation as it does not satisfy the condition of linearity.

Feedback linearization is a common technique employed to linearize nonlinear models [46]. The idea behind feedback linearization involves generat-

ing a signal with an inverse transformation to that of the non-linear model. The mathematical representation of feedback linearization is as follows

$$F_{drive} = f(V) = f(f^{-1}(F_{control})) = F_{control}, \tag{3.7}$$

where F_{drive} is a nonlinear function of voltage V generated by the feedback linearization block by transforming a signal $F_{control}$ with the inverse function of the electromechanical force model. Ultimately, the feedback linearization negates the effect of the electromechanical force model such that the control force $F_{control}$ is approximately equal to the driving force F_{drive}. Fig. 3.5 illustrates the integration of feedback linearization to mitigate the effect of the electromechanical force model. The feedback linearization generates a voltage signal as

$$V = \sqrt{\frac{F_{control}}{a_1 L}}, \tag{3.8}$$

where L is the DMF electrode width and is the maximum value of $\frac{dA}{dx}$. Normalizing $\frac{dA}{dx}$ by its maximum value reduces the sensitivity of the drive force F_{drive} to the position of the droplet.

After feedback linearization, the complete droplet dynamic system can be reduced into a second order system with a control force $F_{control}$ as the input and droplet center position x as the output.

The response of a second order system can easily be described with two specification parameters namely the natural frequency and the damping ratio [26]. The magnitude of these specification parameters determines the characteristic response of a second order system. The natural frequency w_n

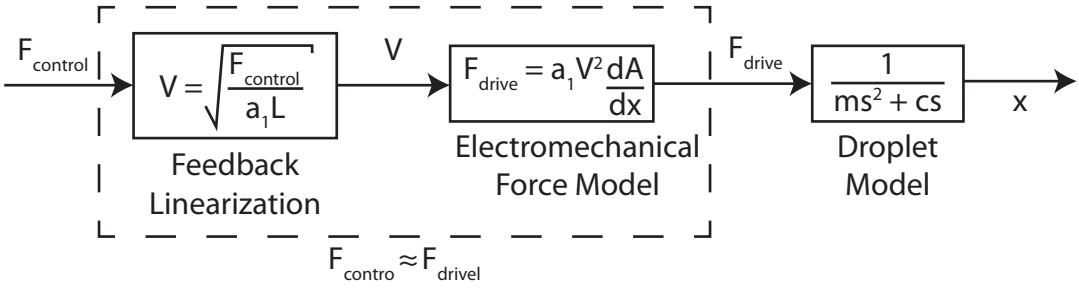

Figure 3.5: Application of feedback linearization to linearize the electromechanical force model.

is the oscillation frequency of the second order system without the damper. The magnitude of the damping ratio ξ dictates whether the system response is under-damped, critically-damped, or over-damped. A desired transient and steady-state response system response can be achieved by tuning the values of these specification parameters with controller gain values. A general second order system has a transfer function in the following form

$$G(s) = \frac{w_n^2}{s^2 + 2\xi w_n s + w_n}, \tag{3.9}$$

where w_n is the natural frequency and ξ is the damping ratio.

Fix. 3.6 illustrates the block diagram of a proportional (P-action) controller. The P-controller consists of a single gain P which amplified the difference between the desired and actual droplet position. The transfer function of the P-controller block diagram is a second order system as

$$\frac{X_{ref}(s)}{X(s)} = \frac{\frac{P}{m}}{s^2 + \frac{c}{m}s + \frac{P}{m}}. \tag{3.10}$$

The controller gain P is can be estimated with the natural frequency and

the mass of the droplet as

$$P = w_n^2 m. \tag{3.11}$$

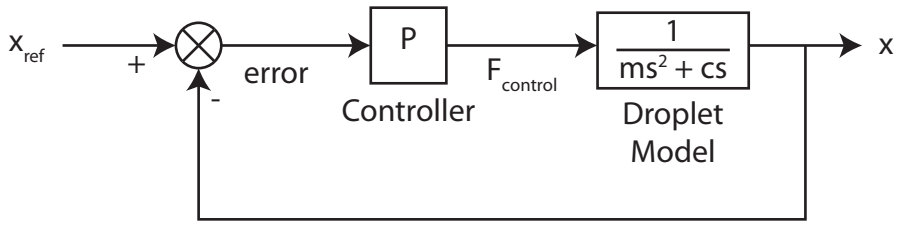

Figure 3.6: Proportional (P) controller block diagram for droplet control in DMF devices.

Fig. 3.7 illustrates the block diagram of a proportional-derivative (PD-action) controller. A PD-controller contains a P grain for amplifying the immediate error value and an additional D gain for amplifying the error rate of change. The transfer function of the PD-controller block diagram is

$$\frac{X_{ref}(s)}{X(s)} = \frac{\frac{P}{m} + \frac{D}{m}s}{s^2 + \frac{c+D}{m}s + \frac{P}{m}}. \tag{3.12}$$

Similarly, the P gain of the controller can be estimated with natural frequency and the mass of the droplet as

$$P = w_n^2 m. \tag{3.13}$$

In a PD controller, the additional D gain can control the value of damping ratio to achieve a faster system response. The controller gain D can be

estimated as

$$D = 2\xi_{PD} w_n m - c, \tag{3.14}$$

where ξ_{PD} is the damping ratio of the PD-control system.

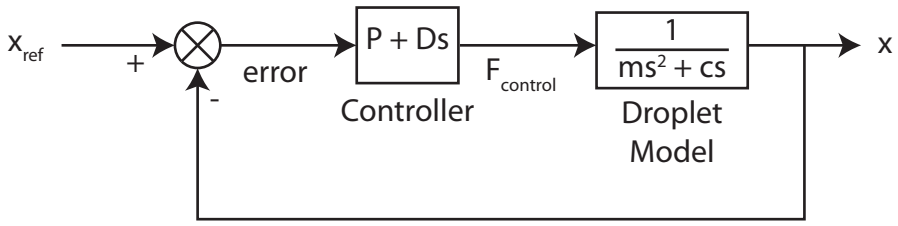

Figure 3.7: Proportional-Derivative (PD) controller block diagram for droplet control in DMF device.

In the design of a control system, there is often a desired system response that one wishes to achieve. The system response is described by several measurements including rise time, settling time, and percent overshoot. These measurements are function of system specification parameters, for example the natural frequency and damping ratio in second order system. In this analysis it was shown how to predict the controller gains with specification parameters whose values were carefully selected to achieve desired system response.

3.4 Simulation Results

The dynamic response of the droplet to actuation signals was simulated in MATLAB®. Prior to analysing the performance of the position feedback control systems, the droplet dynamic system was verified with experimental

data from Pollack *et al.* [20]. Pollack *et al.* [20] documented the maximum droplet switching frequency as a function of applied voltage for a $0.1M$ KCl droplet moving through Silicone Oil medium. The simulation parameters were matched to experimental parameters from [20, 39]. Table 3.1 summarizes simulation parameter values.

Table 3.1: Simulation parameters for a $0.1M$ KCl droplet in a silicone oil medium [20, 39].

Parameter	Value
Upper and bottom plate spacing, h	$300\mu m$
Electrode pitch, L	$1.5mm$
Dielectric layer thickness, t_d	$800nm$
Hydrophobic layer thickness, t_h	$60nm$
Dielectric material permittivity, $\epsilon_r d$ (Parylene C)	3.15
Hydrophobic material permittivity, $\epsilon_r h$ (Teflon AF1600)	2.1
Free space permittivity, ϵ_0	$8.85X10^{-12}\frac{F}{m}$
droplet density, ρ_d	$1000\frac{kg}{m^3}$
droplet viscosity, μ_d	$1.9X10^{-3}Pas$
droplet radius, r	$0.95mm$
Filler fluid density, ρ_f (Silicon Oil)	$760\frac{kg}{m^3}$
Filler fluid viscosity, μf (Silicon Oil)	$1.7X10^{-3}Pas$

Fig. 3.8 plots the simulation results of maximum switching frequency as a function of voltage against experimental data from Pollack *et al.* [20]. The simulation results for low voltages are in agreement with previously published experimental data, but simulation results diverge from the experimental data as the voltage increases. This limits the validity of the droplet

dynamic system to operating in the low voltage range [39, 45]. Therefore, the actuation voltage was set to either 0 V or 30 V in subsequent simulations.

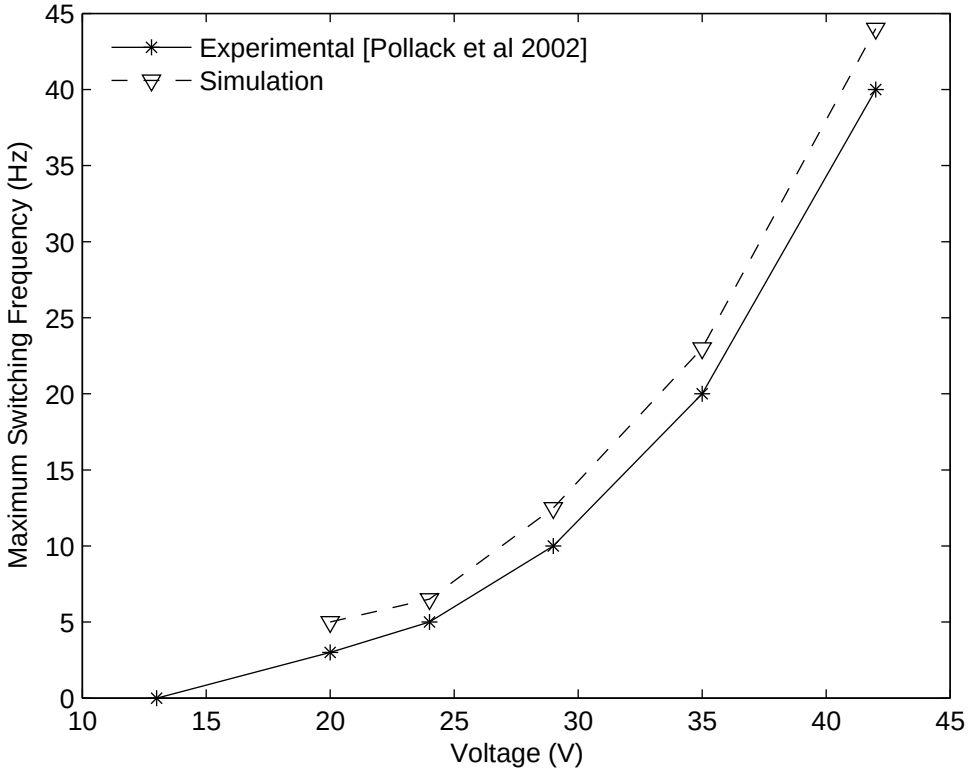

Figure 3.8: Verification of simulation model with experimental data of maximum droplet transport in oil medium as a function of voltage. Simulation model parameters were matched to experimental conditions from Pollack *et al.* [20].

The performance of the droplet position feedback control systems was evaluated with an arbitrary reference signal consisting of step, ramp, and parabolic stimuli. A step stimulation signal is a constant position useful for testing the stability and steady state error of the control system in position-

ing a droplet at a fixed position. The ramp stimulation signal is a linear increasing signal whose rate of change with respect to time is constant. In other words, a ramp stimulation signal is a constant velocity reference signal useful for testing the ability of regulating the droplet velocity. Finally, a parabolic stimulation signal represents constant acceleration. Fig. 3.9 plots the position reference signal for testing the performance of the proposed controller systems (P-controller and PD-controller). The reference signal contains four constant positions between two DMF electrodes including $0mm$, $0.5mm$, $1mm$, and $1.5mm$. In addition, the reference signal has a constant velocity signal of $0.75mm/s$ and a constant acceleration signal of $8mm/s^2$.

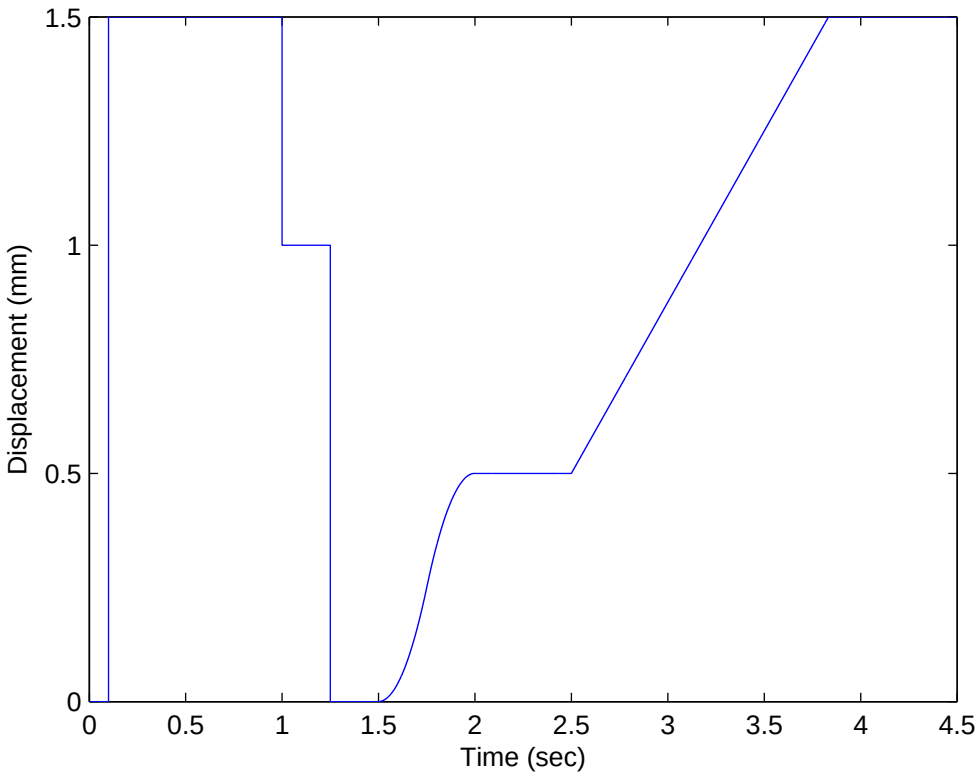

Figure 3.9: Input droplet position reference stimulation signal for evaluating the performance of the intra-electrode droplet control systems for DMF devices.

3.4.1 Proportional (P) Controller Results

The P-controller parameters are summarized in Table 3.2.

Table 3.2: Proportional (P) controller parameters.

Parameter	Value
Natural frequency, f_n	$50Hz$
Damping coefficient, ξ	1.3221
PWM carrier frequency, f_{PWM}	$500Hz$
PWM voltage	$0V or 30V$
Proportional gain, P	0.0816

Fig. 3.10 plots the reference position input signal and the actual droplet position response. The droplet position closely follows the reference input signal with a quick response for reference positions not close to the center of either DMF electrode at $x_1 = 0mm$ and $x_2 = 1.5mm$, respectively. When the reference position is the center of a DMF electrode, the actuation force dramatically decreases as the droplet approaches the center of the DMF electrode.

Fig. 3.11 is a closer look of the reference signal and actual droplet position when the droplet is positioned between two DMF electrodes. Oscillations in the actual droplet position are visible positions between the electrodes as these positions are unstable. The P-controller achieved intra-electrode droplet positioning alternatively applying a voltage pulse to the leading and tailing DMF electrodes in an effort to balance maintain the droplet at the reference position. The magnitude of the oscillations can be decreased by increasing the frequency of the PWM.

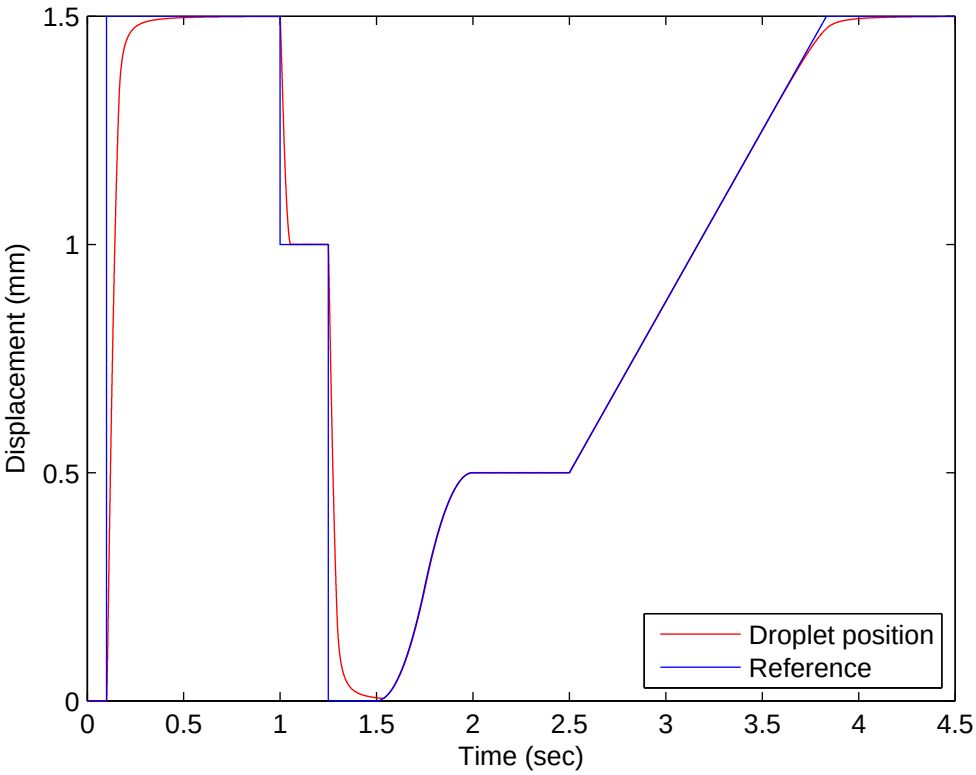

Figure 3.10: Droplet position response from the P-controller.

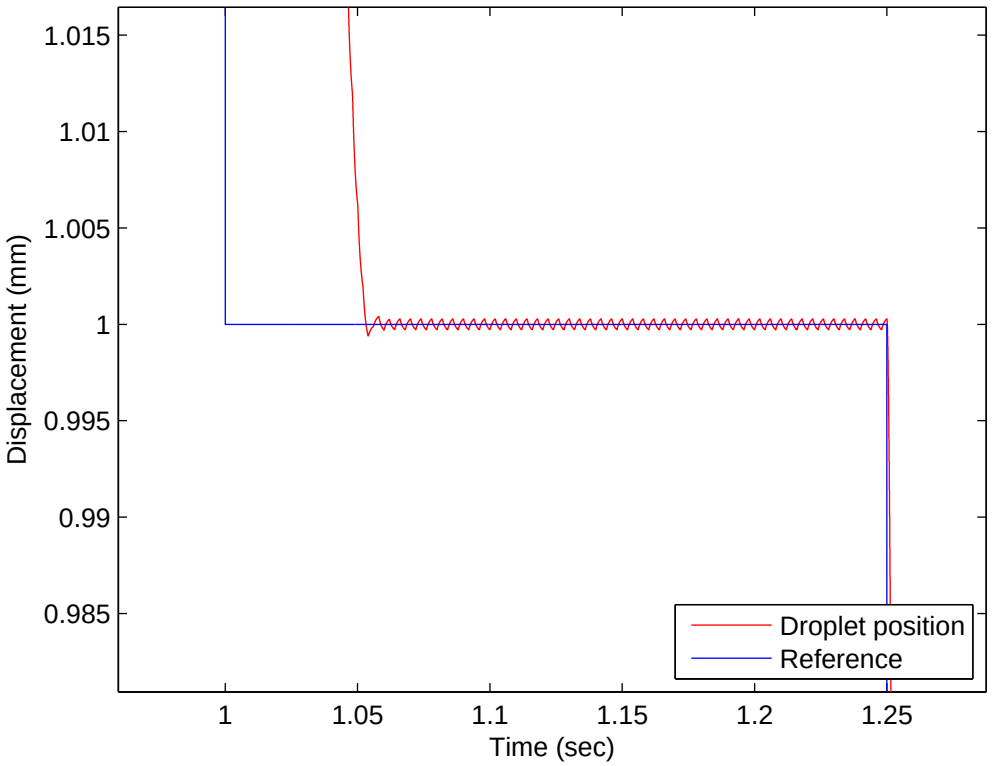

Figure 3.11: Droplet position at the time of $t = 1s$.

Fig. 3.12 plots the velocity of the droplet as it is exited by a step input at the time of $t = 0.1s$. The jitter observed in the velocity plot is the result of on/off voltage pulses produced by the PWM.

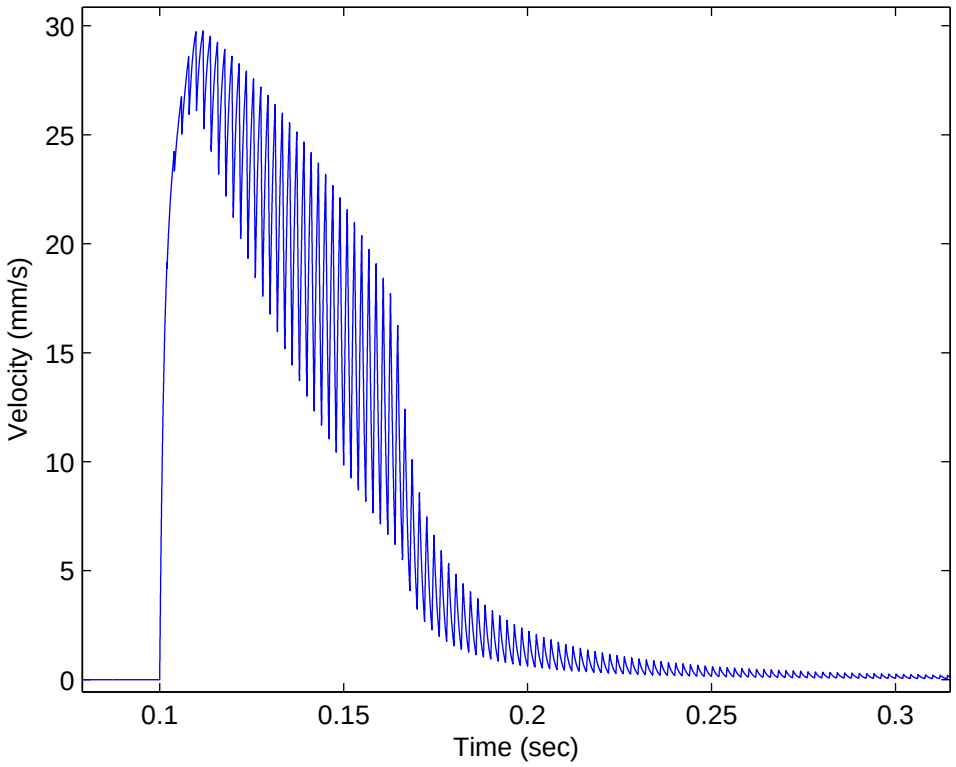

Figure 3.12: Droplet velocity response due to initial step excitation at time $t = 0.1s$.

Fig. 3.13 plots voltage pulses generated by the PWM during the initial step excitation at the time of t = 0.1s. The digital pulse produces by the PWM has a magnitude of either 0V or 30V. In addition, the pulse width decreases as the droplet approached the desired position.

Fig. 3.14 plots the actuation force on the droplet for the initial step

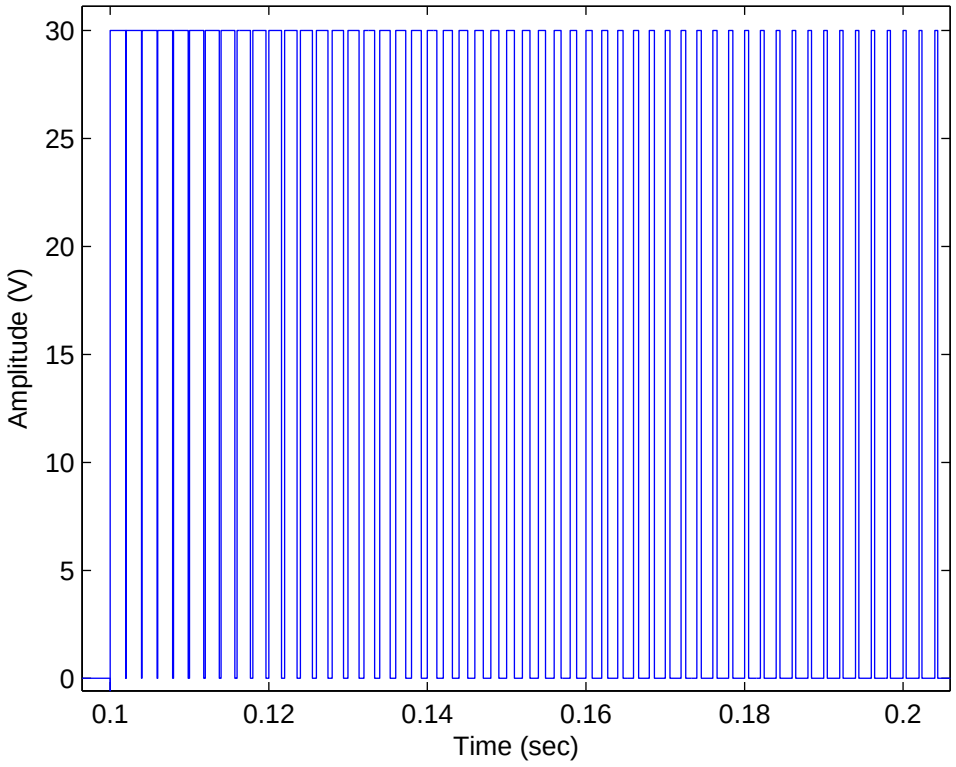

Figure 3.13: Driving voltage signal to induce droplet motion during initial step excitation at time $t = 0.1s$.

excitation at $t = 0.1s$. As it is expected, the actuation force is applied in discrete time intervals which correspond to the time when the driving voltage is 30V. In addition, the magnitude of the actuation force dramatically decreases when the droplet approaches the center of a DMF electrode.

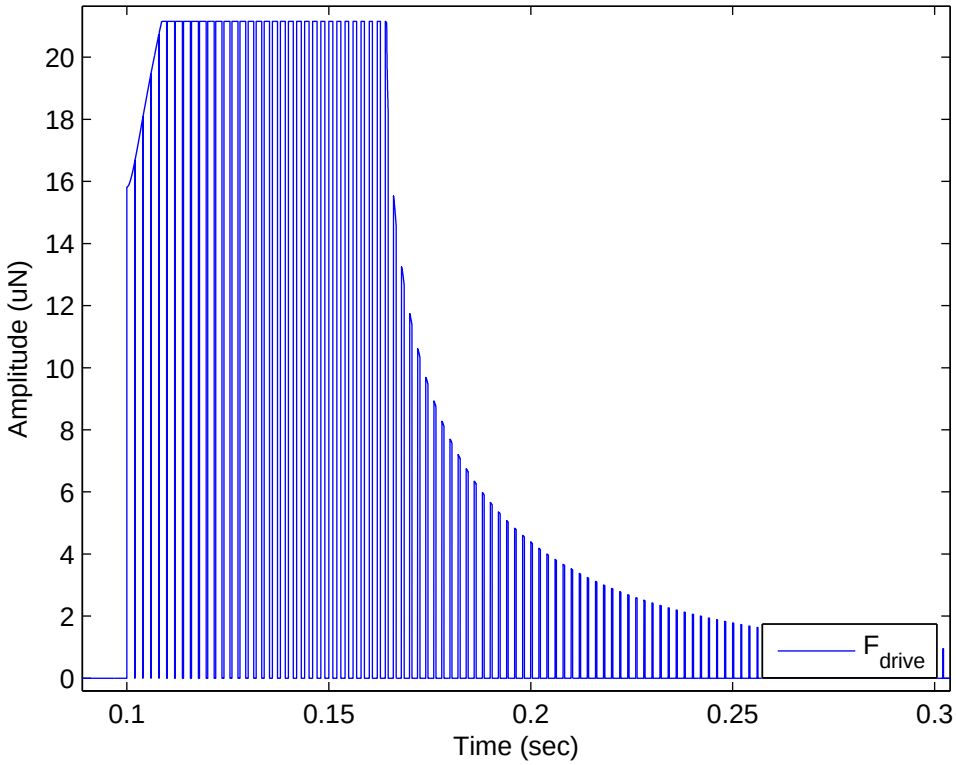

Figure 3.14: Driving force generated from applied voltage during initial step excitation at time $t = 0.1s$.

3.4.2 Proportional-Derivative (PD) Controller Results

The parameters for the PD controller are summarized in Table 3.3.

Fig. 3.15 plots the reference position input signal and the actual droplet

Table 3.3: Proportional-Derivative (PD) controller parameters.

Parameter	Value
Natural frequency, f_n	$50Hz$
Damping coefficient, ξ	1.0
PWM carrier frequency, f_{PWM}	$500Hz$
PWM voltage	$0V or 30V$
Proportional gain, P	0.0816
Derivative gain, D	$-1.6727X10^{-4}$

position response. The performance of the PD-controller appears to be similar to that of the P-controller. However, a close inspection of the reference signal and actual droplet position when the droplet is positioned between two DMF electrodes reveals a more stable response (Fig. 3.16). The added velocity feedback in PD-controllers dampens the instabilities (or oscillations) observed in the P-controller.

No distinguishing difference is observed in the droplet velocity plot, voltage actuation signal, or driving force between the P-controller and PD-controller.

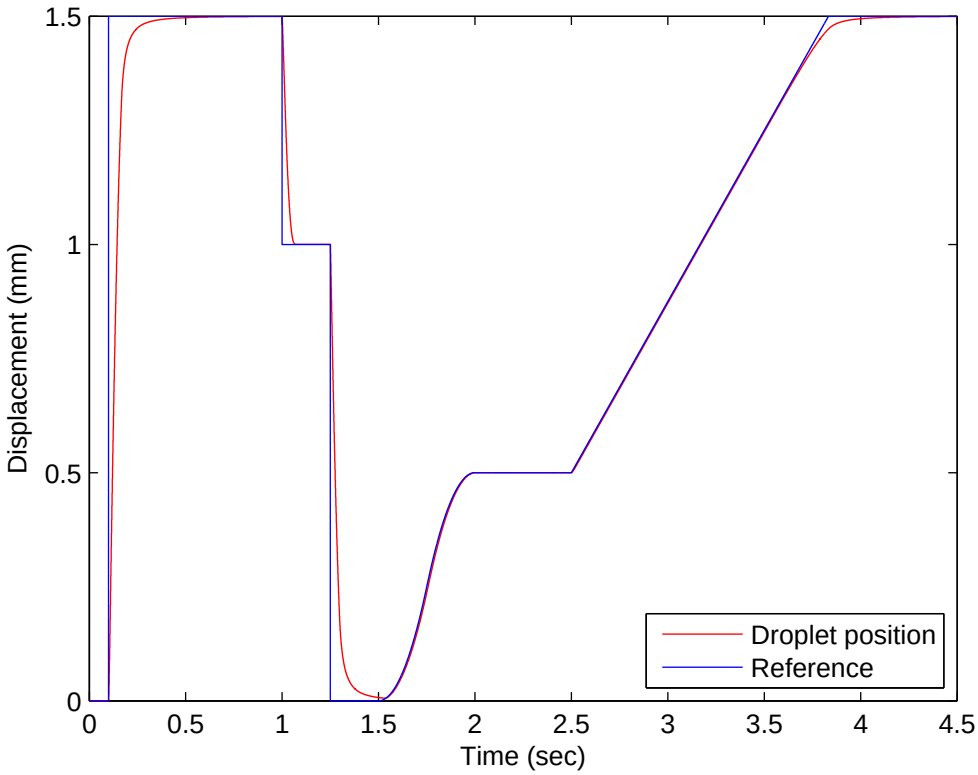

Figure 3.15: Droplet position response from the PD-controller.

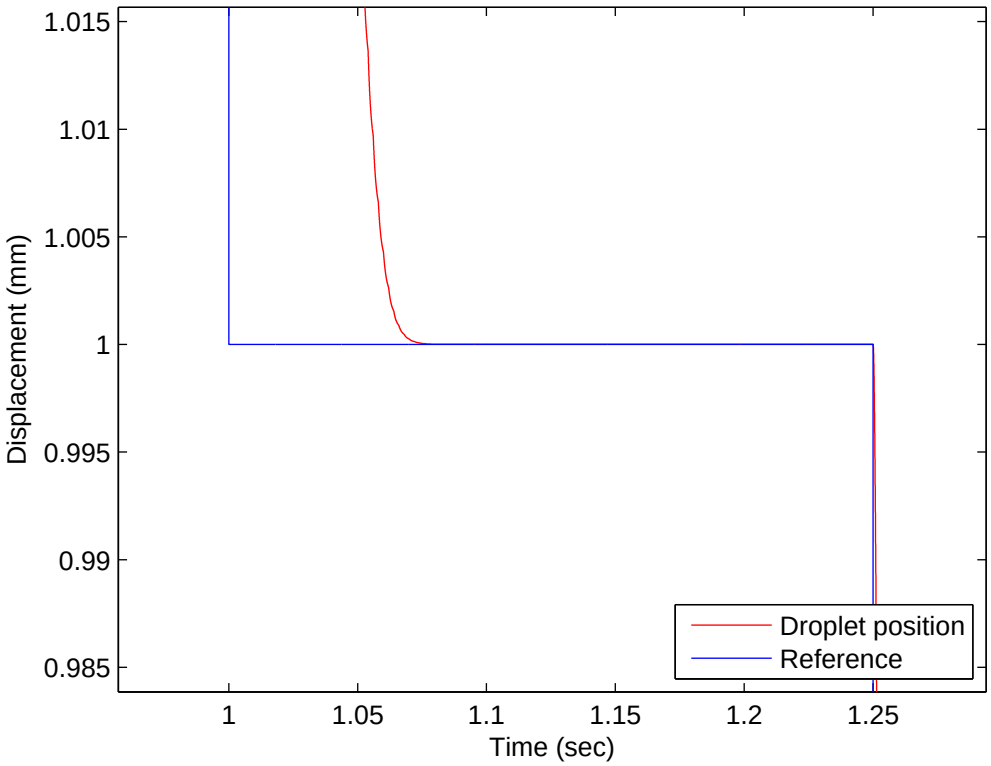

Figure 3.16: Droplet position at the time of $t = 1s$.

3.5 Summary

In this section, a position feedback control system for intra-electrode droplet positioning was designed and analyzed to specify the appropriate controller gains. A method for analytically estimating the gain values for the controller was presented. The dynamics of droplet motion by electromechanical forces were simulated from semi-empirical models proposed in literature. The validity of the droplet dynamic model was tested against experimental data from Pollack *et al.* [20].

Two controllers for intra-electrode droplet positioning were simulated to regulate the position, velocity, and acceleration of a droplet in a DMF device by digital actuation pulses. Both P- and PD- controllers were successful in accurately positing droplets in the interval between two adjacent electrodes. The P controller has a simpler design when compared to the PD-controller, but a P-controller does not have the ability to modify the system damping ratio. In addition, it was found that the actuation voltage has a significant effect on the droplet position overshoot. However, proper controller gains estimated by the proposed method can eliminate this overshoot.

The simulation model was used to demonstrate that a droplet can be positioned anywhere between two DMF electrodes, which is inherently an unstable position in the system, by properly designing a position feedback control system. Furthermore, the DC pulse actuation was found to be a feasible actuation method for controlling the position, velocity, and acceleration of a droplet in a DMF device. These simulation observations led to further investigation into DC pulse train actuation and rapid prototyping

of an intra-electrode droplet positioning feedback control system for DMF devices that will be elaborated in Chapter 4.

Chapter 4

Prototyping of DMF Programmable Controller

4.1 Overview

Digital microfluidics has evolved rapidly in the last decade with many applications in the fields of chemistry, biochemistry, and medicine. This technology hinges on the ability to manipulate droplets on a substrate using electrical signals to perform various droplet operations like droplet transport, merging, splitting, and dispensing. A sequential combination of these droplet operations can be used to execute a complete laboratory protocol on a single DMF device. Typically, complete laboratory analysis in DMF devices are demonstrated in controlled laboratory environments using highly specialized and expensive control instrumentation predominant in well-funded research groups [24, 25]. Such control instrumentation is typically costly and oversized programmable hardware that provides very high signal precision not necessary in most applications. Furthermore, these instruments come equipped with firm-fixed packages (or hardware modules) which offer a handful of design tools with limited re-programmability. Of-

ten, additional expansion hardware modules must be purchased to accommodate future applications. These hardware limitations forces one to work with available instrument functionalities. One of the goals of this thesis was to develop a cost effective and fully customizable control system for DMF devices. The proposed control system is equipped with a microcontroller that in addition to executing fundamental droplet operations can readily interface with auxiliary modules including droplet position feedback sensors, biosensors, heat pump units, and qualitative and quantitative analysis units. The main advantage of this control system over an ensemble of specialized equipment is that it provides researchers with a portable low-cost programmable prototyping environment that is fully customizable to any DMF application and can transfer a laboratory concept based on the DMF technology to a fully functional commercial product in a short turn-around time.

The conceptual schematic of the proposed control system for DMF devices is illustrated in Fig. 4.1. At the core of this programmable control system is a microcontroller and a switch network composed of low-cost off-the-shelf electrical components. The microcontroller can be programmed in high-level language to serve as a logic unit for executing the electrical signals necessary for realizing any droplet operation. The microcontroller is a low voltage device used as a triggering device, and the switch network is an intermediate system that is controlled by the microcontroller to deliver sufficient voltages for actuation to the DMF device.

Noh *et al.* [47] proposed integrating Thin-Film-Transistors (TFT) underneath the dielectric layer of a DMF device. The transistor was used as

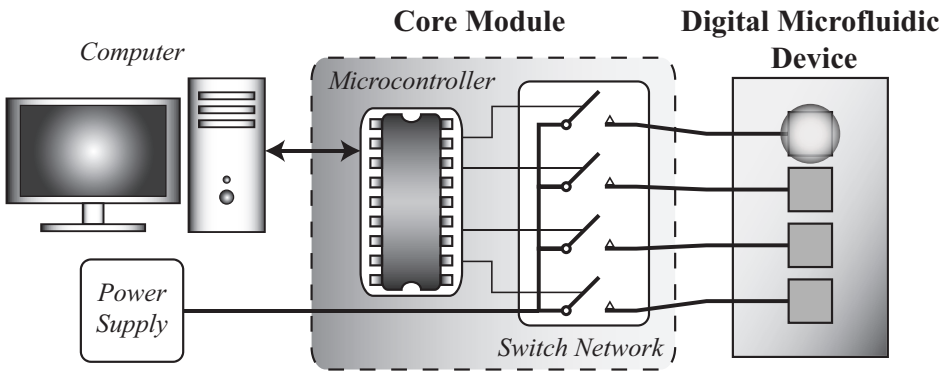

Figure 4.1: Schematic for the controller hardware of DMF devices.

a transmission gate to deliver a DC voltage to an electrode. Two power supplies and solid state relays were used to trigger and deliver sufficient voltage to induce droplet motion. DC pulses were used to actuation the droplet, however it was reported that DC pulse actuation resulted in sluggish droplet motion due to the on/off actuation signal. It was proposed to attach a storage capacitor for every bottom plate electrode and upper plate ground electrode to maintain the voltage on the electrode above the actuation voltage and allow for smooth droplet transport. However, the additional capacitor limits the maximum droplet transport rate due to the slow discharge rate. Integrating the actuation circuitry into the DMF device yields a compact device, but specialized and sophisticated microfabrication facilities are required for the fabrication of such a device. More importantly, DMF devices are quite delicate because the exposed working surface can be easily damaged during normal operation. A damaged working surface makes droplet actuation nearly impossible and the device becomes obsolete. Typically, DMF devices with damaged surfaces are descanted along with

any embedded circuitry beneath the dielectric layer. Therefore, integrating actuation switches into a single chip is not practical for DMF technology.

In this controller design, the switch network was designed separate from the delicate DMF device to allow the reusability and re-configurability of the switch network. Two types of switch network were designed and tested to accommodate either DC or AC droplet actuation signals.

The following sections discuss the implementation and integration of the proposed programmable control system. The electrical components and circuit design for coupling the microcontroller with either DC or AC switch networks are described in detail. Simulation and experimental testing was performed on both switch circuit designs before testing with on a real DMF device. The programmable control system was used to investigate DC pulse train actuation as a feasible and to some extent preferable droplet actuation technique capable of incremental droplet displacement and regulating droplet speeds. Finally, a complete position feedback control system capable of positioning droplets anywhere in between two adjacent electrodes was demonstrated as the ultimate outcome of this thesis.

4.2 Microcontroller Integration

Microcontrollers are programmable integrated circuits with a number of useful modules like counters, pulse width modulation, temperature sensors, digital and analog input/output ports for interfacing with other devices. Microcontrollers are compact and low power devices which are extremely versatile in modern electronic systems including control systems. Typically,

microcontrollers operate in low voltage ranges of less than 5V and low currents in the order of a few milliamps. These low voltages in the order of around 5V, is far from sufficient to overcome the threshold voltage for droplet actuation in the devices fabricated in this thesis. The threshold voltage of actuation was found to be in the range of 50Vdc to 55Vdc. Therefore, the microcontroller for this application is used only as a triggering device for sending control signals to toggle switches which can deliver sufficient voltages to control droplets on a DMF device.

The microcontroller used in this thesis is an 8-bit microcontroller known as Arduino Uno. It operates at 5V and a clock frequency of 16MHz. The Arduino Uno board has 16 digital input/output (I/O) ports capable of reading or writing digital signals. The digital signals have two states; a low state is represented by 0V while a high state is represented by 5V. The microcontroller has an additional 6 analog input pins for reading analog signals with a voltage magnitude between 0V and 5V. When connecting external devices to the microcontroller, special considerations must be taken to ensure that the total maximum current through any microcontroller pin is less than the rated current. Higher currents may permanently damage the microcontroller.

Although other faster microcontrollers are available, the Arduino microcontroller was chosen because of the extensive documentation that is available online for this microcontroller. Also, these microcontrollers were designed with easy access to communication ports available in the ATMEL328 chip. Finally, Arduino provides a C language compiler which translates a program written in C language to machine language. The ability to write

programs in a high-level language such as C is desirable as it significantly facilitates the implementation of complex signal processing functions which would otherwise be tedious and time consuming to implement in machine language.

4.3 Switch Network

The switch network is an intermediate device which is be trigged by the microcontroller to deliver sufficient voltages required to actuate droplets in the DMF device. The switch network draws the necessary voltage for droplet actuation from an external power supply. The network consists of a number of switches where each switch can in turn be connected to any number of electrodes in a DMF device. The advantages for having the switch network as a standalone module include easy re-configurability and reusability. The switches can easily be rearranged to accommodate any number of DMF designs. Furthermore, the switch network can be reused after replacing a damaged DMF device. Two types of solid state switches were designed and tested experimentally to accommodate either DC or AC actuation voltages. Both switch designs were built using off-the-shelf high power semi-conductor devices.

4.3.1 DC Voltage Switch

DC voltages have been used to actuate droplets on DMF devices given that the voltage magnitude is greater than a threshold voltage required for droplet actuation. This threshold voltage is typically an order of magnitude

larger than the operating voltage of most microcontrollers i.e., typically less than 5V. Therefore, an external DC power supply capable of generating sufficient voltage for droplet actuation is needed. The proposed DC switch acts as an inverting amplifier where a digital signal from the microcontroller is inverted and amplified in magnitude. The DC switch is composed of resistors and a single N-channel enhanced-type Metal-Oxide-Semiconductor-Field-Effect-Transistor (MOSFET). A MOSFET is a three terminal semiconductor device that regulates the current flow between the source and drain terminals with a voltage on the gate terminal. When a voltage greater than a threshold voltage is applied to the gate terminal, a conductive channel is created between the source and drain terminals.

The NMOS transistor is connected in common-source circuit as shown in Fig. 4.2. The NMOS transistor used is the IRF540N which is a fast switching high voltage (100Vdc across its drain and source terminals) transistor. The NMOS source terminal is the common ground to both input and output circuits. The input circuit is a microcontroller digital pin connected to the NMOS gate terminal via resistor R_1. Resistor $R_1 = 1k\Omega$ protects the microcontroller digital pin by limiting the current drawn. Resistor R_2 connects the NMOS drain terminal to the positive terminal of the external power supply with a voltage of V_{cc}. Resistor $R_2 = 110k\Omega$ protects the NMOS transistor from operating beyond its rated current. The NMOS drain terminal from each transistor is connected to an individual DMF electrode.

The voltage delivered to the DMF electrode depends on the control signal from the microcontroller. When a 5V digital signal from the microcontroller is applied to the NMOS gate terminal, a conductive channel is created be-

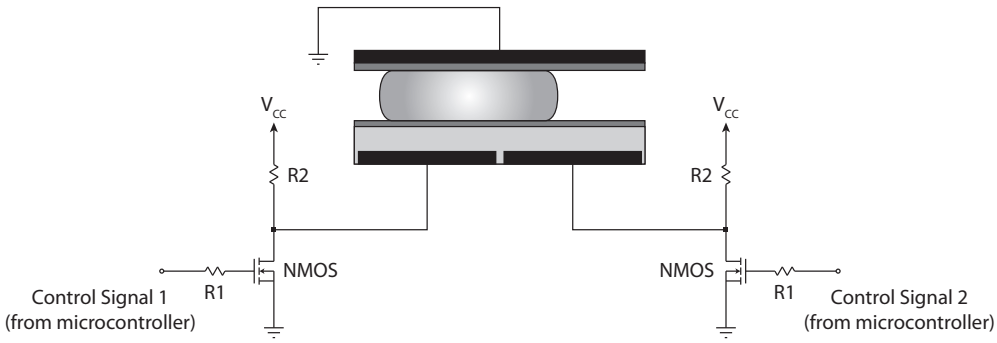

Figure 4.2: DC switch design and integration.

tween the NMOS drain and source terminals, and hence the voltage on the DMF electrode pulled down to 0V. The conductive channel is maintained as long as the voltage on the gate terminal of the NMOS transistor is above a threshold voltage. When the microcontroller brings the gate voltage to 0V, the conductive channel disappears and the voltage on the DMF electrode is pulled up to V_{cc}.

The response of the proposed DC switch was simulated in LTSpice before testing it experimentally. In the simulation, the control signal was a digital signal consisting of three identical pulses spaced 10ms from the next pulse with a pulse width of $10ms$. The external power supply voltage V_{cc} was set to 70Vdc. Fig. 4.3 plots the simulation voltage waveforms of the gate and drain terminals of the NMOS transistor. When the control signal voltage drops to zero, the output voltage of the NMOS drain terminal is pulled to 70Vdc as expected. The DC switch was built and tested experimentally with matching simulation and experimental conditions.

The microcontroller was programmed to generate the identical control signal from the simulation. The voltage on the external power supply was

set to 70Vdc. An oscilloscope was used to capture the voltage waveforms at the gate and drain terminals of the NMOS transistor. Fig. 4.4 plots the experimentally measured voltages from the gate and drain terminals of the NMOS transistor. Simulation results are in agreement with the experimental results. Furthermore, this experiment demonstrates the feasibility of amplifying a digital signal from a microcontroller which can be used for droplet actuation in DMF devices.

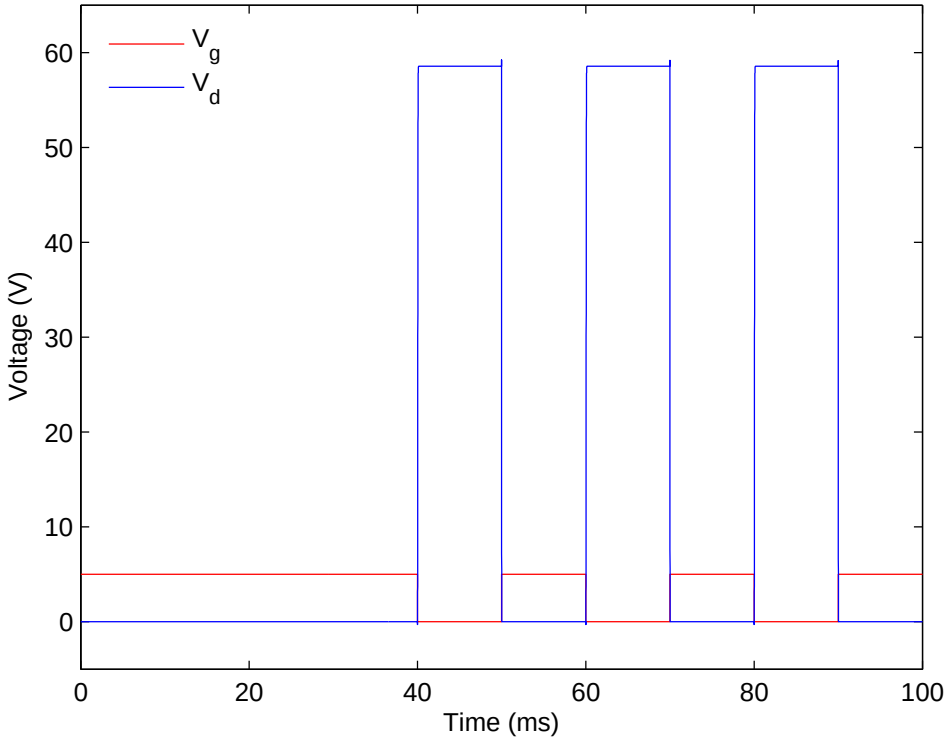

Figure 4.3: DC switch simulation results.

For completeness, the DC switch was tested with a real DMF device by actuating droplets back-and-forth across four electrodes. The fabricated

DMF device consisted of $2mm$ square electrodes spaced 10m from each other. The square electrodes were insulated with a $1.5\mu m$ layer of S1813 photoresist. The working surfaces of the upper and lower plates were coated with a $60nm$ layer of Teflon AF1600. De-ionized water droplets with a volume of $1.4\mu L$ were sandwiched between the upper and lower plates. The plate gap was measured with a micrometer to be $310\mu m$. The microcontroller was programmed to sequentially trigger four transistors each attached to an individual DMF electrode. The external power supply voltage was increased until the droplet was successfully actuated across all four electrodes.

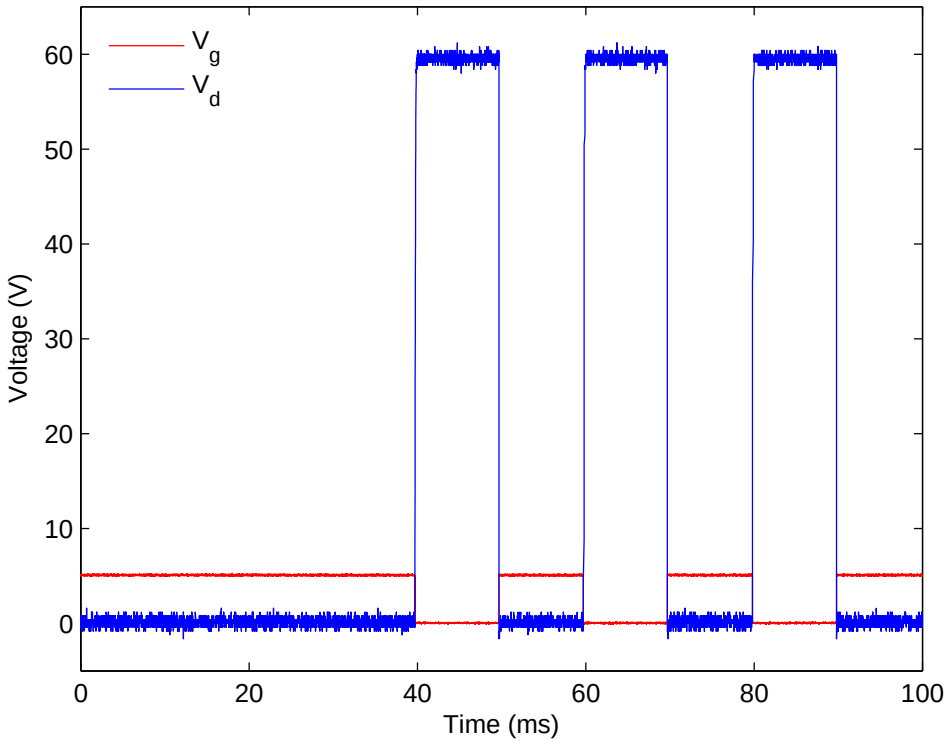

Figure 4.4: DC switch experimental results.

4.3.2 AC Voltage Switch

AC signals can also be used to actuate droplet in DMF devices as an alternative to DC signals. However, the voltage magnitude of AC signals for successful droplet actuation increases as the signal frequency increases [35]. AC signals are also difficult to create with a microcontroller that operates on digital signals. Therefore, the design calls for a bidirectional switch which can be triggered by a digital signal from the microcontroller. The AC switch is connected to an external AC power supply and care must be taken to isolate AC voltages from damaging the microcontroller. For this application an optoisolator was used.

An optoisolator couples the input and output ports via light, thus providing electrical isolation between the ports. The optoisolator transforms an electrical signal into a light signal which triggers a response on the output circuit. A typical optoisolator device contains a light source, a channel, and a photosensor. The light source is a light-emiting-diode (LED) which converts an electrical signal into a light signal. The channel is a medium for confining the light between the light source and the photosensor. The photosensor is a semi-conductor device whose resistivity is modulated by the light intensity.

Fig. 4.5 illustrates the integration of optoisolators for AC voltage actuation in DMF devices. The optoisolator used is this thesis is MOC3021M which can sustain up to 400Vac across its main terminal. A digital pin from the microcontroller is connected through resistor R1 to the input of the optoisolator. The resistance of $R_1 = 500\Omega$ to limit the current drawn

from the microcontroller pin. Resistor R_2 limits the current passing through the MOC3021M to prevent operating above rated conditions. The allowable resistance of R_2 is determined by the maximum rated current and off-mode output resistance of the optoisolator. The resistance of resistor R_2 was set to $200k\Omega$.

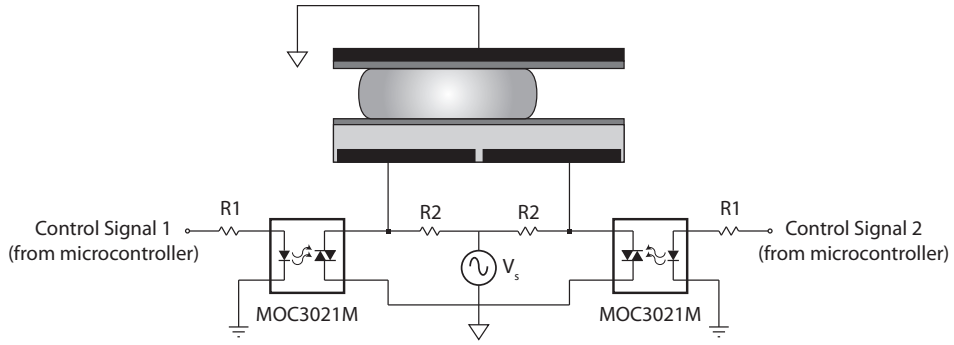

Figure 4.5: AC switch design and integration.

A DMF device was fabricated to experimentally test the AC switch. The bottom place had $2mm$ square electrodes spaced $10\mu m$ from each other. The S1813 photoresist was used as a dielectric layer for insulating the bottom plate electrodes. A $60nm$ layer of Teflon AF1600 coated the working surfaces of the upper and lower plate. De-ionized water droplets with a volume of $1.4\mu L$ were dispensed over the bottom plate and caped with the upper plate. The upper plate was positioned $310\mu m$ over the bottom plate.

The microcontroller was programmed to sequentially trigger four optoisolators to demonstrate continuous droplet actuation across four electrodes. Droplet actuation was noticed at 55Vac with a frequency of 500Hz. However, successful continuous droplet actuation across all four electrodes was possible at 60Vac and frequency 500Hz. In a different experiment, the

merging of two identical droplets was demonstrated with AC switches.

Although AC switches were successful in actuating droplets in DMF devices, DC switches were preferred method for actuation due to simpler implementation when attaching feedback sensors.

4.4 Capacitance Sensor

In Chapter 2, it was proven that the position of a droplet can be estimated from the capacitance values of two adjacent DMF electrodes. This section introduces a circuit that allows a microcontroller to accurately measure the capacitance values. A number of methods exist for measuring capacitance values including voltage divider, RC time constant, RC oscillator circuits, and IC capacitance sensors. However, RC oscillator circuits and IC capacitance sensors are practical methods that can easily be integrated with any microcontroller. Elbuken *et al.* [48] interfaced an IC capacitance sensor (AD7746) with a microcontroller via serial communication for detecting droplets in a continuous flow microfluidic device. The prepackaged IC capacitance sensor eliminates the need to design a sensing circuit; however the capacitance sensing resolution is limited by the number of bits. In this thesis, an RC oscillator circuit was designed for measuring capacitances in the resolution of DMF electrode capacitance. The RC oscillator consists of an inverting amplifier and a feedback circuit of resistors and capacitors. The output of an RC oscillator is a digital signal in the form of a square waveform whose frequency is a function of the capacitance. The frequency of the RC oscillator output signal can be measured using the counter module

in the microcontroller.

Two oscillator chips were investigated including a 555 Timer and Hex Schmitt Trigger inverter. The 555 Timer was preferred over Hex Schmitt Trigger inverter because of its higher operating bandwidth desirable for measuring very small capacitances of DMF electrodes. A 555 Timer is a multipurpose chip for generating accurate delay and oscillation signals. In this application, the 555 Timer is operated in the astable mode to generate an oscillating output signal whose frequency is a function of two resistors R_A and R_B and a single capacitor C. Fig. 4.6 shows the circuit network of resistors and capacitors for astable operation of 555 Timers.

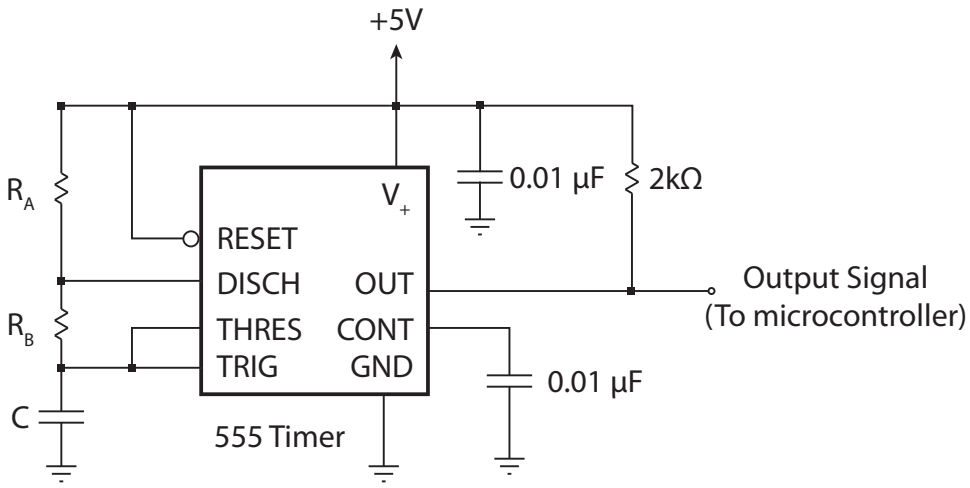

Figure 4.6: 555 Timer astable operation circuit.

In astable operation, the 555 Timer is self-triggered to invert its output signal when the voltage across the capacitor charges to the threshold-voltage level of $(2/3\ V_{cc})$ and discharges to the trigger-voltage level of $(1/3\ V_{cc})$. The

duty cycle of the output signal can be controlled by resistors R_A and R_B as

$$DutyCycle = \frac{R_B}{R_A + 2R_B}. \tag{4.1}$$

For an output signal duty cycle close to 50% with less than 0.5% error, resistors R_A and R_B must satisfy the following constraint where $R_B > 50R_A$.

The frequency of the output signal from the 555 Timer is related to resistors R_A and R_B and capacitor C as

$$f = \frac{1.44}{(R_A + 2R_B)C}. \tag{4.2}$$

Thus, if capacitor C is unknown, its value can be estimated using Eq. 4.2 by measuring the frequency of the output signal given the resistance of resistors R_A and R_B. The frequency of the output signal from the 555 Timer can be measured using a microcontroller by counting the number of positive edges in a given period. When measuring a small capacitance value, which is the case for DMF devices whose electrode capacitance is in the order of pico-Farads, it is recommended to have an output signal frequency in the order of $100kHz$ to reduce the noise and interference from the higher order harmonics in the measurements.

The capacitance sensor performance was simulated in LTSpice and verified experimentally. In the simulation, the power supply voltage V_{cc}, capacitor C, resistor R_A, and resistor R_B were set to 5V, $1nF$, $1k\Omega$, and $1M\Omega$, respectively. Using Eq. 4.2, the frequency of the output signal from the 555 Timer was estimated to be $719.64Hz$. From the simulation results, the output signal frequency was found to be $720Hz$. Fig. 4.7 plots

the simulation voltages of the trigger and output pins from the 555 Timer. As it was expected, the voltage on the trigger pin oscillates between the threshold-voltage level of $(2/3\ V_{cc} = 3.33V)$ and the trigger-voltage level of $(1/3V_{cc} = 1.67V)$. In addition, the output signal is toggled when either of the high or low voltage-thresholds is reached.

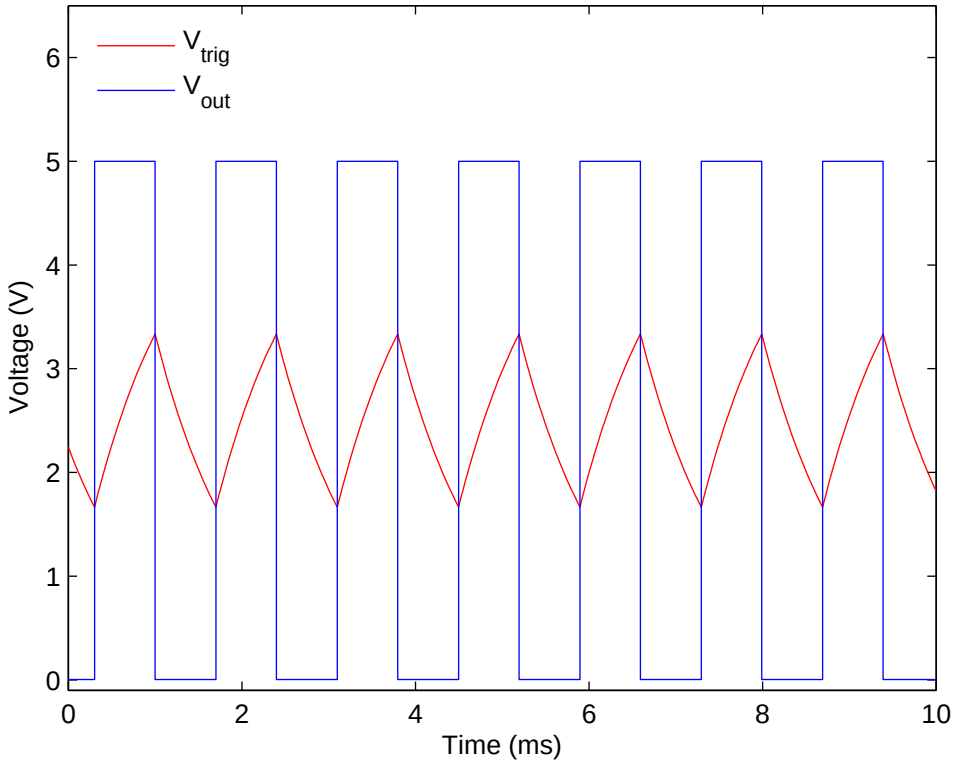

Figure 4.7: Simulation results of the trigger and output pin voltages from a 555 Timer in astable operation.

A similar circuit was built and tested experimentally. The resistors used for the experiment had a tolerance of $\pm 1\%$ while the ceramic capacitor had a tolerance of $\pm 10\%$. An oscilloscope was used to capture the voltages at

the trigger and output pins of the 555 Timer. Fig. 4.8 plots the measured voltages from the trigger and output pins of the 555 Timer. Simulation and experimental voltage waveforms are in agreement. Furthermore, the 555 Timer output signal frequency measured experimentally was $725Hz$ that is less than 1% different from the theoretical and simulation output frequencies. A simulate percent error of less than 1% was noticed when other known capacitor values were tested.

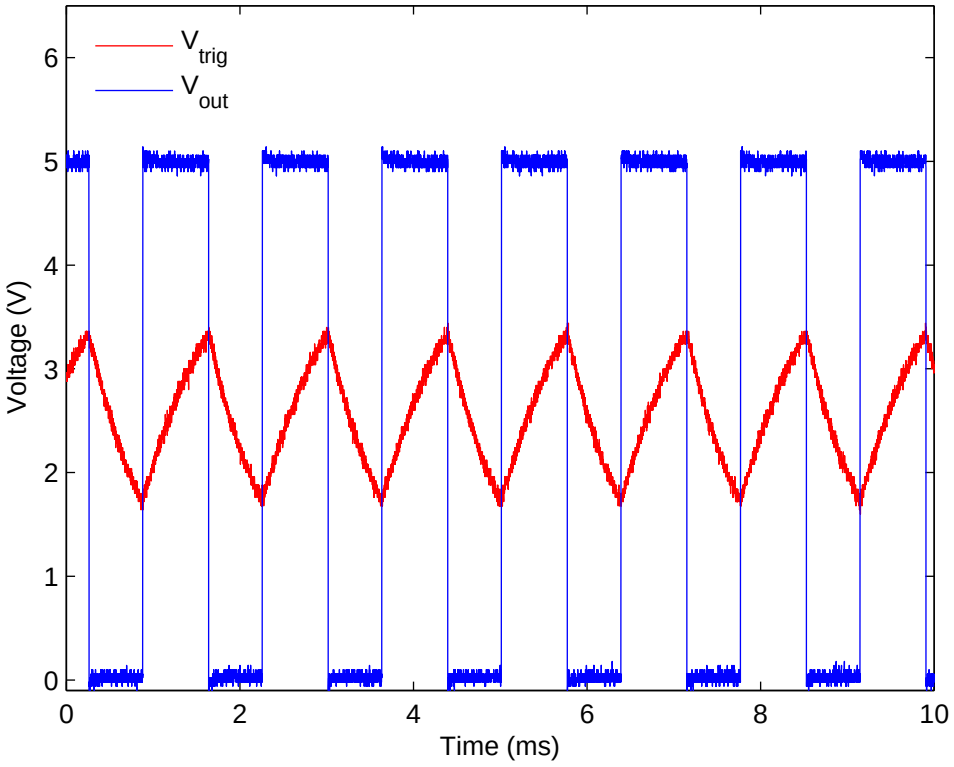

Figure 4.8: Experimental results of the trigger and output pin voltages from a 555 Timer in astable operation.

4.5 DMF Micro-Fabrication

This section describes the many challenges overcome in the process of fabricating DMF devices with basic fabrication facilities. The importance of electrode design, dielectric material selection, and device packaging are discussed. Finally, a detailed step-by-step fabrication recipe for DMF devices is presented.

4.5.1 Electrode Design

Successful operation of DMF devices heavily depends on the design of its electrodes. Careful considerations must be taken when designing the electrode shape and spacing. More precisely, the ability to move droplets depends on the actuation force that depends on the distribution of the electric field between the energized bottom plate electrode and the upper plate grounded electrode. A number of electrode shapes have been reported in the literature. These shape may be categorized in four classes including rectangular [5], interdigitated [10], one-way crescent [49], and two-way crescent [50]. Fig. 4.9 illustrates the four categories of DMF electrode shapes.

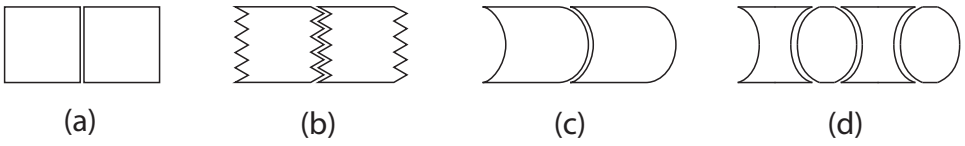

Figure 4.9: Electrode shapes (a) square, (b) interdigitated, (c) one-way crescent, and (d) two-way crescent.

Rectangular electrodes can be easily fabricated because they consist of sharp corners and straight edges. Rectangular shape is a common electrode

design, but the droplet volume is constraint such that the droplet footprint slightly overlaps adjacent electrodes. This slight overlap on adjacent electrodes is necessary to initiate the actuation of a droplet to the next electrode. For rectangular electrodes, it is desirable to minimize the electrode spacing to increase the droplet overlap on adjacent electrode required for continuous electrode actuation. Fig. 4.10 illustrates the importance of minimizing the gap between square electrodes. In Fig. 4.10a, it was not possible to successively actuate droplets beyond two adjacent electrodes because the square DMF electrodes were spaced $200\mu m$ apart. In contrast, successive droplet actuation across multiple electrodes was possible when the square electrodes were spaced $10\mu m$ apart (Fig. 4.10b). Ideally, the spacing between electrodes should be as small as possible to facilitate droplet transport.

Interdigitated electrodes increase the droplet overlap on adjacent electrode because each electrode extends into adjacent electrodes, thereby eliminating the linear gap that is present in rectangular electrode designs. Lienemann *et al.* [51] studied the effect of different interdigitated finger structures including sinusoidal, square, and triangular on the initial droplet motion. Despite this advantage, interdigitated electrodes are not commonly used since this design increases the fabrication complexity and risk of dielectric breakdown. Specifically, when compared to rectangular electrodes, interdigitated electrodes are harder to fabricate because the photoresist layer over the small finger structures is susceptible to pealing during the photoresist development process. Also, the finger structures are prone to undercut etching in the process of patterning the electrodes. Finally, the risk of dielectric breakdown is increased since the electric field is focused on sharp edges sim-

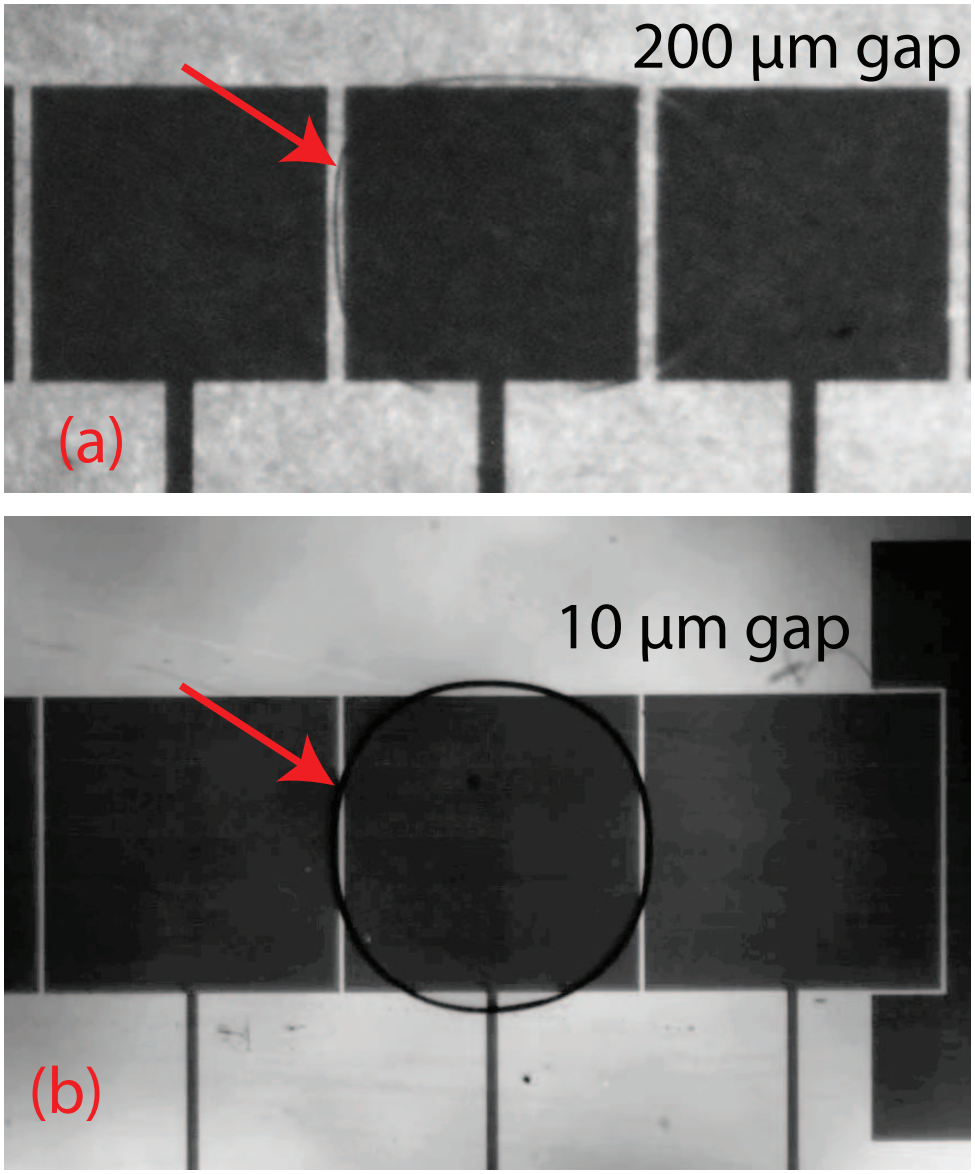

Figure 4.10: Droplet overlap and electrode gap. (a) $200\mu m$ electrode gap, (b) $10\mu m$ electrode gap.

ilar to those of the finger structures. Although, interdigitated electrodes improve droplet overlap and facilitate continuous electrode actuation, Kim *et al.* [10] reported that interdigitated electrodes are not necessary in most cases.

One-way crescent electrodes consist of two curved edges designed such that the electrode edges remain almost parallel to the three phase contact line when the droplet moves from one electrode to the next. This design is capable of achieving faster droplet velocities because it maximizes the droplet overlap on adjacent electrode when compared to the rectangular or interdigitated electrode designs. In addition, one-way crescent electrodes reduce the elongation of droplets because the actuation force is distributed over a larger portion of the droplet. One-way crescent electrode design has a simpler fabrication and has a lower risk of dielectric breakdown when compared to interdigitated electrodes. A drawback of this design is that the actuation force is maximized in one direction, but significantly drops in the opposite direction of droplet motion.

Two-way crescent improves on one-way crescent because it can maximize actuation force in either direction of droplet motion. It consists of two types of electrodes: concave-concave and convex-convex electrodes. The electrodes can be energized in sequence to form a one-way crescent shaped electrode that points to either direction.

In this thesis, a rectangular electrode design was used because of its simple design and easy micro-fabrication. The first fabricated devices were limited by the quality of photoresist and mask feature resolution. The bottom plate electrodes were patterned with a positive photoresist Photophosit

SP 24D. The photolithography masks were printed by a local printing shop with a maximum line width resolution of $100\mu m$ and 2880 X 1440 DPI. Under optimal fabrication conditions, the minimum feature size that was achieved was limited to $200\mu m$ and the device fabrication repeatability was quite low. In particular with the large gap between electrodes, continuous droplet actuation was difficult to achieve due to insufficient droplet overlap.

The next set of DMF devices were fabricated with feature sizes ranging from $10 - 50\mu m$ in a non-clean room environment. The masks were printed by CAD/Art Services with a minimum feature size of $10\mu m$ at 25400 DPI. A better positive photoresist was used to pattern bottom plate electrodes. The S1813 positive photoresist had a higher aspect ratio and allowed smaller features be achieved. Equipped with a finer mask and superior photoresist, $10\mu m$ features were easily fabricated with excellent repeatability and no cleanroom.

4.5.2 Dielectric Material Selection

The ideal dielectric material for DMF devices is the one that has a high dielectric constant as well as a high breakdown voltage and can easily be processed (preferably spin coated) onto a sub-micron thick layer over the bottom plate electrodes. A high dielectric constant is desirable because it can contain a stronger electric field density generating a larger actuation force at lower voltages. Reducing the voltage is essential for realizing the full potential of DMF technology in micro-total analysis systems, lab on a chip technology and point of care devices. The breakdown voltage of the dielectric material must be high enough to enable droplet actuation without

arcing effect (or surge of current) through the dielectric material particularly in thinner dielectric layers.

An important objective in this thesis was to fabricate a practical DMF device using basic lithography and spin coating fabrication equipment to minimize cost and fabrication time. Three dielectric materials applied with spin coating processes were used including Polydimethylsiloxane (PDMS), CyanoethylPullulan (CEP), and recently S1813 photoresist.

PDMS is a two part formula with a base and a currant. Typically, the base material and currant material are mixed at a 10:1 ratio; however, it is not limited to only these proportions. A lower base to currant ratio will yield a stiffer dielectric and may be suitable for other applications. The parts are mixed thoroughly to yield a homogenous solution in a vortex mixer. As a result of mixing many miniscule bobbles are trapped within the solution, which can be removed in a vacuum chamber. Then, the PDMS solution is quickly spin-coated over the slides because the curing time of PDMS. Delayed spin coating thickens the PDMS to a point where it would not spread evenly over the slide. Proper mixing is critical for having a homogeneous PDMS solution. Previously, the PDMS solution was mixed manually and then spin coated. As a result, some partially uncured patches of PDMS appeared on the substrate leaving weak spot on the dielectric surface that can readily be scratched or peeled. Vigorous mixing resolves this issue but introduces air bubbles in the PDMS solution which must be removed in a vacuum chamber before coating. In the end, the PDMS layer was a clear, rubber-like thin film with a very stable surface that could resist scratches and adheres well to the substrate.

CEP was another spin coating material reported by Biddut *et al.* [52]. CEP comes as solid pellets that must be dissolved in a solution of N,N-Dimethylformamide prior to use as a dielectric material. CEP pellets take a few days to dissolve completely, however, the result is a clear viscous liquid that can be spin coated over a substrate. After spin coating, the CEP liquid layer is dried by baking the substrate at 100 °C for 1 hr. The motivation for using CEP over PDMS is that droplets can be actuated at lower voltages because CEP has a higher dielectric permittivity when compared to PDMS. In addition, the CEP liquid solution has longer shelf life than the PDMS solution after mixing the base and a currant. Although CEP is an improvement over PDMS, an objective of this thesis was to optimize the fabrication process of a DMF device by eliminating the need for specialized dielectric materials.

It was found that the S1813 photoresist can also be used as a dielectric material as reported by Newton *et al.* [53]. Newton *et al.* [53] used S1813 as a dielectric layer and demonstrated the actuation of micro-spheres in open DMF systems. S1813 photoresist is a positive photosensitive liquid that is commonly used for microfabrication. Specifically, S1813 photoresist was used for the fabrication of the bottom plate electrodes by photolithography. This photoresist comes in liquid form directly from the supplier and ready, unlike the previously mentioned spin coated dielectric materials. The class of S1800 photoresists has been documented extensively to include accurate photoresist layer thicknesses at various spin coating speeds. In addition, S1800 photoresists have excellent coating uniformity properties desirable for digital microfluidic devices because flat surfaces facilitate the actuation of

droplets. In this thesis, S1813 was used as a dielectric layer for DMF devices. The processing of S1813 as a dielectric involves spin coating directly over the bottom plate electrodes and hardening by baking at 100 °C for 10 minutes. In droplet actuation experiments, reversible EWOD is possible with repeatable results. The threshold voltage for the actuation of DI water droplets in an air filled DMF device with 2mm square electrodes with a $1.3\mu m$ thick layer of S1813 photoresist was 50Vdc. Lower droplet actuation threshold voltages are possible when using less viscous S1800 photoresists like S1805 to achieve smaller dielectric layer thicknesses. The dielectric strength of S1813 was not investigated, however in droplet splitting experiments voltages around 150Vdc have been used on a $1.3\mu m$ thick S1813 dielectric layer. The dual purpose of S1813 as both a photoresist in the fabrication of bottom plate electrodes and a dielectric layer for EWOD droplet actuation dramatically reduces fabrication time and material costs. A digital microfluidic device can be fabricated in less than 35 minutes because the dielectric material S1813 does not need to be processed.

4.5.3 Device Packaging

Device packaging is referred as the mechanical process of interconnecting external wires to the millimeter-scale electrode contact pads in a DMF device. This is the last process before attaining a fully functional DMF device because it enables external macro-devices full control of the droplets. Three approaches have been used in this thesis to attach external wires to electrode contact pads which are classified by as mechanical, adhesive, or solder contact.

Mechanical contact was the first technique used in early experiments. One approach was place a wire in contact with an electrode pad and fix-in-place with a strip of tape. Though this approach is quite feasible for a small number of electrodes, it becomes logistically harder to attach additional wires as the number of electrodes increases. Besides, the major issue was false contact where the external wire does not conduct electricity to the electrode on the DMF device. Often, oily fingerprints or tape adhesive between the external wire and the electrode pad resulted in a false connection. Above all and more commonly, handling the external wires during the experiments was cumbersome as they can be easily decoupled.

Another mechanic contact approach was to use a PCI (Peripheral Component Interconnect) connector from a computer as shown in Fig. 4.11. The PCI connector has two rows of spring loaded electrodes that press against both sides of a PCI card. The spring loaded electrodes of the PCI connector can be accessed through the bottom of the PCI connector via the pins. To accommodate a DMF device, the PCI connector must be trimmed to remove bridges which are used to guide and secure a PCI card. Unlike the previous mechanical contact approach, the device was fully secured within the PCI connector and false contact was not an issue due to the tight fit. In addition, higher electrode pad densities could be accommodated easily by properly designing the electrode pads on the DMF device. On the other hand, a drawback was the tight fit of the microscope slide in the PCI connector as the sharp glass edges would irreversibly damage some spring loaded electrodes in the PCI connector. Also, the spring loaded electrode of the PCI connector can scratch the thin copper layer of the electrode pads on the

DMF device. The biggest drawback was the lack of suppliers of PCI connectors that provide small quantities. The few PCI connectors that were used where stripped from an old computer motherboard by mechanical means.

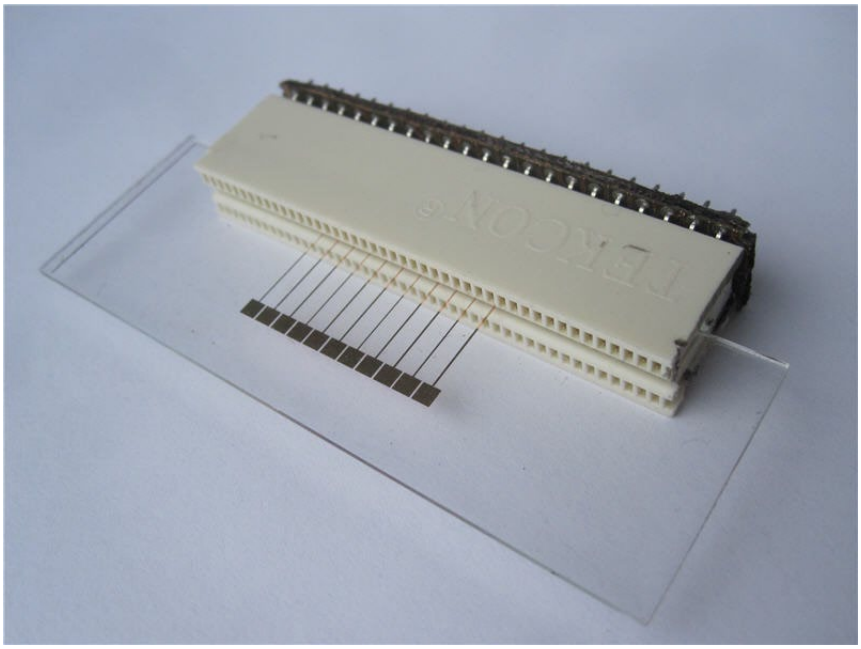

Figure 4.11: DMF device inside a PCI Connector.

Adhesive contact involved using a conductive adhesive to attach an external wire onto an electrode pad in a DMF device. The conductive adhesive used was a 2 part epoxy enriched with silver particles. The conductive resin was formed by mixing equal parts of the epoxy. The resin was spread over an electrode pad and an external wire was placed and fixed over the electrode pad. This approach has two limitations: i) the cost of the silver epoxy and ii) handling of the viscous resin.

Solder contact was the most reliable contact that was used but care must be taken to minimize the damage on the electrode pads. In the first

attempts, an external wire was soldered directly onto an electrode pad of a DMF device at the lowest solder melting temperature of 250 °C. The high melting temperature of solder caused significant damage to the DMF electrode pad. The excess heat burned away the 45nm copper layer of the DMF electrode pad which resulted in a weak and brittle solder bond. More precisely, the bond failed abruptly upon handling the rigid external wire. An improvement was to use an intermediate length solder wire between the rigid external electrode and the DMF electrode pad as shown in Fig. 4.12. The solder wire is quite malleable and can sustain large deformations reducing the stress on the weak bond. In addition, a quick curing liquid adhesive can be applied around the solder bond for strengthening.

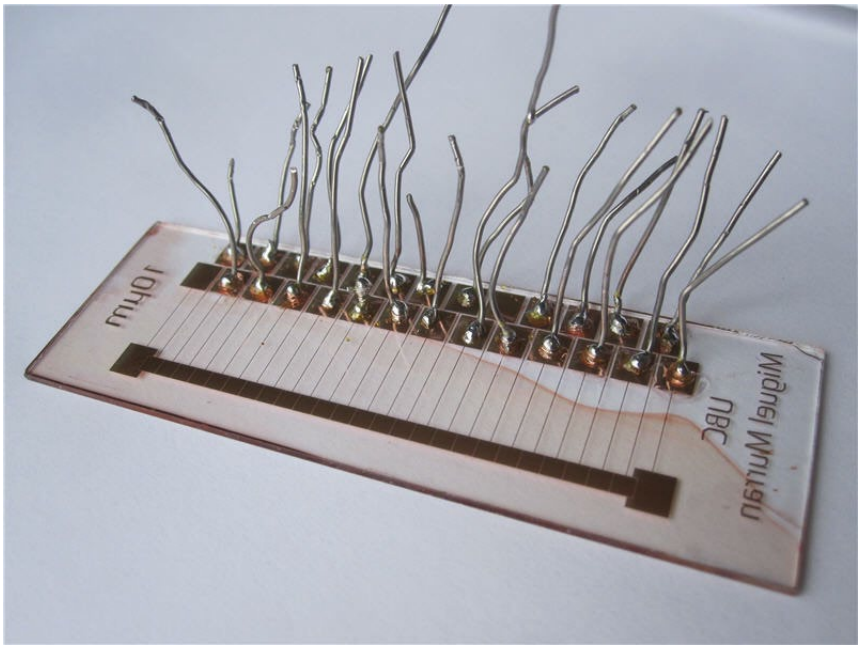

Figure 4.12: Solder wires bonded onto electrode pads in a DMF device.

4.5.4 Fabrication Recipe

The fabrication process for DMF devices is illustrated in Fig. 4.13. In addition, step-by-step instructions of the fabrication process are summarized below.

1.0 Resist Coating (S1813 Positive Resist)

- 1.1 Spin coat photoresist at $v = 3500rpm$, $a = 500rpm/s$ for 26 seconds
- 1.2 Heat substrate to $T = 100\,^{\circ}\mathrm{C}$ for 1 minute to harden resist

2.0 Resist Patterning ($350 - 450nm$ UV light)

- 2.1 Place mask flat over photoresist layer
- 2.2 Expose substrate to $350 - 450nm$ UV light at a distance of $10cm$ for 5 minutes

3.0 Resist Developing (MF-319 Developer)

- 3.1 Rinse substrate in MF-319 developer solution for 1 minute until pattern is revealed
- 3.2 Rinse substrate in DI water to stop the developing process

4.0 Copper Etching (Ferric Chloride)

- 4.1 Rinse substrate in diluted etchant solution (ferric chloride to DI water 1 droplet : $10mL$)
- 4.2 Rinse substrate in DI water to stop etching process

4.3 Air blow substrate until dry

5.0 Dielectric Layer (S1813 Positive Resist)

5.1 Spin coat photoresist at $v = 3500rpm$, $a = 500rpm/s$ for 26 seconds

5.2 Bake substrate to 100 °C for 10 minutes

6.0 Dielectric Layer (PDMS)

6.1 Prepare PDMS solution (Base to Currant $10 : 1$ by volume) in Vortex Machine

6.2 Vacuum PDMS solution for $3060min$ at room temperature $T = 22$ °C to remove air bubbles

6.3 Spin coat PDMS solution at $v = 5000rpm$, $a = 500rpm/s$ for 36 seconds

6.4 Bake substrate to $T = 100$ °C for 2 hours

7.0 Hydrophobic Layer (Teflon AF1600)

7.1 Prepare Teflon solution (Teflon AF1600 to FC-40 Solvent $1-3\%$ of final weight)

7.2 Spin coat Teflon solution $v = 2000rpm$, $a = 500rpm/s$ for 26 seconds

7.3 Bake substrate to T = 120 °C for 5 minutes

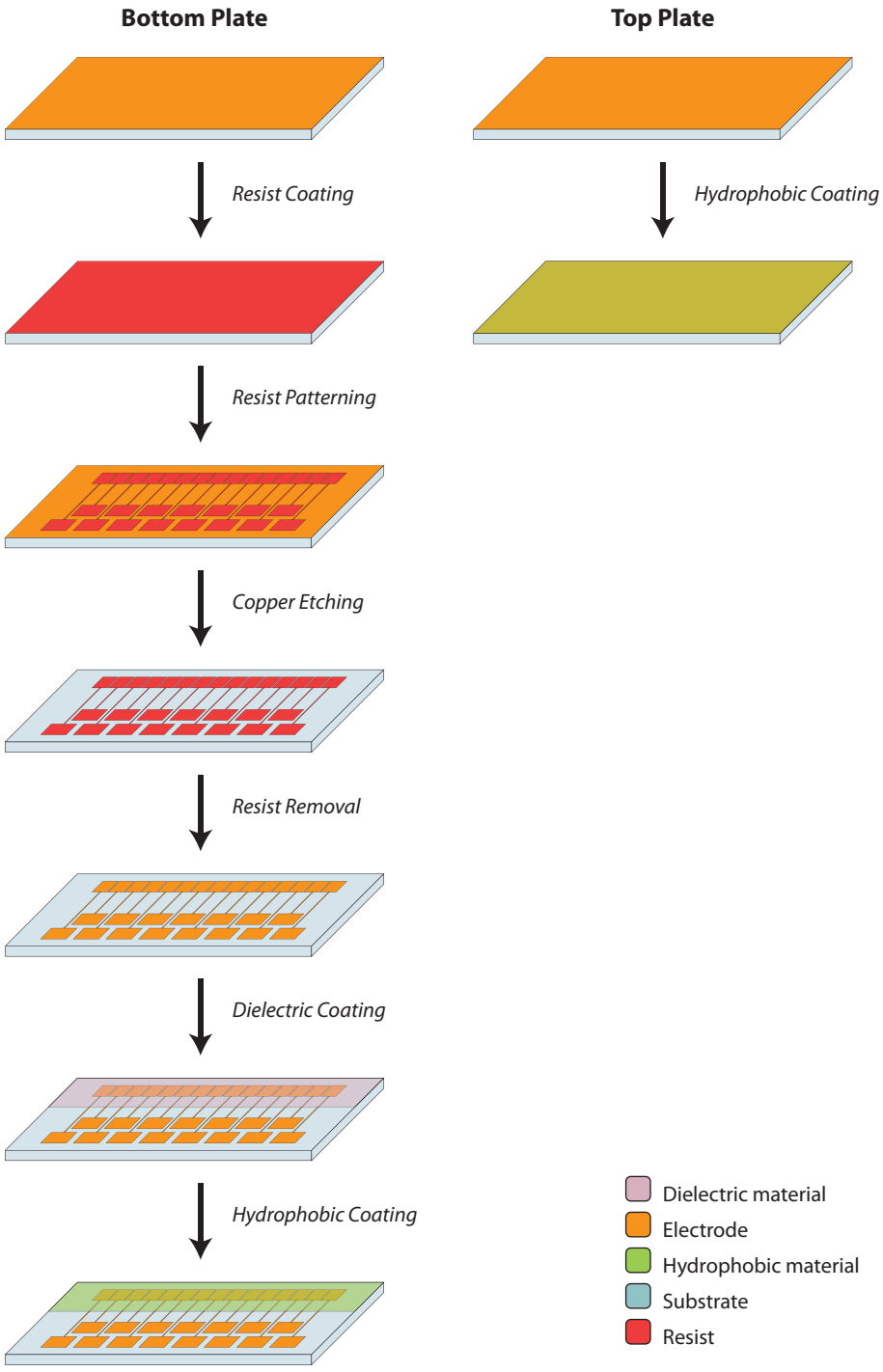

Figure 4.13: Fabrication process for DMF devices.

4.6 DC Pulse Train Actuation

The actuation of droplets on DMF devices with DC voltage typically involves the application of a single DC pulse of sufficient duration to achieve complete droplet transport to the adjacent electrode. Larger droplet displacements are achieved by sequentially applying a single DC pulse to the next electrode. Fig. 4.14 illustrates the progression of single DC pulses to a sequence of adjacent DMF electrodes to induce a continuous droplet transport across a DMF device.

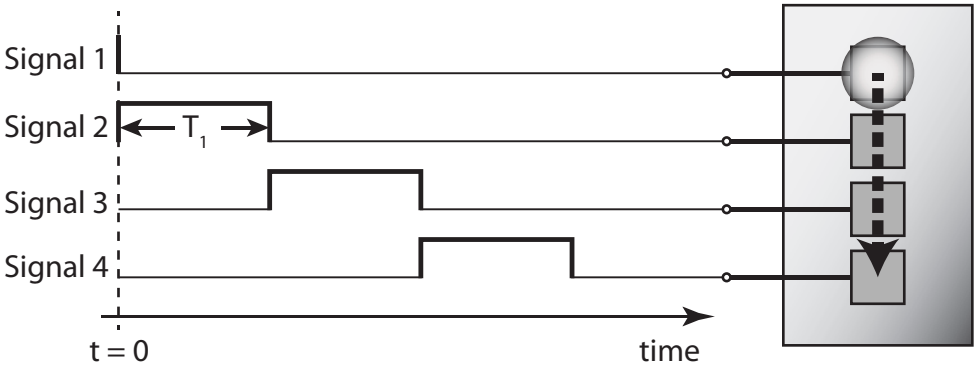

Figure 4.14: Continuous droplet transport actuation sequence using a single DC pulse.

When a single DC pulse is applied to a DMF electrode adjacent to a droplet, the droplet rapidly accelerates toward the energized DMF electrode because the actuation force is continuous and non-linear during the entire pulse width. The only stable droplet positions are limited to the position of DMF electrodes because the net actuation force is minimized when a droplet resided over the energized electrode. Attempting to position droplet between DMF electrodes an unstable position is a difficult task because the

inertia of the droplet results in position overshoot. Therefore, single DC pulse actuation offers limited control over position and speed of the droplet when fixing the voltage magnitude.

An alternative DC actuation technique referred to as DC pulse train actuation offers greater droplet position and speed controllability even though the actuation voltage is still fixed. In DC pulse train actuation, a single DC actuation pulse is divided into many small pulses that collectively displace a droplet from one DMF electrode to the next as shown in Fig. 4.15.

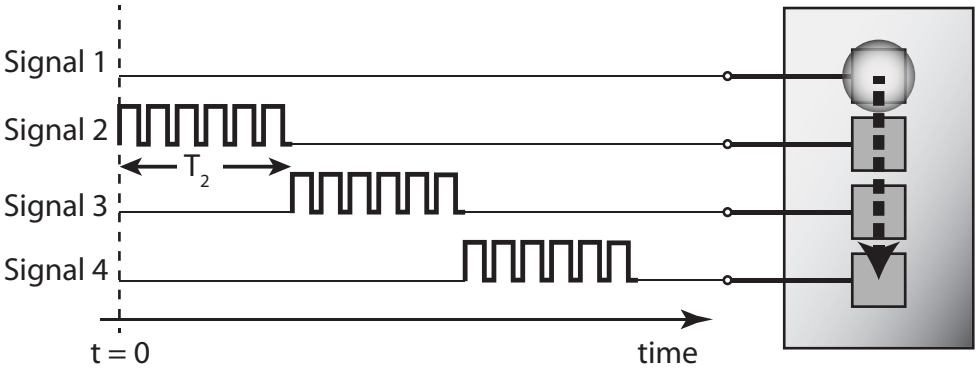

Figure 4.15: Continuous droplet transport actuation sequence using sequential DC pulses.

Each individual pulse has a high-voltage-level duration followed by a low-voltage-level duration. The ratio of high-voltage-level duration to the pulse duration is the pulse duty cycle. In the time interval of high-voltage-level, voltage is applied to a DMF electrode which generates an actuation force that momentarily displaces the droplet. In the time interval of low-voltage-level, the actuation force disappears as the voltage of the DMF electrode is reduced to 0V, and the droplet rolls to a stop due to opposing resistance forces. If the pulse frequency is sufficiently high typically greater than

$100Hz$, then the droplet motion appears to be continuous. The sequential train of small DC pulses enables the incremental droplet displacement desirable for intra-electrode positioning as well as regulating the non-linear droplet speed.

A DMF device was fabricated to demonstrate DC pulse train actuation. The DMF device contained a linear array of $2mm$ square electrodes spaced 10m from each other. The dielectric material was a $1.5\mu m$ thick layer of S1813 photoresist over the square electrodes. A $60nm$ layer of Teflon AF1600 was coated over the ground electrode of the upper plate and the dielectric layer of the bottom plate. A De-Ionize water droplet with a volume of $1.4\mu L$ was dispensed over a square electrode and caped by the upper plate. The upper plate was positioned $310\mu m$ from the bottom plate.

The proposed control system consisting of a microcontroller and a set of DC switches was used to verify the efficacy of DC pulse train for droplet actuation in a DMF device. The microcontroller was programmed to energize four electrodes sequentially and move the droplet from one end to another back and forth. The actuation signal applied to each DMF electrode is a train of pulses where each pulse had a period of $10ms$. The DC switches were attached to a 120Vdc power supply whose voltage was regulated to achieve complete droplet transport across four DMF electrodes.

Droplet displacement was noticed at 50-55Vdc, but it was not possible to successively actuate the droplet beyond two DMF electrodes as the droplet had little inertia to roll onto the adjacent electrode. Fig. 4.16 shows time-lapse frames at intervals of $100ms$ of droplet transport across four DMF electrodes with DC pulse train actuation. The frames where extracted from

a video (30 frames/sec) of droplets being moved to adjacent DMF electrodes with 70 pulses where each pulse had a voltage magnitude, period, and duty cycle of 60.2Vdc, $10ms$, and 90%, respectively.

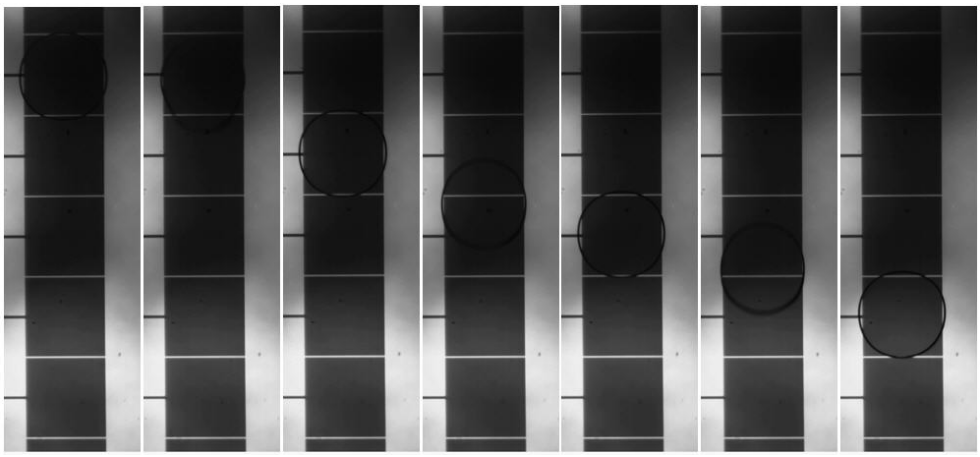

Figure 4.16: Video frames of a $1.4\mu L$ DI water droplet moving from top-to-bottom across four successive electrodes at $100ms$ intervals. View is looking down at the droplet through the copper ground electrode. The actuation signal applied to each electrode consisted of 70 pulses each with a $10ms$ period, 90% duty cycle, and voltage magnitude of 60.2Vdc.

The effect of different pulse duty cycles on the droplet speed was investigated in the maximum switching frequency versus voltage plots proposed by Fair *et al.* [13]. The maximum switching frequency for a fixed voltage magnitude is the maximum rate at which the actuation signal can be switched to the next DMF electrode for successive droplet transport. The maximum switching frequency corresponds to the minimum period of time that the droplet needs to transfer to the adjacent electrode completely and immediately before it can be actuated to the next electrode. Fig. 4.17 plots the maximum switching frequency as a function of applied voltage for different

pulse duty cycles where the pulse period was fixed at $10ms$. Experimental results indicate that the maximum switching frequency at a fixed voltage magnitude increases with an increase in the pulse duty cycle. In the extreme case where the duty cycle approaches 100%, the train of individual $10ms$ pulses combine to form a single pulse that generates a continuous and non-linear actuation force with the fastest droplet transport speed for a given actuation voltage. As the pulse duty cycle decreases to near 0%, the actuation force is momentarily applied at fixed time intervals of high-voltage-level. During low-voltage-level time intervals the droplet transport speed slows down due to opposing resistance forces. The DC pulse train actuation is a feasible approach to regulate the droplet transport speed.

An observation from DC pulse train actuation that worth noting was that the DC pulse train actuation can reduce the droplet deformation during actuation. Droplet deformation is greatest during initial actuation as the actuation force is focused on a small portion of the droplet. Fig. 4.18 (a) and (b) are video frames that capture the deformation of a droplet caused by the actuation force. The pulse voltage magnitude and period is similar for both figures, but the pulse duty cycle for Fig. 4.18a was 80% while the pulse duty cycle for Fig. 4.18b was 20%. The figures visually confirm that a higher duty cycle results in faster droplet transport speed consistent with earlier experimental results. Furthermore, larger droplet deformation was observed in Fig. 4.18a than in Fig. 4.18b. The reason is that lower pulse duty cycles allow more time for the droplet to assume a quasi-equilibrium transport process when compared to higher pulse duty cycles. The impact of pulse duty cycle on droplet deformation is important to this thesis because the

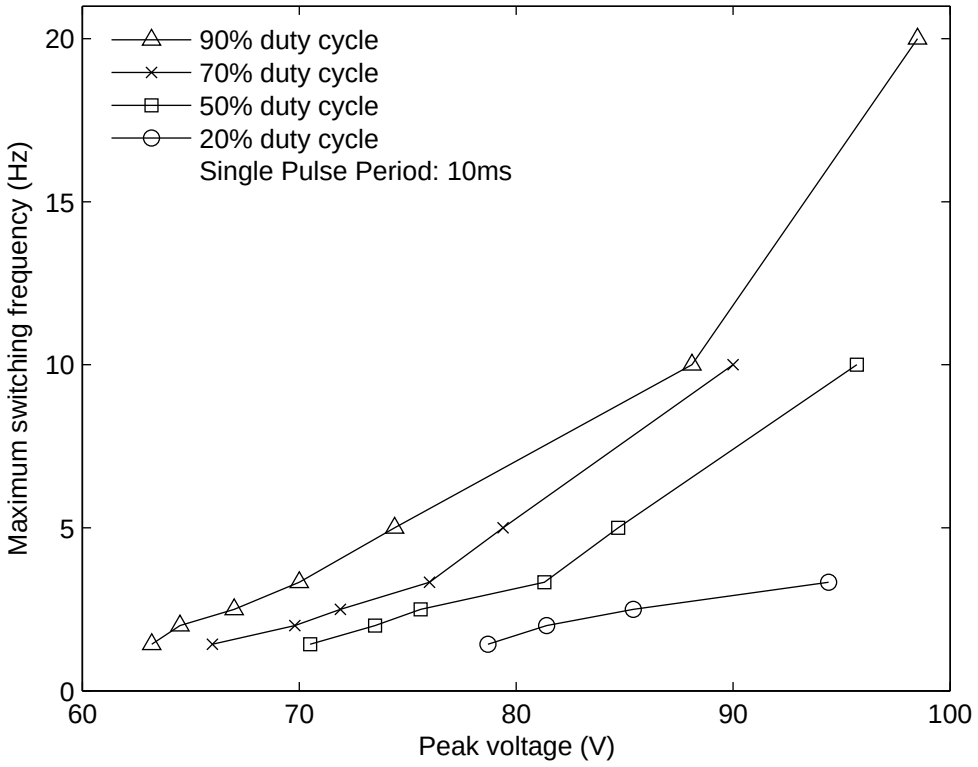

Figure 4.17: Pulse duty cycle effect on the maximum switching frequency for a 1.4μL DI water droplet as a function of peak voltage.

accuracy of the proposed droplet position sensing is affected as the droplet shape deviates from a circular shape. These visual observations support the assumption made in Chapter 2 that droplet deformation are minimal during normal droplet transport speeds (or low pulse duty cycles). In other words, the estimation of the droplet position using the proposed capacitance measurement approach is not limited to stationary droplets, thus a control system can operate faster which is required for continuously moving droplets.

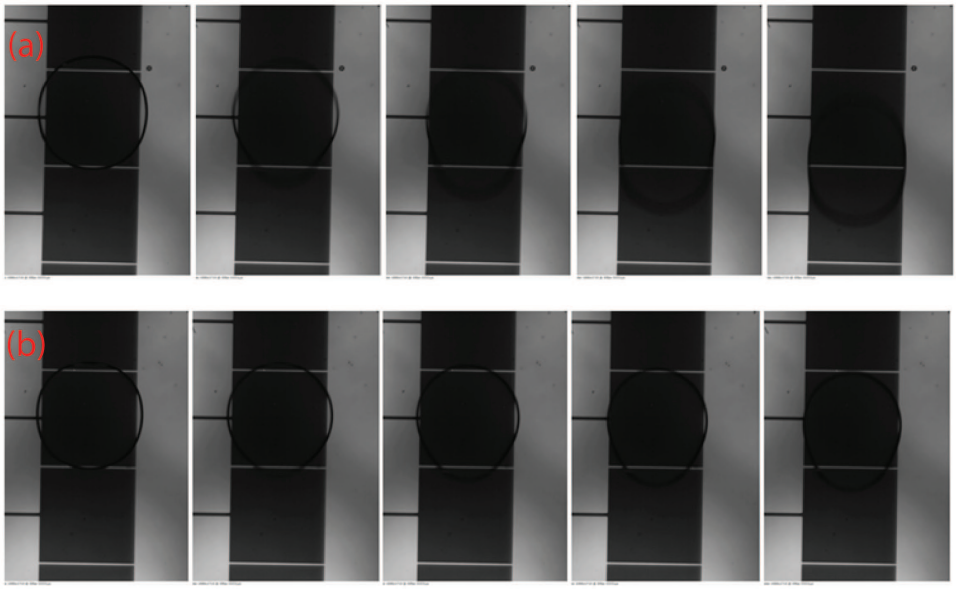

Figure 4.18: Video frames of a $1.4\mu L$ DI water droplet during initial actuation at $33.3ms$ intervals. View is looking down at the droplets through the copper ground electrode. The pulse voltage magnitude was 73Vdc and period was $10ms$ is common for both (a) and (b). The only difference is that in (a) the pulse duty cycle was 80% and (b) the pulse duty cycle was 20%.

4.7 Intra-Electrode Droplet Positioning

Positioning droplets between electrodes in a DMF device is important for a range of droplet operation such as transport, splitting and mixing, but it is difficult without a fast and accurate control system because of the unstable position of the droplet in between electrodes. When applying a voltage to an electrode, droplets are pulled towards the energized electrode until they reach a stable position where the actuation force is balanced which occurs when a droplet resides directly over an electrode. In order to achieve intra-electrode droplet positioning, droplet position feedback is required to incrementally displace a droplet back-and-forth until the droplet reaches the desired position. The DC pulse train actuation was found feasible for intra-electrode droplet positioning because a single pulse displaces the droplet slightly towards the energized electrode. The control system for intra-electrode droplet positioning must therefore locate the position of a droplet and then decide which electrode (leading or tailing) to energize. The position of the droplet can be determined using the capacitance-based approach described in Chapter 2 of this thesis. The capacitance-based droplet position sensing involves integrating a capacitance sensor which can detect the changes in capacitance of an electrode in a DMF device. The circuit for integrating the capacitance sensor with the proposed programmable control system is illustrated in Fig. 4.19.

Several challenges must be addressed to achieve a working feedback control system. The first challenge is connecting the feedback sensor circuitry to the DMF electrodes to which voltages greater than 50V are applied. The

feedback sensor has a 555 Timer chip which is rated for voltages less than 15V. However, greater voltages are required to actuate the droplet. A practical solution was to use coupling capacitors (denoted as C_1 in Fig. 4.19). The coupling capacitors allow the free passage of high frequency AC signals from the feedback sensor to the DMF electrode. While low frequency signals such as the actuation signal from the DC switch are blocked from damaging the 555 Timer chip due to the high impedance of the capacitor at low frequencies.

Coupling capacitors work well at blocking DC voltages which change slowly. However, in this application, the actuation signal is a DC pulse that contains high frequency transient signals to create the sharp edges of a pulse. These transient signals create voltage spikes with magnitudes greater than the rated voltages of IC. Therefore, these voltage spikes must be mitigated to avoid damaging the delicate IC components. Electro-Static Discharge (ESD) protection circuits are commonly used to reduce voltage spikes (electrostatic discharge). The ESD protection circuit used is high-speed dual-rail clamp diodes. It consists of two high-speed diodes (1N914) and a Zener diode (1N4733). Two regular diodes clamp the feedback signal line to the ground and to the positive 5V power rail. A positive voltage spike drains through the diode connected to the positive 5V rail and down the Zener diode. A negative voltage spike is pulled to the ground by the diode connected to the ground. Although a single Zener diode may be used to protect the IC components, the Zener diode response time is slower than the high-speed diodes.

The magnitude of the coupling capacitors C_1 must be chosen carefully

as its presence affects the capacitance measurements because it is in series with the capacitance of a DMF electrode. The feedback sensor will measure the equivalent capacitance of the coupling capacitor C_1 in series with the capacitance of a DMF electrode C_{DMF}. The magnitude of C_1 must be larger than C_{DMF} so that the equivalent series capacitance is approximately equal to C_{DMF}. On the other hand, the size of C_1 cannot be too large because the capacitor charge time increases leading to a slower droplet actuation sequence. In this thesis, C_1 was chosen to be four times larger than the maximum capacitance value of C_{DMF}. The magnitude of C_{DMF} varied from $29.1pF$ when no droplet is present to $60pF$ when a DI droplet is completely overlapping the DMF electrode. Therefore, C_1 was chosen to be $200pF$.

Finally, a large resistor R_3 is required between the DC solid state switch and the DMF electrode to avoid shunting the DMF electrode capacitor when the NMOS is in "On" mode (or conduction path exists between the drain and source terminals). This issue is not present when the NMOS transistor is in "Off" mode because the drain resistor R_2 provides a high-impedance path to ground at V_{CC}. Without resistor R_3, the bottom plate DMF electrode is grounded by the NMOS transistor when it is in "On" mode and the coupled AC signal from the feedback sensor would not pass through the DMF electrode capacitor of interest. As a result, the feedback sensor would measure the capacitance of the coupling capacitor. The magnitude of resistor R_3 must be much larger than resistor R_B to avoid interfering with the discharge time constant that affects capacitance measurements. Resistor R_3 was chosen to be $200k\Omega$ which is four times larger than resistor R_B which was set at $50k\Omega$. Resistor R_A was set at $1k\Omega$ that is much smaller than

resistor R_B to achieve an output square waveform from the 555 Timer with 50% duty cycle.

The analog switch (TS12A4515P) enables one to measure the capacitance of one or two DMF electrodes with one capacitance sensor.

Fig. 4.20 shows the operational flowchart of the intra-electrode droplet control system. The control system first determines the position of the droplet then energizes the appropriate electrode until the droplet arrives at the desired position. The droplet position is estimated from the capacitance of two electrodes as detailed in Chapter 2. If the estimated droplet position is within an allowable error from the desired position X_{ref}, the pulse train is terminated. However, if the desired position is further than the estimated position DC pulses are applied to the leading electrode such that it displaces the droplet towards the desired position. Finally, if the droplet has for any reason overshot beyond the desired position, DC pulses are applied to the tailing DMF electrode to recede the droplet. An overshoot is however unlikely to occur in pulse train actuation mode with small duty cycles.

A DMF device was fabricated to test the proposed control system featuring the proposed intra-electrode droplet positioning and the pulse train actuation technique. The bottom plate consists of a linear array of $2mm$ square electrodes spaced $10\mu m$ apart. The square electrodes were coated with $1.5\mu m$ of S1813 photoresist followed by a $60nm$ of Teflon AF1600. The upper plate was a continuous electrode coated with $60nm$ of Teflon AF1600.

Droplets of $1.4\mu L$ DI water were dispensed over two square electrodes and the upper plate was fixed $310\mu m$ from the bottom plate. The electrical circuit from Fig. 4.19 was built and attached to the electrodes beneath

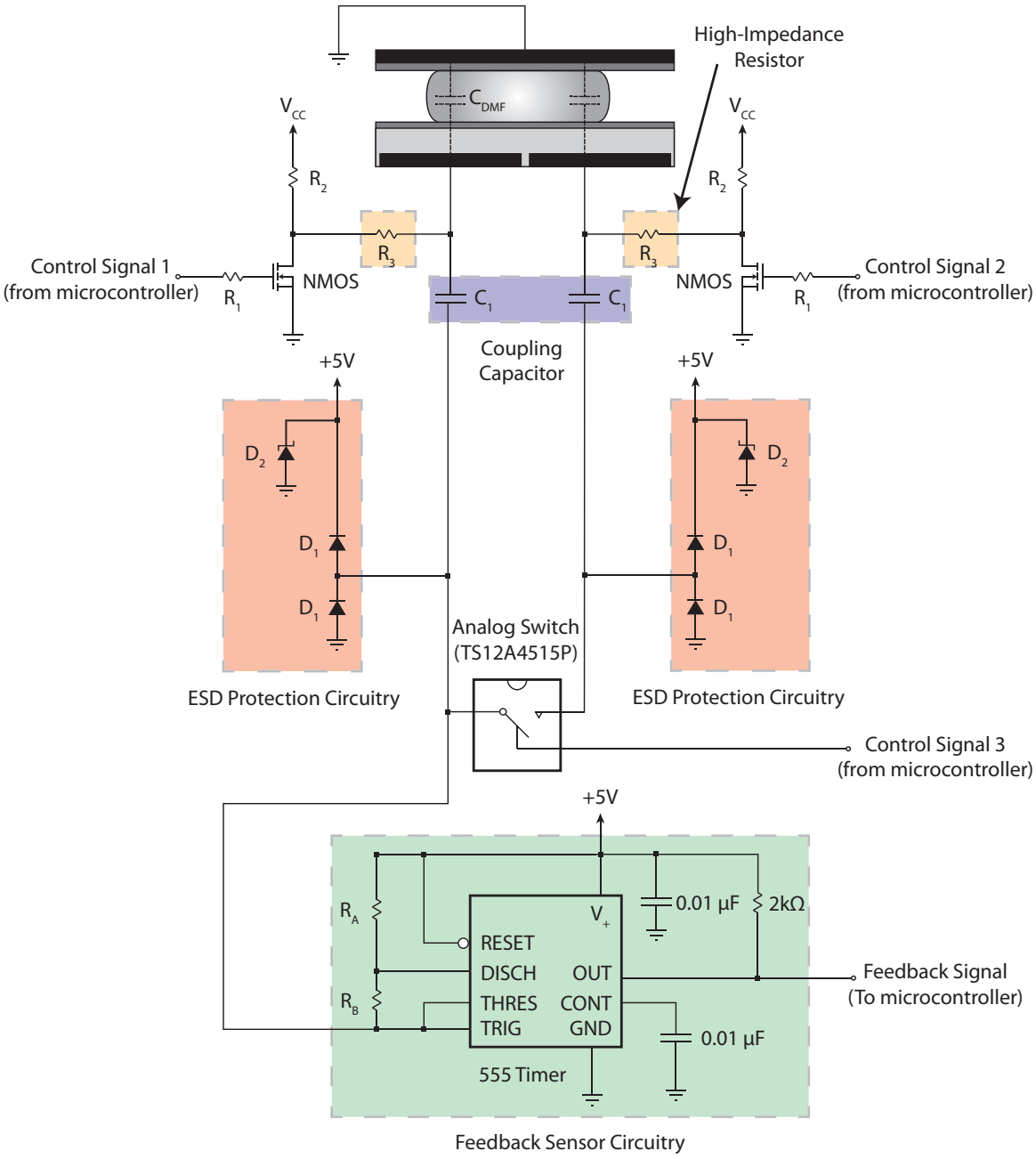

Figure 4.19: Feedback control system circuit for intra-electrode droplet positioning in DMF devices.

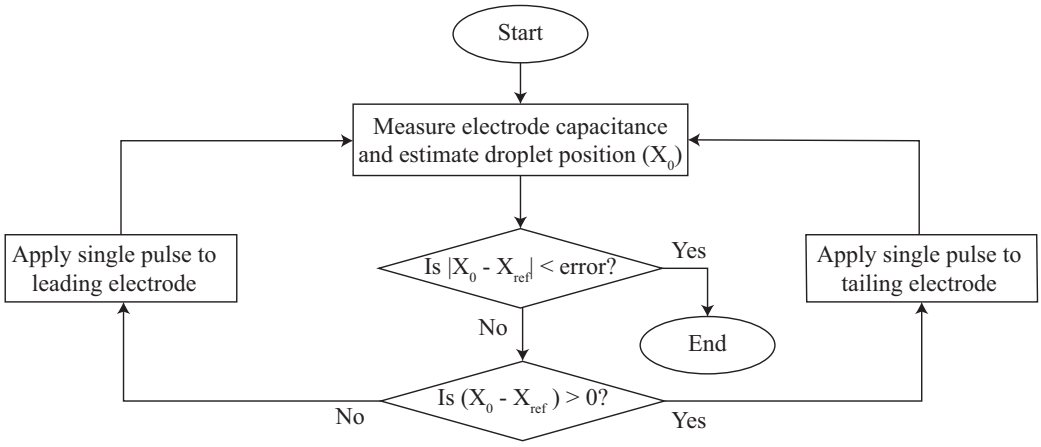

Figure 4.20: Control system finite state machine (FSM).

the droplet. The microcontroller was programmed to implement the finite state machine in Fig. 4.20. The control signal for the actuation pulse was programmed with a 40% duty cycle and a $5ms$ period. The magnitude of the actuation pulse was set to 60Vdc by an external power supply.

Previous feedback control systems proposed by Shih *et al.* [25] and Shin *et al.* [24] require sensor calibration and are incapable of positioning droplet in the domain of two DMF electrodes an inherently unstable position. Experimental observations verified that this feedback control system can position droplets anywhere between two electrodes in a digital microfluidic device in real time. Numerous reference positions between two adjacent electrodes were tested and successfully executed by this feedback control system. The controller had no difficulty positioning droplets near the middle of two electrodes. Clearly, the actuation pulse duty cycle had to be increased for reference positions close to the center of either electrode as the electromechanical force decreases in magnitude when the droplet approaches

the center of either electrode. The actuation pulse duty cycle has an effect on the system damping ratio; near unity duty cycles yield an underdamped system response where the droplet position overshoots the reference position, while near zero duty cycles yield an overdamped response where no droplet position overshoot was observed.

Chapter 5

Conclusions and Future Research

This section summarizes the accomplishments of this thesis and their roles in advancing the state-of-the-art in digital microfluidics are discussed. In addition, further research avenues resulting from an extension of this thesis are presented as future research.

5.1 Conclusions

Digital microfluidic devices must be able to manipulate droplets over a planar surface in order to achieve complete laboratory analyses on a single device. Droplets are typically controlled through the application of electrical signals to an array of electrodes beneath the droplets. Fundamental droplet operations, which are the building blocks for any on-chip laboratory protocol, include droplet transport, mixing, and splitting. Under ideal device operating conditions, each of these droplet operations can be executed through precisely timed electrical signals applied sequentially to the array of electrodes. However in practice, device operating conditions may vary over the run time. For example, compromised surface condition of a device can

negatively affect the device's ability to manipulate droplets. Surface imperfections likely caused by material impurities and foreign particles impede the motion of a droplet. In certain conditions, surface imperfections can thus completely halt the transport phenomenon, compromising the overall performance of DMF devices. This research mainly focuses on improving the accuracy and control of droplet transport operations.

Previous efforts to reduce the device's sensitivity to variations in operating conditions have included the integration of closed loop (feedback) control systems. Such control systems are capable of correcting the timing of electrical signals to compensate for a failure in droplet transport. Feedback control systems have significantly improved the reliability of droplet operations, ultimately enhancing the performance capabilities of DMF devices. However, the state-of-the-art feedback control systems require calibration before they can be used to ensure proper device operation. Current feedback control systems are limited to positioning droplets over electrodes. The controller uses a droplet detection sensing technique which is only able to detect the presence of a droplet when it is positioned over an electrode. As a result, these sensing techniques are limited by the spatial density of electrodes. Conventional approaches for sensing a droplet require high electrode densities to improve the accuracy of droplet position sensing. However, increasing the electrode density increases the cost of device fabrication and logistically complicates the supporting hardware. Furthermore, these droplet sensing techniques fail to capture the continuous motion of a droplet as it transitions from one electrode to the next, particularly in situations where the droplet is situated between two electrodes.

This research addresses the need to choose between sensing accuracy and system complexity attributed to electrode density. A calibration-free droplet sensing technique was proposed to estimate the precise position of any type of droplet between electrodes. This sensing approach requires no prior calibration to estimate the position of a droplet because the approach applies a dimensionless mathematical expression to the capacitance of multiple electrodes. The output from the mathematical expression is the droplet position. This sensing technique has unprecedented droplet position monitoring capabilities with applications in position feedback control systems for accurately controlling droplet position, velocity and acceleration at sub-electrode size resolutions.

During the course of this research six additional contributions were made. First, the proposed droplet sensing technique was optimized through DMF physical parameters to minimize the error in the droplet position estimate. Statistical analysis was performed on a model of the calibration-free capacitance sensing technique to determine its sensitivity to structural and physical parameters of a DMF device. The analysis suggests that the error in the droplet position estimate can be minimized by properly tuning the DMF parameters including dielectric thickness, droplet radius, electrode pitch, electrode separation, filler fluid permittivity, and plate gap. Iso-performance curves were generated to describe the interaction between DMF parameters and the droplet position estimate error. Iso-performance curves are useful plots to help in the design of a DMF device when implementing the proposed calibration-free droplet sensing technique.

Second, a position feedback controller for DMF devices was simulated

to demonstrate its feasibility to position droplets anywhere in between two electrodes prior to prototyping the controller. An analytical method for estimating the controller gains using classical control theory analysis techniques was presented. With this method of estimating controller gains, the controller response can be predicted prior to experimental trials. Two types of controllers (P-action and PD-action) were designed and simulated that demonstrate the capability of accurately controlling the position, velocity, and acceleration of a droplet in a DMF device. Simulation results demonstrate the possibility of controlling droplets in the unstable region between electrodes using Pulse-Width-Modulation (PWM) actuation voltages. In addition, PWM actuation voltages can be used to control the velocity and acceleration of droplets by controlling the width or duty cycle of the actuation pulse.

Third, DC pulse train actuation (or PWM actuation) was investigated as an alternative approach to single-pulse DC or AC actuation. In DC pulse train actuation, a single-pulse DC actuation is divided into many small pulses that incrementally displace a droplet from one electrode to the next. Experimental observations demonstrate that DC pulse train actuation offers a greater degree of control over the position and speed of a droplet. The sequential train of small DC pulses enables the incremental droplet displacement desirable for intra-electrode positioning. In addition, DC pulse train actuation can be used to regulate the non-linear speed of a droplet as it transverse to an adjacent electrode by controlling the pulse width or duty cycle of the actuation pulse. DC pulse train actuation reduces droplet deformation or elongation during actuation because during the low voltage level

of each actuation pulse, the droplet is allowed to assume a quasi-equilibrium transport process. The impact of pulse duty cycle on droplet deformation is important to this thesis because the accuracy of the calibration-free droplet position sensing technique is affected as the droplet footprint deviates from a circular shape. More importantly in a practical application, excessive elongation of droplets containing particles is undesirable because the abrupt deformation of the droplet can result in the contamination of the DMF surface. DC pulse train actuation reduces droplet elongation and abrupt droplet motion, thus has the potential to minimize surface contamination.

Fourth, a portable, low-cost, and programmable control system for DMF devices was prototyped. The proposed control system is fully customizable and can be applied to any DMF application. The controller consists of a microcontroller and a network of solid-state switches which are reusable and reconfigurable to any DMF design. Two types of switches were designed and tested to accommodate either AC or DC actuation voltages. This control system can readily be integrated with external sensors, thus realizing a portable complete total analysis system. In addition, this control system can serve as a prototyping development environment to promote the commercialization of DMF technology.

Fifth, an intra-electrode droplet positioning feedback controller for DMF devices was prototyped. This feedback control system integrates the proposed calibration-free droplet position sensing technique to demonstrate the full capabilities of the droplet sensing technique. The controller estimates the position and then determines which of the two electrodes must apply a single voltage pulse to incrementally displace the droplet towards the desired

reference position. This feedback control system has unparalleled control over the droplet transport phenomena with sub-electrode size resolution. The feedback control system has applications in DMF micro-conveyor systems where it can increase the conveyor positioning resolution.

Sixth and final, the fabrication process of defect-free DMF devices was optimized using basic microfabrication facilities. A step-by-step fabrication recipe for DMF device fabrication is presented. With this fabrication recipe, DMF devices with $10\mu m$ features can readily be fabricated with excellent repeatability without the need for a cleanroom environment. In addition, the fabrication time and cost for DMF device was optimized by eliminating the need for specialized dielectric materials. In this thesis, S1813 photoresist was used as a photoresist in the fabrication of bottom plate electrodes and a dielectric layer for EWOD DMF devices. A DMF device can be fabricated in less than 35 minutes because the dielectric material S1813 comes ready to use.

In conclusion, this research presents a calibration-free droplet sensing technique, a low-cost and programmable controller development environment for DMF devices, and an optimized fabrication recipe of defect-free DMF devices. The contributions of this research thesis enhance the control of droplet transport phenomenon significantly and can be applicable to other droplet operations including mixing, splitting on DMF devices.

5.2 Future Research

This research has opened many possible venues of research beyond the scope of a single masters thesis. The development of a low cost, fully customizable, and programmable controller for DMF devices has great potential to study dynamics of droplet actuation and rapid prototyping of true integrated Lab-On-a-Chip systems. The proposed controller can be programmed on-the-fly to execute a desired sequence of trigger signals used to manipulate droplets on a DMF device. Expansion modules such as droplet position sensors or other sensors can readily be incorporated into the programmable controller development platform.

An extension of this thesis can involve further research into the DC pulse train actuation. In this thesis, the proposed DC pulse train actuation was used to demonstrate the incremental droplet displacement of droplets, which was proven useful for positioning droplets in between electrodes on a DMF device. It was shown that the droplet transport speed or incremental displacement unit can be controlled by varying the pulse duty cycle of the actuation signal. Future research can study the effects of pulse duty cycle to regulate the droplet transport speed. The velocity of a droplet during actuation varies non-linearly as the droplet travels from one electrode to another because the magnitude of the electromechanical force is a function of the droplet position. In the case of square electrodes, the droplet velocity increases sharply as the droplet approaches halfway between the two electrodes and then decreases as the droplet reaches its final destination on the center of the adjacent electrode. An interesting research can be the study

of regulating the velocity of a droplet during actuation by controlling the duty cycle or voltage magnitude of the actuating signals. Preliminary experiments have shown that duty cycle and the magnitude of voltage both have an effect on the droplet transport speed as discussed in Chapter 4. Intuitively, to regulate the droplet velocity on square electrodes, the duty cycle has to decrease as the droplet approaches the halfway point between two electrodes to prevent the droplet from accelerating. Then, the duty cycle has to increase as the droplet approaches the next electrode to overcome resisting forces. This technique can be seen in simulation results in Chapter 2 when attempting to regulate the velocity of a droplet with a position feedback controller.

Another venue of research related to the DC pulse train actuation that was not studied in this thesis is the effect of pulse frequency on the droplet actuation. Experiments of this thesis constrain the pulse frequency to $100Hz$. However, it can be interesting to investigate whether or not the pulse frequency has an effect on the droplet actuation dynamics.

The proposed programmable controller hardware in this thesis draws power from a standard DC power supply. It would be desirable for future applications to include the necessary circuitry to draw power from a standard household wall outlet, thereby achieving a portable control system by eliminating the need of an external power supply. The power circuitry involves the design of an AC to DC converter with the capability of adjusting the DC voltage level to actuate a variety droplet composition with different threshold actuation voltages. In addition, the control system could have control over the droplet transport speed by varying the pulse amplitude.

Another interesting research may involve the application of the DC pulse train actuation to address the issue of unequal droplet splitting ratios. Droplet splitting into two equal size droplets can be readily executed on a linear array of three electrodes by applying sufficient voltage to the end electrodes when the droplet is centered over the middle electrode. It is suspected that applying different duty cycle signals to the end electrodes have an effect on droplet splitting ratios.

Little research has been done on particle absorption with DC pulse train actuation. It would be interesting to see if an oscillating (on/off) driving signal can mitigate particle absorption on the surface.

Finally, it is the hope of the author that this proposed programmable controller can be integrated into a portable Lab-On-a-Chip device for Point-of-Care applications.

References

[1] M. Murran and H. Najjaran, "Capacitance-based droplet position estimator for digital microfluidic devices," *Lab Chip*, 2012 (In press).

[2] A. M. M. Murran and H. Najjaran, "Capacitance-based droplet position sensing optimization through digital microfluidic parameters," in *ASME 9th International Conference on Nanochannels, Microchannels, and Minichannels (ICNMM)*, June 2011.

[3] R. L. H. Martin, M. Murran and H. Najjaran, "Experimental technique for sensing droplet position in digital microfluidic systems using capacitance measurement," in *ASME International Mechanical Engineering Congress and Exposition*, November 2010.

[4] J. Berthier, *Microdrops and digital microfluidics*. William Andrew Pub., 2008.

[5] I. Barbulovic-Nad, H. Yang, P. S. Park, and A. R. Wheeler, "Digital microfluidics for cell-based assays," *Lab Chip*, vol. 8, pp. 519–526, 2008.

[6] M. J. Jebrail and A. R. Wheeler, "Digital microfluidic method for protein extraction by precipitation.," *Anal. Chem.*, vol. 81, pp. 330–335, 2009.

[7] Y.-H. Chang, G.-B. Lee, F.-C. Huang, Y.-Y. Chen, and J.-L. Lin, "Integrated polymerase chain reaction chips utilizing digital microfluidics," *Biomedical Microdevices*, vol. 8, pp. 215–225, 2006.

[8] K. Chakrabarty and F. Su, *Digital microfluidic biochips: synthesis, testing, and reconfiguration techniques*. CRC/Taylor & Francis, 2006.

[9] R. Fair, A. Khlystov, T. Tailor, V. Ivanov, R. Evans, P. Griffin, V. Srinivasan, V. Pamula, M. Pollack, and J. Zhou, "Chemical and biological applications of digital-microfluidic devices," *Design Test of Computers, IEEE*, vol. 24, pp. 10 –24, jan.-feb. 2007.

[10] S. K. Cho, H. Moon, and C.-J. Kim, "Creating, transporting, cutting, and merging liquid droplets by electrowetting-based actuation for digital microfluidic circuits," *Microelectromechanical Systems, Journal of*, vol. 12, pp. 70–80, feb 2003.

[11] F. Brochard, "Motions of droplets on solid surfaces induced by chemical or thermal gradients," *Langmuir*, vol. 5, no. 2, pp. 432–438, 1989.

[12] M. Washizu, "Electrostatic actuation of liquid droplets for microreactor applications," *Industry Applications, IEEE Transactions on*, vol. 34, pp. 732–737, jul/aug 1998.

[13] M. G. Pollack, R. B. Fair, and A. D. Shenderov, "Electrowetting-based actuation of liquid droplets for microfluidic applications," *Applied Physics Letters*, vol. 77, no. 11, pp. 1725–1726, 2000.

[14] M. O. A. Abdelgawad, *Digital Microfluidics for Integration of Lab-on-*

a-Chip Devices. PhD thesis, University of Toronto, Ontario, Canada, 2009.

[15] N.-T. Nguyen, K. M. Ng, and X. Huang, "Manipulation of ferrofluid droplets using planar coils," *Applied Physics Letters*, vol. 89, no. 5, p. 052509, 2006.

[16] K. Ichimura, S.-K. Oh, and M. Nakagawa, "Light-driven motion of liquids on a photoresponsive surface," *Science*, vol. 288, no. 5471, pp. 1624–1626, 2000.

[17] A. Wixforth, C. Strobl, C. Gauer, A. Toegl, J. Scriba, and Z. v. Guttenberg, "Acoustic manipulation of small droplets," *Analytical and Bioanalytical Chemistry*, vol. 379, pp. 982–991, 2004.

[18] E. Yakhshi-Tafti, H. J. Cho, and R. Kumar, "Discrete droplet manipulation on liquid platforms using thermal gradients," *Procedia Chemistry*, vol. 1, no. 1, pp. 1519 – 1522, 2009.

[19] J. Gong and C.-J. C. Kim, "All-electronic droplet generation on-chip with real-time feedback control for ewod digital microfluidics," *Lab Chip*, vol. 8, pp. 898–906, 2008.

[20] M. G. Pollack, A. D. Shenderov, and R. B. Fair, "Electrowetting-based actuation of droplets for integrated microfluidics," *Lab Chip*, vol. 2, no. 2, pp. 96–101, 2002.

[21] K.-S. Yun and C.-J. Kim, "Low-voltage elctrostatic actuation of droplet on thin superhydrophobic nanoturf," in *Micro Electro Mechanical Sys-*

tems, 2007. MEMS. IEEE 20th International Conference on, pp. 139 –142, jan. 2007.

[22] C. Cooney, C.-Y. Chen, M. Emerling, A. Nadim, and J. Sterling, "Electrowetting droplet microfluidics on a single planar surface," *Microfluidics and Nanofluidics*, vol. 2, pp. 435–446, 2006.

[23] A. Torkkeli, "Droplet microfluidics on a planar surface," *Vtt Publications*, p. 217, 2003.

[24] Y.-J. Shin and J.-B. Lee, "Machine vision for digital microfluidics," *Review of Scientific Instruments*, vol. 81, no. 1, p. 014302, 2010.

[25] S. C. C. Shih, R. Fobel, P. Kumar, and A. R. Wheeler, "A feedback control system for high-fidelity digital microfluidics," *Lab Chip*, vol. 11, pp. 535–540, 2011.

[26] N. S. Nise, *Control Systems Engineering*. 111 River street, Hoboken, N.J: Wiley, 2008.

[27] I. Moon and J. Kim, "Using ewod (electrowetting-on-dielectric) actuation in a micro conveyor system," *Sensors and Actuators A: Physical*, vol. 130131, no. 0, pp. 537 – 544, 2006.

[28] V. Srinivasan, V. K. Pamula, and R. B. Fair, "An integrated digital microfluidic lab-on-a-chip for clinical diagnostics on human physiological fluids," *Lab Chip*, vol. 4, 2004.

[29] J. Valentino, S. Troian, and S. Wagner, "Microfluidic detection and analysis by integration of evanescent wave sensing with thermocapillary

actuation," in *Micro Electro Mechanical Systems, 2005. MEMS 2005. 18th IEEE International Conference on*, pp. 730 – 733, jan.-3 feb. 2005.

[30] J. Nichols, A. Ahmadi, M. Hoorfar, H. Najjaran, and J. F. Holzman, "In situ digital microfluidic conductance sampling," *Sensors and Actuators A: Physical*, vol. 152, no. 1, pp. 13 – 20, 2009.

[31] J. Z. Chen, A. A. Darhuber, S. M. Troian, and S. Wagner, "Capacitive sensing of droplets for microfluidic devices based on thermocapillary actuation," *Lab Chip*, vol. 4, 2004.

[32] M. Schertzer, R. B. Mrad, and P. Sullivan, "Automated detection of particle concentration and chemical reactions in ewod devices," *Sensors and Actuators B: Chemical*, vol. 164, no. 1, pp. 1–6, 2012.

[33] M. Schertzer, R. B. Mrad, and P. Sullivan, "Using capacitance measurements in ewod devices to identify fluid composition and control droplet mixing," *Sensors and Actuators B: Chemical*, vol. 145, no. 1, pp. 340–347, 2010.

[34] D. Chatterjee, H. Shepherd, and R. L. Garrell, "Electromechanical model for actuating liquids in a two-plate droplet microfluidic device," *Lab Chip*, vol. 9, pp. 1219–1229, 2009.

[35] T. B. Jones, J. D. Fowler, Y. S. Chang, and C.-J. Kim, "Frequency-based relationship of electrowetting and dielectrophoretic liquid microactuation," *Langmuir*, vol. 19, no. 18, pp. 7646–7651, 2003.

[36] T. B. Jones, K.-L. Wang, and D.-J. Yao, "Frequency-dependent elec-

tromechanics of aqueous liquids: electrowetting and dielectrophoresis," *Langmuir*, vol. 20, no. 7, pp. 2813–2818, 2004. PMID: 15835158.

[37] T. B. Jones, "An electromechanical interpretation of electrowetting," *Journal of Micromechanics and Microengineering*, vol. 15, no. 6, p. 1184, 2005.

[38] A. Ahmadi, J. Holzman, H. Najjaran, and M. Hoorfar, "Electrohydrodynamic modeling of microdroplet transient dynamics in electrocapillary-based digital microfluidic devices," *Microfluidics and Nanofluidics*, vol. 10, pp. 1019–1032, 2011.

[39] V. Bahadur and S. V. Garimella, "An energy-based model for electrowetting-induced droplet actuation," *Journal of Micromechanics and Microengineering*, vol. 16, no. 8, p. 1494, 2006.

[40] E. Baird, P. Young, and K. Mohseni, "Electrostatic force calculation for an ewod-actuated droplet," *Microfluidics and Nanofluidics*, vol. 3, no. 6, pp. 635–644, 2007.

[41] H. Ren, R. B. Fair, M. G. Pollack, and E. J. Shaughnessy, "Dynamics of electro-wetting droplet transport," *Sensors and Actuators B: Chemical*, vol. 87, no. 1, pp. 201 – 206, 2002.

[42] E. Bertrand, T. D. Blake, and J. D. Coninck, "Influence of solidliquid interactions on dynamic wetting: a molecular dynamics study," *Journal of Physics: Condensed Matter*, vol. 21, no. 46, p. 464124, 2009.

[43] H. N. Biddut Bhattacharjee, "Size dependent droplet actuation in digital microfluidic systems," in *SPIE*, April 2009.

[44] F. Mugele and J.-C. Baret, "Electrowetting: from basics to applications," *Journal of Physics: Condensed Matter*, vol. 17, no. 28, p. R705, 2005.

[45] A. Ahmadi, H. Najjaran, J. F. Holzman, and M. Hoorfar, "Two-dimensional flow dynamics in digital microfluidic systems," *Journal of Micromechanics and Microengineering*, vol. 19, no. 6, p. 065003, 2009.

[46] J.-J. E. Slotine and W. Li, *Applied Nonlinear Control*. Englewood Cliffs, New Jersey: Prentice-Hall, Inc, 1991.

[47] J. H. Noh, J. Noh, E. Kreit, J. Heikenfeld, and P. D. Rack, "Toward active-matrix lab-on-a-chip: programmable electrofluidic control enabled by arrayed oxide thin film transistors," *Lab Chip*, vol. 12, 2012.

[48] C. Elbuken, T. Glawdel, D. Chan, and C. L. Ren, "Detection of microdroplet size and speed using capacitive sensors," *Sensors and Actuators A: Physical*, vol. 171, no. 2, pp. 55 – 62, 2011.

[49] N. Rajabi and A. Dolatabadi, "A novel electrode shape for electrowetting-based microfluidics," *Colloids and Surfaces A: Physicochemical and Engineering Aspects*, vol. 365, pp. 230 – 236, 2010.

[50] M. Abdelgawad, P. Park, and A. R. Wheeler, "Optimization of device geometry in single-plate digital microfluidics," *Journal of Applied Physics*, vol. 105, no. 9, p. 094506, 2009.

[51] J. Lienemann, A. Greiner, J. G. Korvink, G. K, and D. Freiburg, "Electrode shapes for electrowetting arrays," *Proc nanotech*, vol. 1, pp. 94–97, 2003.

[52] H. N. Biddut Bhattacharjee, "Effects of the properties of dielectric materials on the fabrication and operation of digital microfluidic systems," in *ASME International Mechanical Engineering Congress and Exposition*, November 2010.

[53] M. I. Newton, D. L. Herbertson, S. J. Elliott, N. J. Shirtcliffe, and G. McHale, "Electrowetting of liquid marbles," *Journal of Physics D: Applied Physics*, vol. 40, no. 1, p. 20, 2007.